



8-2001

Analysis of extended Constant Power Speed Range of the Permanent Magnet Synchronous Machine driven by Dual Mode Inverter Control

João Onofre Pereira Pinto

Follow this and additional works at: https://trace.tennessee.edu/utk_graddiss

Recommended Citation

Pereira Pinto, João Onofre, "Analysis of extended Constant Power Speed Range of the Permanent Magnet Synchronous Machine driven by Dual Mode Inverter Control. " PhD diss., University of Tennessee, 2001. https://trace.tennessee.edu/utk_graddiss/8195

This Dissertation is brought to you for free and open access by the Graduate School at TRACE: Tennessee Research and Creative Exchange. It has been accepted for inclusion in Doctoral Dissertations by an authorized administrator of TRACE: Tennessee Research and Creative Exchange. For more information, please contact trace@utk.edu.

To the Graduate Council:

I am submitting herewith a dissertation written by João Onofre Pereira Pinto entitled "Analysis of extended Constant Power Speed Range of the Permanent Magnet Synchronous Machine driven by Dual Mode Inverter Control." I have examined the final electronic copy of this dissertation for form and content and recommend that it be accepted in partial fulfillment of the requirements for the degree of Doctor of Philosophy, with a major in Electrical Engineering.

Jack S. Lawler, Major Professor

We have read this dissertation and recommend its acceptance:

J. Milton Bradley, Paul B. Crilly, Leon Tolbert, Luiz E. Borges Silva, Tse-Wei Wang

Accepted for the Council:

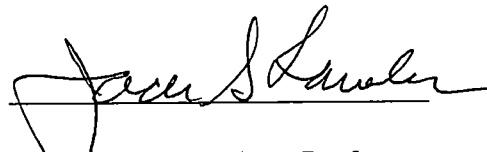
Carolyn R. Hodges

Vice Provost and Dean of the Graduate School

(Original signatures are on file with official student records.)

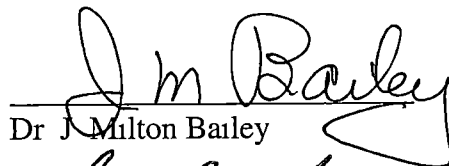
To the Graduate Council

I am submitting herewith a dissertation written by João Onofre Pereira Pinto entitled "Analysis of Extended Constant Power Speed Range Of The Permanent Magnet Synchronous Machine Driven by Dual Mode Inverter Control" I have examined the final copy of this dissertation for form and content and recommended that it be accepted in partial fulfillment of the requirements for the degree of Doctor of Philosophy, with a major in Electrical Engineering

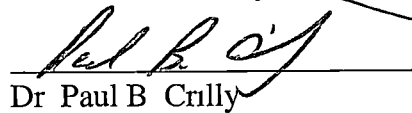


Jack S. Lawler, Major Professor

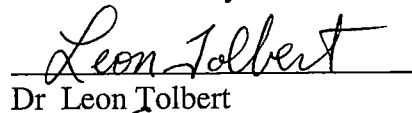
We have read this dissertation
and recommend its acceptance



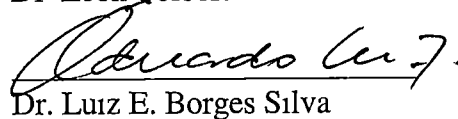
Dr. J. Milton Bailey



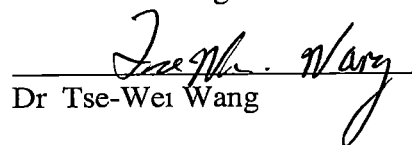
Dr. Paul B. Crilly



Dr. Leon Tolbert

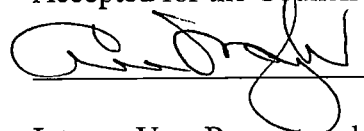


Dr. Luiz E. Borges Silva



Dr. Tse-Wei Wang

Accepted for the Council



Interim Vice Provost and
Dean of the Graduate School

**ANALYSIS OF EXTENDED CONSTANT POWER SPEED
RANGE OF THE PERMANENT MAGNET
SYNCHRONOUS MACHINE DRIVEN BY DUAL MODE
INVERTER CONTROL**

A Dissertation
Presented for the
Doctor of Philosophy Degree
The University of Tennessee, Knoxville

João Onofre Pereira Pinto
August 2001

DEDICATION

This dissertation is dedicated to my parents

Mr Benedito Pereira Pinto[†]

and

Mrs Damiana de Freitas Pinto

who have taught me the values of belief and perseverance

ACKNOWLEDGEMENTS

Before acknowledging anyone, I would like to convey that this is very difficult for me because I know that my best English is not good enough to fully express my gratitude to the people who were my guides, my friends, and my support during this journey through the PhD program.

I would like to thank Dr. Jack S Lawler His unconditional support was one of the main reasons for my success. Dr. Lawler showed me that advising and kindness are perfectly compatible From Dr. Lawler I have not only learned the interesting topics of research involved in this dissertation but have also learned to adopt a practical way of thinking.

In addition to Dr. Lawler, I would like to thank the other members of the dissertation committee, Dr J. Milton Bailey, Dr Paul B Crilly, Dr. Leon M. Tolbert, Dr Luiz E. B Silva, and Dr. Tse-Wei Wang, for their careful review of my work and their suggestions for the improvement that resulted in this dissertation. I also want to thank them for sparing some of their busy time to review my work in such a short amount of time.

There are some people whose kindness and help are immeasurable. Among them, I would like to highlight my great friend Burak Ozpineci, for his friendship, technical discussions, careful review of my writings, and encouragement. I would like to thank Dr. Luiz Eduardo Borges da Silva, my friend and also a member of my dissertation committee Luiz's wisdom helped me pass through rough times during

my stay in the U S As if that was not enough, he gifted me with his presence in my dissertation defense, leaving his business and his family in Brazil and traveling such a long distance I also would like to specially recognize the precious assistance of Dr Subrata Mondal and Nicolau Pereira Filho who helped me improve the results of this work

I also want to thank the Brazilian community, which I consider to be my family in Knoxville, for their friendship and support. During this time, many people have come and gone, but their friendship has always stayed, and also the memories of the good and bad times as well

During my stay in the Ph D program in Knoxville, I had the opportunity to meet very nice people from all over the world with whom I exchanged valuable cultural experiences that helped me to grow as a human being They are from the U.S , like Alev and Wesley, from Turkey like Omer and Orkun, from Lebanon like Ibrahim, from Germany like Claudia, from India and Mexico, like the couple Samuel and Claudia, from Korea like Dr Jong-Son Ko and Sewoong Kim, and so many other people from so many other places

I would also like to thank my brothers and sisters for their support throughout my life and particularly during this time in which I was geographically separated from them They are Maria, Marinalva, Mauro, Marina, Marlene, Maurilio, Maura, Mara and Sebastião Although they were in Brazil, I could still feel their caring presence all the time.

Finally, I would like to thank those who made this journey more enjoyable, my wife Alexandra, and my son João Vitor. I thank them for being so understanding of my absence during many moments of their lives due to my work, but I also offer my apologies for those times.

I would like to recognize the importance of CAPES from Brazil, Universidade Federal de Mato Grosso do Sul and The Electrical, and Computer Engineering Department of The University of Tennessee in Knoxville, without their financial support this work could not have been completed.

DEDICATÓRIA

Esta tese é dedicada aos meus pais

Sr Benedito Pereira Pinto[†]

e

Sra Damiana de Freitas Pinto

que me ensinaram a acreditar e a perseverar

AGRADECIMENTOS

Antes de fazer qualquer agradecimento, eu gostaria de dizer que isso é muito difícil para mim, porque sei que não conseguirei expressar, em linguagem escrita, a minha gratidão às pessoas que foram meus guias, meus amigos, e meu suporte durante minha jornada no programa de doutorado

Gostaria de agradecer ao Dr Jack. S Lawler Seu apoio incondicional foi uma das principais razões para o meu sucesso Dr. Lawler me mostrou que orientação e carinho são perfeitamente conciliáveis Com Dr Lawler, aprendi não somente os tópicos interessantes da minha tese, mas também a adoção de uma forma prática de pensar

Além do Dr Lawler, agradeço aos demais membros da Banca Examinadora da minha tese, Dr J Milton Bailey, Dr Paul B Crilly, Dr Leon M Tolbert, Dr Luiz E B Silva e Dr Tse-Wei Wang, pela cuidadosa revisão do meu trabalho e pelas sugestões de melhorias, as quais resultaram nesta tese Gostaria de agradecê-los ainda por seus esforços e disponibilidade na revisão deste trabalho em tão curto espaço de tempo.

Há algumas pessoas, cujo carinho e a ajuda são imensuráveis. Entre elas, destaco o meu grande amigo Burak Ozıpineci, pela sua amizade, discussões técnicas, cuidadosa revisão dos meus textos e pelo incentivo. Agradeço também ao Dr Luiz Eduardo Borges da Silva, meu amigo e também membro da minha Banca de tese, sua maturidade e seu discernimento me ajudaram a passar por difíceis fases durante o

tempo que permaneci nos Estados Unidos. Como se isso não fosse suficiente, ele me presenteou com sua participação na minha defesa, deixando sua família e seus negócios no Brasil e fazendo essa longa viagem do Brasil aos Estados Unidos. Gostaria também de reconhecer, especialmente, a preciosa assistência do Dr. Subrata Mondal e do Prof. Nicolau Pereira Filho, os quais me ajudaram a melhorar os resultados do meu trabalho.

Agradeço também à comunidade Brasileira, extensão da minha família em Knoxville, pela amizade e apoio. Durante esse tempo, muitas pessoas vieram e muitas pessoas se foram, mas a amizade deles permanece, e também as lembranças dos bons e dos difíceis momentos.

Durante minha estada no programa de doutorado em Knoxville, tive a oportunidade de encontrar excelentes pessoas do mundo todo, com as quais pude trocar experiências culturais, que me ajudaram a crescer como ser humano. São pessoas dos Estados Unidos, como Alev e Wesley, da Turquia, como Omer e Orkun, do Líbano, como Ibrahim, da Alemanha, como Claudia, da Índia e do México, como o casal Samuel e Claudia, da Coreia, como Dr. Jong-Son Ko e Sewoong Kim, e muitas outras pessoas de muitos outros lugares.

Expresso também minha gratidão às minhas irmãs e aos meus irmãos, pelo apoio que me deram durante toda a minha vida e, particularmente, durante o período em que estive geograficamente separado deles. São eles, Maria, Marinalva, Mauro, Marina, Marlene, Maurílio, Maura, Mara e Sebastião. Mesmo estando eles no Brasil, senti a presença carinhosa de cada um todo o tempo.

Finalmente, minha eterna gratidão àqueles que fizeram minha jornada mais agradável, minha esposa Alexandra e meu filho João Vitor. Agradeço-os por entenderem minha ausência em muitos momentos de suas vidas, por causa do meu trabalho. Peço-lhes perdão por isso.

Gostaria de reconhecer a importância da CAPES, da Universidade Federal de Mato Grosso do Sul e do *The Electrical, and The Computer Engineering Department of The University of Tennessee*, de Knoxville, sem apoio financeiro desses órgãos, este trabalho não poderia ter sido concluído.

ABSTRACT

The scope of this work is the Permanent Magnet Synchronous Machine (PMSM) operating at Constant Power Speed Range (CPSR). The proposed technique to drive the PMSM at CPSR is the Dual Mode Inverter Control (DMIC). The main idea behind DMIC is to change the three-phase operation of the PMSM below base speed to hybrid, single-phase and three-phase, operation above the base speed. This technique allows driving the PMSM in a wide CPSR. The DMIC uses three facts to achieve wide CPSR. First, it introduces the idea of the advance angle, which allows driving current into the machine while the back-emf is smaller than the DC link voltage. Second, the blanking angle is used to maximize the electrical to mechanical power conversion by increasing the on time of the transistors of the Voltage-Fed Inverter (VFI) and therefore slowing down the decreasing voltage in the outgoing phase. Finally, this technique avoids regeneration through the bypass diodes by introducing an ac-voltage controller interfacing the VFI and the PMSM.

The analysis of DMIC/PMSM drive system shows that it uses the same principle of Vector Control with Field Weakening (VCFW) i.e., the armature current is controlled to have a field component that weakens the air gap field, and therefore opposes the back emf. However, the armature current vector must satisfy the voltage and current constraints, which are the maximum current and armature voltage. In VCFW, the voltage limit circle shrinks fast as speed increases because the maximum armature voltage is the maximum output voltage of the VFI, which is limited by the

DC link voltage In DMIC, on the other hand, the voltage limit circle shrinks slower, since after the commutation period the machine is operating in single-phase mode. The total armature voltage is the contribution of the DC link voltage, the back emf, and the induced voltage provided by the derivative of the on-phase currents. In fact, this operation eliminates the voltage constraint, and the machine can operate at any speed, and then the only constraint is the current limit. Therefore, it is shown in this work that theoretically there is no speed limit for DMIC driving PMSM over constant power operation range.

PREFACE

Permanent Magnet Synchronous Machines (PMSM) have high efficiency, high power density, high torque-to-inertia ratio, and fast dynamic response. These features make this machine very attractive for applications such as actuators, robotics, servo drives, etc. Electric Vehicles is another potential application of this type of machine. However, because of its nature, i.e., constant magnet flux provided by magnets, these machines have a narrow constant power operation range. This limitation is a strong drawback for application of PMSM in electric vehicles, where high speed is a top requirement. This dissertation proposes, describes, evaluates, and analyzes Dual Mode Inverter Control (DMIC). DMIC is a technique that provides a wide CPOR for PMSM.

Chapter I Briefly reviews the recent advances in PMSM drive systems, their advantages and their drawbacks and states the necessity of a scheme that truly can drive PMSM in wide constant power speed range.

Chapter II presents PMSM models. Initially, it gives the three-phase model of the PMSM in the stationary frame, which is used in chapter III to describe how DMIC works. Then, the d-q model of PMSM in rotating frame is given. This model is used in chapter IV and V for analysis and comparison of Vector Control with Field Weakening and DMIC.

Chapter III proposes DMIC driving PMSM. Initially, it describes the Phase-Advance method (PHA), gives simulation results for PHA driving a low inductance Brushless DC machine (BDCM) and discusses its limitations doing so. In the sequence it describes DMIC driving BDCM. The superiority of DMIC compared to PHA for low inductance BDCM is given and the reason for this superiority is identified. Finally, in this chapter, DMIC driving PMSM is described. Simulation results are given and the effectiveness of the DMIC/PMSM drive system is shown. Analysis showing why DMIC/PMSM drive system has a good performance for operation above base speed is addressed in Chapter V.

Chapter IV discusses Vector Control with Field Weakening (VCFW) of PMSM. VCFW is the most popular method of driving PMSM above base speed. The VC principles driving PMSM is described in details for Constant Torque Operation Region (CTOR) as well as for Constant Power Operation Region (CPOR). The speed limit of the CTOR and CPOR is given using the voltage and current constraints. The system driving a low inductance PMSM is simulated and simulation results are given. The CPOR is found to be narrow for low inductance PMSM.

Chapter V explains why DMIC works from the machine perspective, compares DMIC and VCFW, and proves that there is no theoretical speed limit for CPOR when DMIC drives PMSM. In this chapter, the d-q model of PMSM in rotating reference frame is used. Analytical expression of the phase currents and voltages provided by DMIC are given. The d-q currents and voltages are found by doing the inverse vector rotation of the phase currents and voltages. The average

values of the pulsating d-q currents and voltages are found. The d-q currents and voltages of the PMSM controlled by VCFW and by DMIC are plotted in the same plot in such a way that the two techniques can be compared. The superiority of DMIC over VCFW with respect to speed limit of CPOR is shown. Finally, the theoretical speed limit of CPOR is found to be infinity for DMIC driving PMSM.

Chapter IV draws conclusions from the presented work, and gives recommendations for future research topics.

TABLE OF CONTENTS

CHAPTER	PAGE
III. INTRODUCTION.....	1
I 1 Background	1
I.2 Objective of the Research	7
II. PERMANENT MAGNET SYNCHRONOUS MACHINE MODELS.	9
II 1 Introduction	9
II 2 PMSM three-phase model	10
II 3 PMSM d-q model.	14
II 4 Conclusions	19
III. DUAL MODE INVERTER CONTROL.....	20
III 1 Introduction	20
III 2 PHA driving a BDCM	21
III 3 DMIC driving a BDCM	27
III 4 DMIC driving a PMSM	33
III.5. Conclusion	37
IV. FIELD WEAKENING TECHNIQUE FOR PMSM.....	39
IV 1 Introduction	39
IV 2 Vector Control of PMSM	40
IV.3 Analysis of limits of operation of PMSM with Vector Control	46
IV.3 1 Voltage and current limits	46
IV 3 2 Constant Torque Operation Region	52
IV 3 3 Constant Power Operation Region.. . . .	55
IV 4 System Description of Vector Control of PMSM with Field Weakening Operation.	61
IV 5 Simulation Results of Vector Control of PMSM with Field Weakening Operation	68
IV.6 Conclusions	84
V. ANALYSIS OF DUAL MODE INVERTER CONTROL.....	86
V.1 Introduction.. . . .	86
V 2 Analytical Equations of the PMSM Armature Phase Currents and Phase Voltages in DMIC/PMSM System	87

CHAPTER	PAGE
V 2.1 Analytical Equations of the PMSM Armature Phase Currents.....	88
V.2 2 Analytical Equations of the PMSM Phase Voltages ..	99
V 3 Equations of the dq Components of the Armature Current and Voltage	101
V 3 1 Equations of the dq Components of the Armature Current	102
V 3 2 Equations of the dq Components of the Armature Voltage	105
V 4 Analysis of PMSM Driven by DMIC Using the PMSM d-q Model	107
V 5 Limit of Constant Power Operation Range of the PMSM Driven by DMIC	114
V 6 Conclusions	121
VI. SUMMARY.....	123
VI 1 Conclusions	123
VI 2 Recommendation for future work	125
REFERENCES.....	128
APPENDIX.....	135
Simulation Block Diagram.	136
VITA.....	144

LIST OF FIGURES

FIGURE	PAGE
1.1 Typical phase <i>a</i> current excitation for a Brushless DC motor.	3
1.2 Typical phase <i>a</i> current excitation for a Permanent Magnet Synchronous Machine... ..	4
2.1 PMSM three-phase model.... ..	10
2.2 Phasor diagram showing abc and dq reference frames.	16
2.3 d-q equivalent circuit in synchronously rotating frame (I)..... ..	18
3.1 Standard VFI.	21
3.2 Gate signal For Q_1 and Q_4 in the phase advance method.... ..	23
3.3 Current in phase <i>a</i> , transistor Q_1 and Diode D_1 for $n=5$ and $\theta_a = 50^\circ$.. .	25
3.4 Instantaneous total power, phase <i>a</i> power, and power flowing through the phase <i>a</i> transistors and diodes for $n=5$ and $\theta_a = 50^\circ$	26
3.5 Inverter Topology for the DMIC	28
3.6 Firing scheme for motoring mode of DMIC driving a BDCM	30
3.7 Current in phase <i>a</i> , transistor Q_1 and Q_4 and Diode D_1 and D_4 for $n=5$, $\theta_a = 36.6^\circ$, $\theta_b = 20^\circ$	32
3.8 Instantaneous total power, phase <i>a</i> power (transistors) for $n=5$, $\theta_a = 36.6^\circ$, $\theta_b = 20^\circ$	32
3.9 Firing scheme for motoring mode of DMIC driving a PMSM.	35
3.10 Current in phase <i>a</i> , transistor Q_1 and Diode D_1 for $n=5$, $\theta_a = 42^\circ$, $\theta_b = 20^\circ$	36
3.11 Instantaneous total power, phase <i>a</i> power (all flowing through the transistors) for $n=5$, $\theta_a = 42^\circ$, $\theta_b = 20^\circ$	37
4.1 d-q equivalent circuit in synchronously rotating frame (II).	41
4.2 Phasor diagram showing the variables of the d-q model of the PMSM....	43
4.3 Normalized current limit circle in the synchronously rotating reference frame..	47
4.4 Voltage limit circles in the synchronously rotating reference frame.....	51

FIGURE	PAGE
4 29 Machine output power during machine acceleration.. .. .	83
4.30 i_q and i_d behavior during machine acceleration.	84
5 1 DMIC driving a PMSM	89
5 2 DMIC driving a PMSM during commutation period	91
5 3 Line-to-line Back emf waveform with respect to the reference at DMIC/PMSM system	92
5.4 DMIC driving a PMSM after commutation period.....	96
5 5 Armature phase currents for the machine operating at 5 times base speed	98
5 6 Armature phase voltages for the machine operating at 5 times base speed	101
5 7 i_d and i_q currents for the machine operating at 5 times base speed	105
5 8 v_d and v_q voltages for the machine operating at 5 times base speed.	107
5 9 Current and voltage limits of the PMSM using DMIC and VCFW for machine operating at twice the base speed	112
5 10 Current and voltage limit of the PMSM using DMIC and VCFW for machine operating 5 times base speed	113
5 11 Current and voltage limits of the PMSM using DMIC and VCFW for machine operating 9 times the base speed.. . . .	114
5 12 Minimum radius of the voltage limit circle for PMSM to develop rated power	116
5 13 Voltage radius provided by DMIC, VCFW, and the minimum radius.	118
5 14 Actual and fitting function of the voltage limit radius provided by DMIC	120

LIST OF TABLES

TABLE	PAGE
3 1 Drive system parameters	24
4 1 Drive system parameters – VCFW	69
5.1 Average Values of Voltages and Currents.	110

LIST OF SYMBOLS*

λ_{abc}	Total flux linkages in phases a , b and c
i_a, i_b, i_c	Phase currents
v_{an}, v_{bn}, v_{cn}	Terminal phase to neutral voltages
R	Winding resistance per phase
L_s	Self-inductance per phase
M	Mutual inductance
ϕ_a	Phase flux linkages established by the permanent magnets
ϕ_m	Amplitude of the flux linkages established by the permanent magnet
N_0	Power supply neutral point
N_1	PMSM neutral point
P	Number of pole pairs
ω_e	Electrical speed
ω_r	Angular speed of the rotor
T_e	Electromagnetic torque
T_L	Load torque
B	Damping constant

*Symbols are given in order of appearance

J	Rotor inertia
f_{an}, f_{bn}, f_{cn}	Phase variables in the abc stationary frame
f_d, f_q, f_0	Variables in the dqo rotating reference frame
$Q_1 \sim Q_6$	Voltage fed inverter main devices
$D_1 \sim D_6$	Anti-parallel diodes of $Q_1 \sim Q_6$
V_{dc}	DC link voltage
e_{an}, e_{bn}, e_{cn}	Phase to neutral back-emf
P_{rated}	Machine rated power
N_b	Mechanical base speed in rpm
f_b	Base frequency in Hz
E_b	Peak phase-to-neutral back-emf at base speed
$I_{rated (peak)}$	Rated peak current of the inverter devices
$I_{rated (rms)}$	Rated rms current of the inverter devices
n	Actual speed to base speed ratio
$T_1 \sim T_6$	AC voltage controller thyristors
θ_b	Blanking angle
θ_a	Advance angle
θ_c	Commutation angle
θ_d	Delay angle
$\Delta\theta_e$	Difference between θ_a and θ_d
v_q	Quadrature component of the PMSM terminal

	voltage
v_d	Direct component of the PMSM terminal voltage
i_q	Quadrature component of the PMSM current
i_d	Direct component of the PMSM current
I_{max}	Maximum stator current
m	PWM modulation index
V^*	Peak value of the fundamental voltage generated by the PWM modulator
V_{1sw}	Peak value of the fundamental voltage at square-wave operation
V_a	Amplitude of the applied armature voltage
V_{max}	Maximum amplitude of the applied armature voltage
ω_{rb}	Base speed
ω_{rc}	Critical speed
ω_r^*	Rotor speed command
$K_{\omega I}$	Integral constant for the rotor speed controller
$K_{\omega P}$	Proportional constant for the speed controller
K_{qI}	Integral constant for the i_q controller
K_{qP}	Proportional constant for the i_q controller
K_{dI}	Integral constant for the i_d controller
K_{dP}	Proportional constant for the i_d controller

i_q^*	i_q command
i_d^*	i_d command
v_{q0}, v_{d0}	Decoupling voltages
v_{qc}	Compensated value of v_q
v_{dc}	Compensated value of v_d
f_s	PWM switching frequency
T_s	PWM sample time
k	Load constant
e_{ab}	Line-to-line back emf
I_q	Average value of i_q
I_d	Average value of i_d
V_q	Average value of v_q
V_d	Average value of v_d
V_{R-DMIC}	Voltage circle limit radius provided by DMIC
V_{R-VCFW}	Voltage circle limit radius provided by VCFW
V_{Rn}	Minimum voltage circle limit radius at n times base speed

CHAPTER I

INTRODUCTION

I.1 Background

Permanent magnet AC machines (PMAC) are becoming more and more popular because of their high efficiency, high power density, and high torque-to-inertia ratio. The efficiency of the PMAC is high because no excitation winding is used since the air gap magnetic flux is provided by the permanent magnets. The high density and the high torque-to-inertia ratio are achieved when rare-earth magnet materials are used. Fast dynamic response is another feature that makes this machine attractive for applications such as actuators, robotics, and servo drives. The electric vehicle is another potential application for this type of machines, mainly because of their appealing efficiency, which is a top requirement for battery or fuel-cell supplied vehicles. These machines are synchronous type machines and therefore their excitation frequency (stator frequency) must be perfectly synchronized with their rotational frequency (rotor speed). PMAC machines may or may not have auxiliary rotor windings. If auxiliary rotor windings are provided, these machines can be easily controlled, since they start as an induction machine, and after the rotor frequency gets close to the excitation frequency, it is pulled into synchronism by a combination of the reluctance and synchronous motor torques provided by the magnets [1]. However,

the auxiliary rotor windings decrease the efficiency, the power density, and the torque-to-inertia ratio of the PMAC. The dynamic response is also affected by the auxiliary rotor windings. For that reason, PMAC without auxiliary rotor windings is generally desired. However, the absence of the auxiliary rotor windings makes the control of PMAC complex and power electronics is essential to achieve perfect rotational-excitation synchronization and to generate useful steady-state torque [2]. In the past few years, many researchers have put much effort on this subject. In general, their research involve selecting permanent magnet materials, designing machine configurations [3], achieving motor and drive physical integration [4], using sensorless PMAC control [5], [6], developing PWM techniques for controlling PMAC machines, and so forth.

With respect to the back-EMF shape, the PMAC machine can be classified into two types: trapezoidal back-EMF, which is also known as Brushless DC machine (BDCM), and sinusoidal back-EMF, known as Permanent Magnet Synchronous Machine (PMSM). The back-EMF shape will result in different rules for their motion control. For instance, the BDCM must be excited with a six-step switched current in order to develop almost constant torque. Figure 1.1 shows a typical phase *a* current excitation waveform for a three-phase BDCM. There is a 120° conduction angle in both positive and negative half-cycle, meaning that in BDCM only two phases are on at a time, which characterizes single-phase operation. The *b* and *c* phase current excitation waveforms are respectively 120° and 240° phase shifted with respect to phase *a*. A PWM technique is then used to control the amplitude of the current wave,

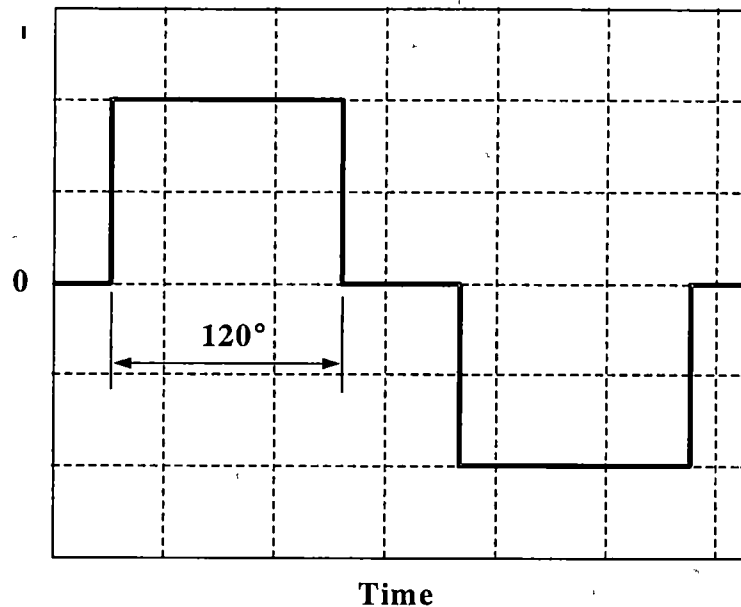


Fig 1 1 Typical phase *a* current excitation for a Brushless DC motor

and consequently control the torque magnitude. The hysteresis band PWM current control is the most accepted PWM control for this type of machine [1]. On the other hand, the PMSM must be excited with a sinusoidal current. Figure 1 2 shows a typical phase *a* current excitation waveform for a three-phase PMSM. Notice that in this type of machine there is 180° conduction angle in both positive and negative half-cycle, i.e., the three phases are on all the time, which characterizes three-phase operation. The *b* and *c* phase current excitation waveforms are respectively 120° and 240° phase shifted with respect to phase *a*. Again, a PWM technique is used to control current amplitude and consequently to control the torque magnitude, and to eliminate the low order harmonics and therefore to make the torque smooth. Among many PWM techniques used for this type of machine are: sinusoidal PWM, hysteresis band PWM

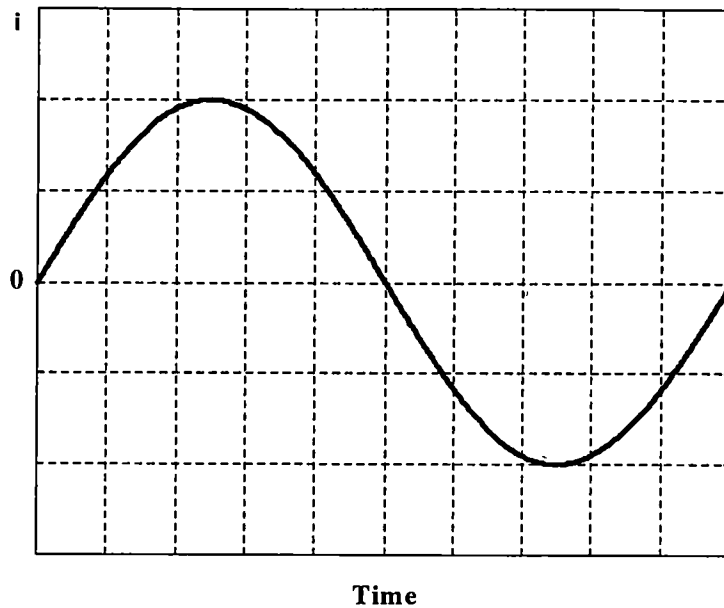


Fig 1 2 Typical phase *a* current excitation for a Permanent Magnet Synchronous Machine

current control, space vector PWM [2]. In both machines, the fundamental switching frequency of the six switches of the inverter will dictate the operation frequency and therefore the rotational frequency (rotor speed)

Another important issue for BDCM and PMSM control is the synchronization between the stator frequency and the rotor frequency. The precision in synchronization is obtained by using the absolute angular position of the rotor. The absolute angular position of the rotor can be obtained through a sensor-based technique, where an absolute angular position sensor is mounted in the machine shaft; or via sensorless technique [5], [6], where estimation algorithms use the machine

terminal voltage and current waveforms as inputs to obtain the rotor position. The difference between BDCM and PMSM in the rotor position requirement comes from the nature of the back-emf shape. In a trapezoidal back-emf, the required rotor position signal is discrete, every 60° interval, which makes the synchronization much simpler and requires less resolution of the rotor position signal. The sinusoidal back-emf on the other hand, requires feedback of a continuous rotor position signal and therefore high resolution in such signal is required.

Although much research is being conducted in order to improve the inverter/machine overall performance, the control of BDCM and PMSM at low speed is well understood [1], [7]. However, in both, BDCM and PMSM, the back-EMF magnitude increases linearly with the rotor speed and consequently after the back-EMF amplitude reaches the same value as the DC link voltage, at so called Base Speed, the current cannot be controlled any longer. Until this point the machine is said to be in the constant torque operation region. At this speed the inverter output voltage has reached its maximum value and so has the machine developed power. From this point on, the machine is said to be operating in constant power range. Unfortunately, the constant power range, without the use of any special control strategy, is very narrow and maximum speed is low if the rated current cannot be exceeded [8]. However, high-speed operation capability is a very important feature especially for electric vehicle applications [9]. Vector control, with so-called field weakening technique (VCFW), can make the constant power speed range wider by introducing a field current component (i_d) in the stator current [10], [11], [12].

However, this technique requires d-q transformation, and although it can readily be applied to sinusoidal back-emf type of machine (PMSM), it cannot be directly applied to the trapezoidal back-emf type (BDCM). Fourier series can be applied to the square-wave in order to decompose it into sine waves and then apply the d-q transformation, but this increases the signal processing complexity [13].

Vector Control of PMSM is well-understood and largely accepted for the operation below base speed. In this operation region, the machine is controlled to operate with optimum torque/ampere ratio. To achieve this operation condition, the field component of the armature current i_d is controlled to be zero, and therefore the armature current is only composed of the torque component i_q . Beyond the base speed, the optimum torque/ampere ratio is no longer a priority. The priority is to accomplish the widest possible constant power operation range. The i_d component is then controlled to be negative and therefore produces flux that weakens the air gap flux, which in the constant torque operation range is only provided by the permanent magnets. However, the flux produced by the i_d current is also proportional to the inductance of the machine, and if the inductance is low, the i_d current must be really large in order to effectively oppose permanent magnet flux. Therefore, in order for the armature current not to exceed the current limit of the drive system, the current i_q must decrease as i_d increases, which makes the developed torque smaller than the torque at the rated power. In other words, in the field weakening technique, the speed range is machine parameter dependent, i. e., the maximum speed is proportional to

the machine inductance, and therefore a low inductance machine will have a low speed limit.

Another technique proposed to overcome the low speed limit is Phase Advance Method (PHA) [14]. This technique was proposed only for BDCM and it is successful only for a high inductance BDCM.

I.2 Objective of the Research

Recently, the Dual Mode Inverter Control (DMIC) [9] has been proposed to drive a BDCM over a wide constant power speed range. This method was shown to be effective in driving both low and high inductance machines. The objective of this work is to analyze the DMIC and to show its feasibility for driving the PMSM. It is also an objective of this work to compare the performances of DMIC and VCFW driving PMSM above the base speed with respect to their constant power operation range widths.

Initially in this work, the PMSM is modeled. In the sequence, the PHA method is analyzed. Simulation results are given and the reasons of its failure driving a low inductance BDCM are pointed out. Then, the DMIC driving a BDCM is addressed. The similarities and differences between this method and PHA are presented. The effectiveness of DMIC/BDCM drive system regarding the width of the constant power operation range is shown through simulation results. The DMIC concept is extended to PMSM machines and simulation results are given. Next,

description, analysis and simulation of the Vector Control (VC) technique with Field Weakening are given. Finally, the explanation of DMIC driving PMSM using dq model of PMSM is given and the derivation of the theoretical limit of the CPSR for the PMSM driven by DMIC is done. Comparison between DMIC and VCFW concerning the capability of driving low inductance PMSM in a wide constant power operation range is also given. The results of this comparison show the superiority of DMIC over VCFW.

CHAPTER II

PERMANENT MAGNET SYNCHRONOUS MACHINE MODELS

II.1 – Introduction

Regarding excitation, Permanent Magnet Machines can be classified into two groups. Trapezoidal back-EMF (BDCM) and sinusoidal back-EMF (PMSM). This difference in the back-EMF waveform dictates a different control strategy for each machine. This work is concerned about the sinusoidal excitation machine control in constant power operation range. Therefore, the objective of this chapter is to present two models for the surface-mounted three-phase PMSM to give theoretical support for the proposed control strategy. First, a three-phase (a, b, c) PMSM model in the stationary reference frame is presented. In sequence, a three-phase in stationary frame to two-phase in the synchronously rotating reference frame transformation is applied, and the two-phase PMSM model in the rotating reference frame is obtained. The importance of these two models lies in the fact that the three-phase model in the stationary frame allows us to show the theory behind the Dual Mode Inverter Control (DMIC) from the converter point of view while the two-phase model allows us to show the theory behind the DMIC from the machine point of view.

II.2 – PMSM three-phase model

Figure 2.1 shows the PMSM three-phase model. Equation 2.1 describes this model [15]

$$\begin{bmatrix} \frac{d\lambda_a(i_{abc}, \theta_r)}{dt} \\ \frac{d\lambda_b(i_{abc}, \theta_r)}{dt} \\ \frac{d\lambda_c(i_{abc}, \theta_r)}{dt} \end{bmatrix} = - \begin{bmatrix} R & 0 & 0 \\ 0 & R & 0 \\ 0 & 0 & R \end{bmatrix} \begin{bmatrix} i_a \\ i_b \\ i_c \end{bmatrix} + \begin{bmatrix} v_{an} \\ v_{bn} \\ v_{cn} \end{bmatrix} \quad (2.1)$$

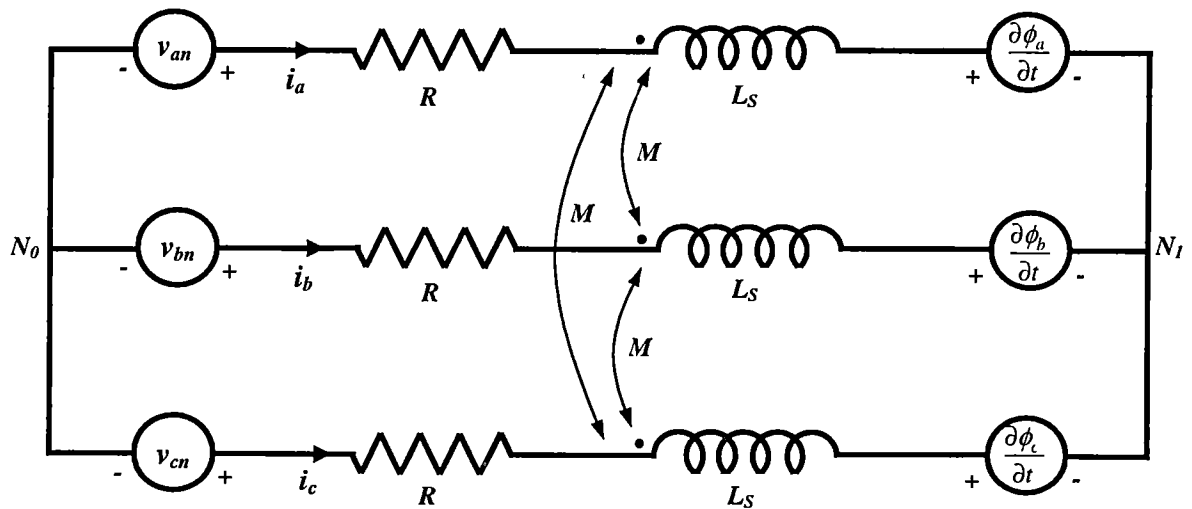


Fig 2.1 PMSM three-phase model

where

λ_{abc} – flux linkages

i_a, i_b, i_c – phase currents

θ_r – rotor position

R – winding resistance per phase

v_{an}, v_{bn}, v_{cn} – terminal phase to neutral voltages

The flux linkages are given by

$$\begin{bmatrix} \lambda_a \\ \lambda_b \\ \lambda_c \end{bmatrix} = \begin{bmatrix} L_s & -M & -M \\ -M & L_s & -M \\ -M & -M & L_s \end{bmatrix} \begin{bmatrix} i_a \\ i_b \\ i_c \end{bmatrix} + \begin{bmatrix} \phi_a \\ \phi_b \\ \phi_c \end{bmatrix} \quad (2.2)$$

where

L_s – Self-inductance per phase

M – Mutual inductance

ϕ_a – phase flux linkages established by the permanent magnets

The phase flux linkages established by the permanent magnets are

$$\begin{bmatrix} \phi_a \\ \phi_b \\ \phi_c \end{bmatrix} = \begin{bmatrix} \phi_m \cos(P\theta_r) \\ \phi_m \cos(P\theta_r - 2\pi/3) \\ \phi_m \cos(P\theta_r - 4\pi/3) \end{bmatrix} \quad (2.3)$$

where

ϕ_m - is the amplitude of the flux linkages established by the permanent magnet

P - number of magnetic pole pairs

Since the neutral points are isolated, the node equation in any of the neutral points N_0 or N_1 is

$$i_a + i_b + i_c = 0 \quad (2.4)$$

Making

$$L = L_s + M \quad (2.5)$$

Then, combining Equations 2.2, 2.3, 2.4 and 2.5, the flux linkage equations become

$$\begin{bmatrix} \lambda_a \\ \lambda_b \\ \lambda_c \end{bmatrix} = \begin{bmatrix} L & 0 & 0 \\ 0 & L & 0 \\ 0 & 0 & L \end{bmatrix} \begin{bmatrix} i_a \\ i_b \\ i_c \end{bmatrix} + \begin{bmatrix} \phi_m \cos(P\theta_r) \\ \phi_m \cos(P\theta_r - 2\pi/3) \\ \phi_m \cos(P\theta_r - 4\pi/3) \end{bmatrix} \quad (2.6)$$

Finally, substituting Equation 2.6 in Equation 2.1 and rearranging it, the phase equations are obtained as given below

$$\begin{bmatrix} v_{an} \\ v_{bn} \\ v_{cn} \end{bmatrix} = \begin{bmatrix} R & 0 & 0 \\ 0 & R & 0 \\ 0 & 0 & R \end{bmatrix} \begin{bmatrix} i_a \\ i_b \\ i_c \end{bmatrix} + \begin{bmatrix} L & 0 & 0 \\ 0 & L & 0 \\ 0 & 0 & L \end{bmatrix} \frac{d}{dt} \begin{bmatrix} i_a \\ i_b \\ i_c \end{bmatrix} - \begin{bmatrix} P\omega_r \phi_m \sin(P\theta_r) \\ P\omega_r \phi_m \sin(P\theta_r - 2\pi/3) \\ P\omega_r \phi_m \sin(P\theta_r - 4\pi/3) \end{bmatrix} \quad (2.7)$$

The relationship between rotor speed ω_r and stator speed ω_e , and rotor position θ_r and stator position θ_e respectively are

$$\omega_r = \frac{\omega_e}{P} \quad \text{and} \quad \theta_r = \frac{\theta_e}{P} \quad (2.8)$$

Equation 2.4 shows that the currents sum to zero, therefore only two of the three equations above are independent and a second order model can be derived.

Equation 2.9 shows the second order model of the PMSM [9].

$$\begin{bmatrix} v_{ab} \\ v_{cb} \end{bmatrix} = \begin{bmatrix} 2R & R \\ R & 2R \end{bmatrix} \begin{bmatrix} i_a \\ i_c \end{bmatrix} + \begin{bmatrix} 2L & L \\ L & 2L \end{bmatrix} \frac{d}{dt} \begin{bmatrix} i_a \\ i_c \end{bmatrix} - \begin{bmatrix} P\omega_r \phi_m \sin(P\theta_r) \\ P\omega_r \phi_m \sin(P\theta_r - 4\pi/3) \end{bmatrix} \quad (2.9)$$

where v_{ab} and v_{cb} are the line-to-line armature voltages

The mechanical dynamics of the PMSM are given by

$$\frac{d\omega_r}{dt} = \frac{(T_e - T_L - B\omega_r)}{J} \quad (2.10)$$

$$\frac{d\theta_r}{dt} = \omega_r \quad (2.11)$$

where

T_e – electromagnetic torque

T_L – load torque

B – damping constant

J – rotor inertia

II.3 – PMSM d-q model

In this section a two-phase model of the PMSM in synchronously rotating reference frame is presented. This model is obtained by applying the Park

Transformation [15] to the three-phase model presented in section 2.1. This transformation is a mathematical tool that maps the three-phase coupled variables in the stator reference frame into three orthogonal (decoupled) variables in any reference frame. In some specific cases, for example, the isolated wye connected PMSM, one of the three orthogonal components becomes zero, and therefore the transformation becomes a three to two phase transformation. It is convenient to choose the synchronous frame as the new reference frame because the sinusoidal three-phase variables of the stationary frame become DC quantities and this makes the analysis simpler.

Equation 2.12 shows a transformation matrix that maps three-phase variables in stationary frame to three-phase variables in any other reference frame.

$$\begin{bmatrix} f_q \\ f_d \\ f_0 \end{bmatrix} = \frac{2}{3} \begin{bmatrix} \cos \theta & \cos(\theta - 2\pi/3) & \cos(\theta + 2\pi/3) \\ \sin \theta & \sin(\theta - 2\pi/3) & \sin(\theta + 2\pi/3) \\ 1/2 & 1/2 & 1/2 \end{bmatrix} \begin{bmatrix} f_{an} \\ f_{bn} \\ f_{cn} \end{bmatrix} \quad (2.12)$$

In this transformation, f is the variable that undergoes transformation. The variables f_{an} , f_{bn} , and f_{cn} are the phase variables in stationary frame. The variables f_d , f_q , and f_0 are variables in the new reference frame. Figure 2.2 shows the phasor diagram illustrating the abc and dq reference frames. The three new axes quadrature (q), direct (d) and zero sequence component (0) are simultaneously orthogonal, where

q -axis and d -axis are in the same plane as a_n , b_n and c_n axis while 0 axis is perpendicular to that plane. If the sum of f_{a_n} , f_{b_n} , and f_{c_n} is zero, then the 0 -axis component is zero and the transformation becomes a three-phase to two-phase transformation. In Equation 2.12, the angle θ represents the angle between the q -axis and the a_n -axis as shown in the phasor diagram in Figure 2.2.

As noted above, the transformation given in 2.12 is a generic transformation, i.e., it maps variables from the stationary frame to a new reference frame, which is displaced by θ , and $\theta - \pi/3$ angles from that of the old frame. The new reference frame is defined by the value of θ . For instance, if the angle θ is made constant and is equal to zero, then the two-phase machine model is in the stationary frame. If the angle θ varies at the rate of the synchronous speed, then the two-phase machine model is in the synchronously rotating frame.

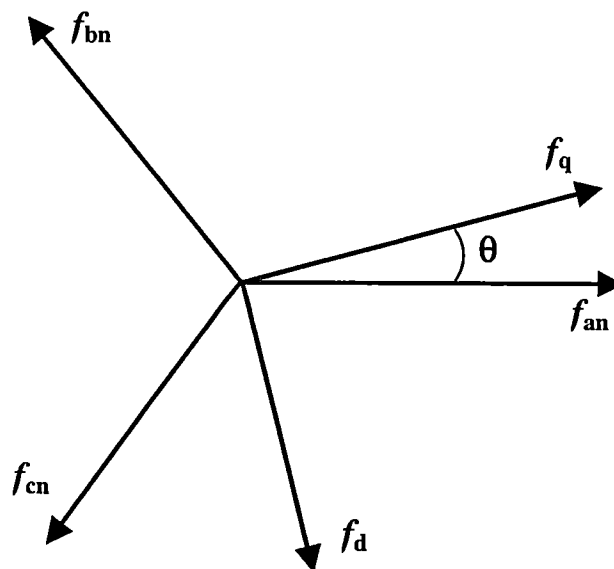


Fig 2.2 Phasor diagram showing abc and dq reference frames

The two-phase machine model at the synchronously rotating frame is obtained by applying the transformation given by Equation 2.12, in the three-phase model at the stationary rotating frame with $\theta = \omega_e t$. The two-phase machine model in synchronously rotating frame is then given by Equation 2.13

$$\begin{bmatrix} v_q \\ v_d \end{bmatrix} = \begin{bmatrix} P\omega_r L & R + L \frac{d}{dt} \\ R + L \frac{d}{dt} & P\omega_r L \end{bmatrix} \begin{bmatrix} i_d \\ i_q \end{bmatrix} + \begin{bmatrix} P\omega_r \phi_m \\ 0 \end{bmatrix} = \begin{bmatrix} P\omega_r L & R + L \frac{d}{dt} \\ R + L \frac{d}{dt} & P\omega_r L \end{bmatrix} \begin{bmatrix} i_d \\ i_q \end{bmatrix} + \begin{bmatrix} e \\ 0 \end{bmatrix} \quad (2.13)$$

where e is the back-emf

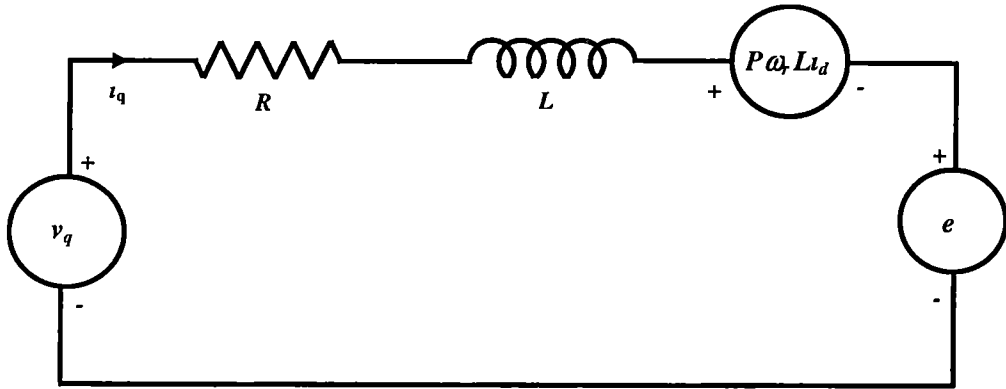
Notice that this is a model for a surface mounted permanent magnet machine, and therefore the direct-axis inductance and the quadrature-axis inductance are equal and their value is equal to the sum of the self-inductance per phase L_s and the mutual inductance M , i.e., the same as given in Equation 2.5

Neglecting rotational losses, the electromagnetic torque is then given by

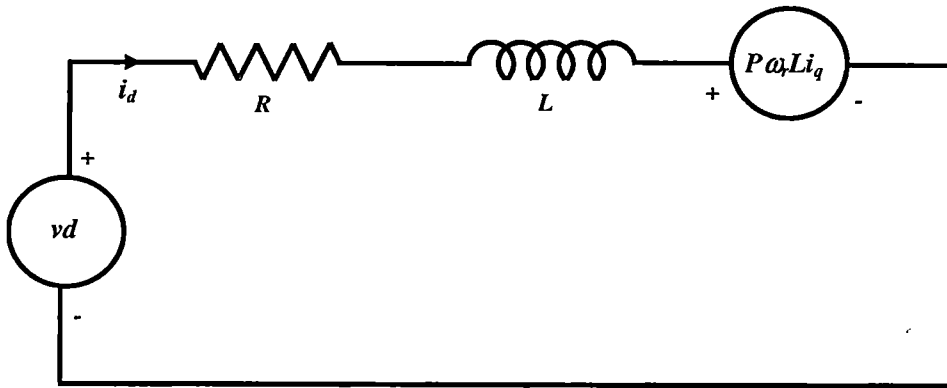
$$T_e = \frac{3}{2} P \phi_m i_q \quad (2.14)$$

The mechanical variables do not undergo transformation, therefore the mechanical dynamics are the same as given in Equations 2.9 and 2.10.

Figure 2.3 shows the two-phase machine model in the synchronously rotating frame



(a) q-axis equivalent circuit



(b) d-axis equivalent circuit

Fig 2 3 d-q equivalent circuit in synchronously rotating frame (I)

II.4 – Conclusions

This chapter presented the three-phase model of PMSM in the stationary reference frame and the dq model of PMSM in the rotating reference frame. The three-phase model of PMSM will be used in the next chapter to help describe DMIC driving a PMSM. The d-q model of PMSM will be used to describe and to analyze vector control with field weakening of PMSM in Chapter IV, and also to explain why DMIC works in Chapter V.

CHAPTER III

DUAL MODE INVERTER CONTROL

III.1 – Introduction

As discussed in Chapter 1, the problem in driving a permanent magnet machine above base speed is that the back-emf increases above the DC bus voltage and therefore no current can be driven into the machine. If current is not driven into the machine, no electrical to mechanical energy conversion is possible. Therefore, the target of any scheme to drive this type of machine above base speed is to find a way to drive current into the machine in order to make the electrical to mechanical energy conversion.

The Dual Mode Inverter Control (DMIC) is a control technique that allows operation of the Permanent Magnetic Machine over a wide constant power speed range. This technique was proposed by *Lawler et al.* [9] and is well described to drive a Brushless DC motor (BDCM). However it seems to be feasible for Permanent Magnet Synchronous Machine (PMSM) as well. The aim of this chapter is to describe the DMIC and to show its effectiveness driving a PMSM. Initially, Phase Advanced Method (PHA) driving a BDCM is described and simulation results are given. The description of PHA and the analysis of its drawbacks help to explain the DMIC strategy. In the sequence, DMIC driving BDCM is described and simulated. The

performances of PHA and DMIC driving a BDCM regarding their capability of driving low inductance BDCM without exceeding the current limit, are analyzed and compared. Then the concept of DMIC is extended to PMSM, and finally some simulation results are given showing its feasibility

III.2 – PHA driving a BDCM

The so-called Phase Advanced Method [14] was developed to drive a BDCM over a wide constant power operation region (CPSR). This technique uses a standard voltage-fed inverter topology as shown in Figure 3 1

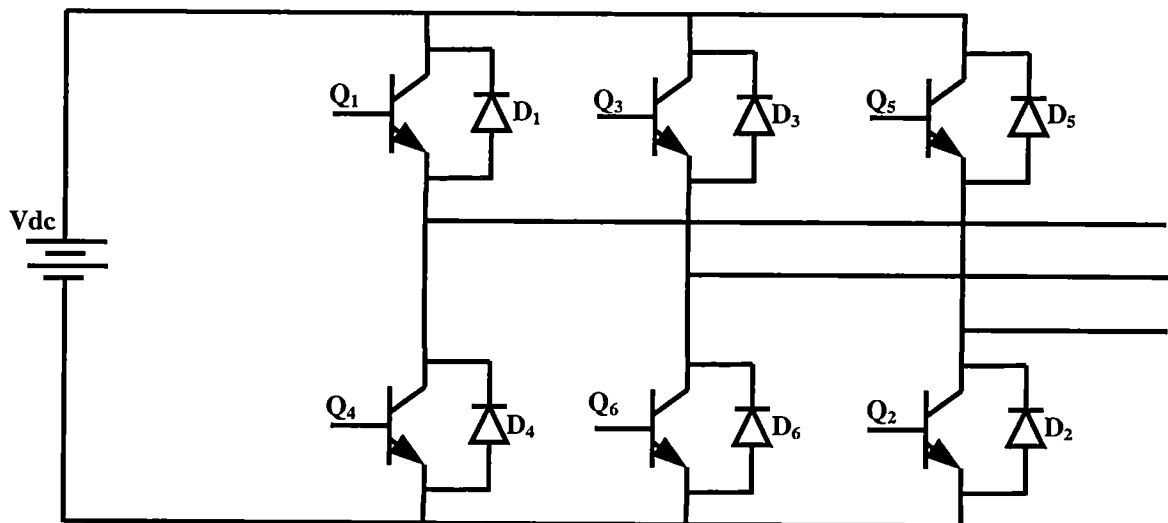


Fig 3 1 Standard VFI [14]

Figure 3.2 shows typical gate signals to fire the transistors Q_1 and Q_4 in the PHA method. The back-emf for phase a (e_{an}) is also shown in this figure. The transistor control pulses are θ_a radians ahead of the instant that phase to neutral back-emf e_{an} reaches its maximum value. The angle θ_a is called Advance Angle and is defined as the angle between the instant that a transistor is turned on and the point where the phase to neutral back-emf related to that transistor reaches its maximum. For instance, Figure 3.2 shows the advanced angle between the instant that the transistor Q_1 is turned on and the instant that phase to neutral back-emf e_{an} reaches its maximum positive value. This figure also shows the advance angle for the transistor Q_4 and the time that e_{an} reaches its minimum. The gate signals for the transistor in phase b and c are similar to those for phase a, the difference is 120° and 240° delay for phases b and c respectively. The pulse width of each transistor is 120° .

Below base speed, θ_a is zero and the power driven into the machine (developed torque) is controlled by any PWM method, such as hysteresis current control. However as the speed increases toward the base speed, the PWM controllers start to saturate, meaning that the current cannot be controlled anymore since the back-emf has reached the same value as the DC bus voltage. In other words, current cannot be driven into the machine any longer. The Phase Advance Method uses the fact that during transition from the negative flat portion of back-emf to its positive flat portion, and vice-versa, the back-emf assumes values that are momentarily smaller than DC bus voltage in absolute value. Therefore, the PHA technique makes the

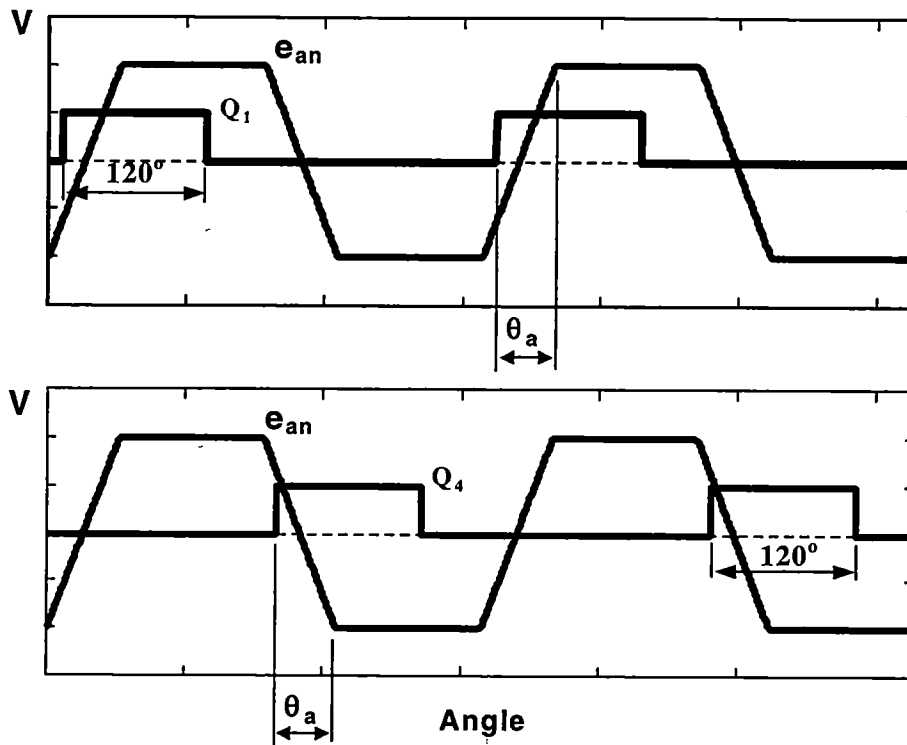


Fig. 3.2 Gate signal for Q_1 and Q_4 in the phase advance method [14]

advance angle different from zero, i.e., the transistors are fired while the back emf is smaller than V_{dc} , and during this time a large amount of current can be driven into the machine and power can be developed. This technique has two main drawbacks: first, the current increases too much and its overall performance is poor. The second is the negative current that passes through the bypass diodes, caused by the high value that the back-emf assumes at high speed. At this point the voltage is positive and the current is negative, i.e., during this time the power is flowing back from the machine to the power supply. Therefore, the three phases will be conducting all the time, and the machine loses the single-phase operation mode that it had below base speed. The

problem with that is that each phase will be operating in both motoring and regenerating mode. Therefore, for a low inductance machine, the motoring and regenerating currents must be much larger than the rated current in order to develop rated motoring power.

As an example of the PHA performance, consider inverter/machine system parameters given in Table 3.1.

The system described in Table 3.1 operating at 5 times base speed $\left(n = \frac{N_r}{N_{rb}} = 5 \right)$,

Table 3.1 Drive system parameters

DC-link voltage	162 V
Brushless DC motor	$P_{\text{rated}} = 49.5 \text{ hp (36,927 Watts)}$, 12-pole, ORNL Base Speed: $N_b = 2600 \text{ rpm}$ Base frequency: $f_b = 260 \text{ Hz}$ Peak phase-to-neutral back-emf at base speed $E_b = 74.2 \text{ V}$ Stator resistance: $R_s = 0.0118 \Omega$ Stator inductance: $L_s = 61.8 \mu\text{H}$ Stator mutual inductance: $M = 11.8 \mu\text{H}$ Rated peak current: $I_{\text{rated (peak)}} = 249 \text{ A}$ Rated rms current: $I_{\text{rated (rms)}} = 203.3 \text{ A}$

using the PHA method results in current waves given in Figure 3.3. Instantaneous total power, power developed in phase *a*, power flowing through phase *a* transistors, and power flowing through phase *a* diodes are given in Figure 3.4. Notice that in order to develop the rated power, the phase *a* current peak is close to 900 A and the rms current is around 600 A, while the rated peak and rms currents are 249 A and 203.3 A respectively. From Figure 3.4, one can see clearly that during certain period of time the machine is regenerating, and therefore much more motoring power must flow to the machine in order for the net power/cycle to be the motoring rated power. In other words, the system is operating in a very low power factor.

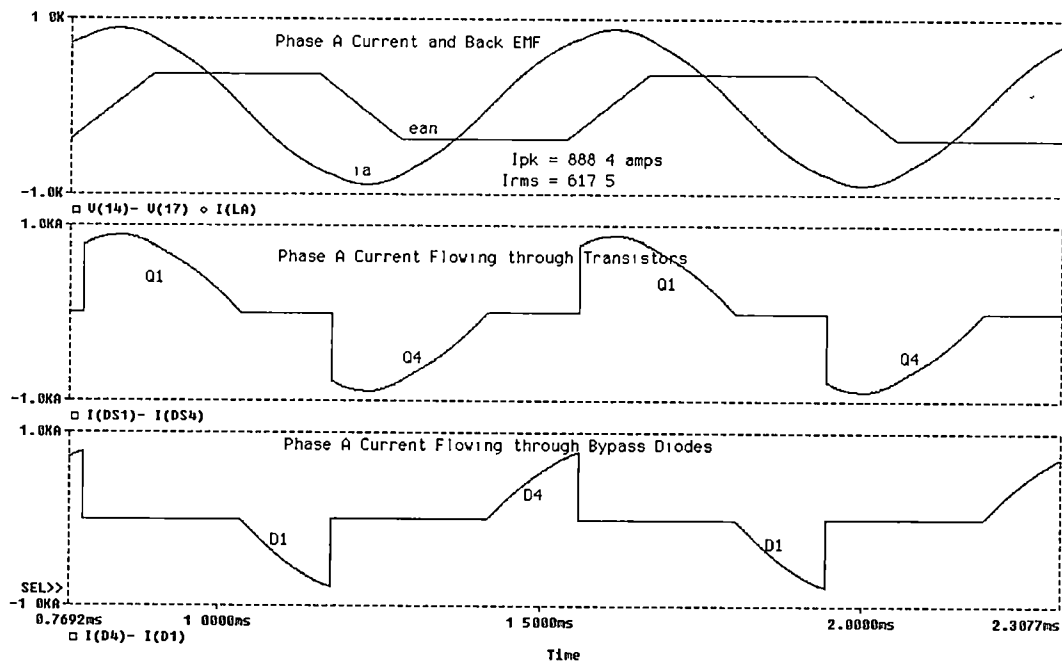


Fig. 3.3 Current in phase *a*, transistor Q_1 and Diode D_1 for $n=5$ and $\theta_a = 50^\circ$

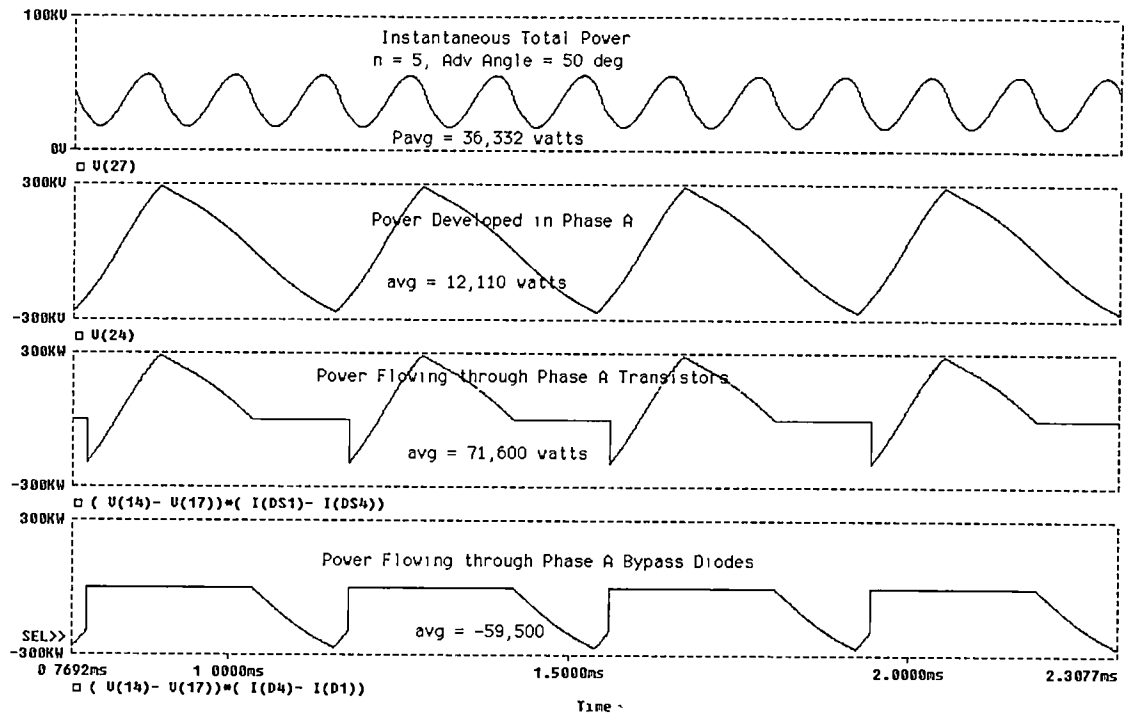


Fig 3 4 Instantaneous total power, phase *a* power, and power flowing through the phase *a* transistors and diodes for $n=5$ and $\theta_a = 50^\circ$

The increase in current causes two problems. First, the switching device current ratings must be increased. The second problem is related to electrical losses, which are proportional to the square of the current, i.e., a substantial increase in the current will lead to an even more substantial increase in the electrical losses. These are the two main facts that make the PHA method not viable for low inductance BDCMs.

The performance of the PHA can be improved if a high inductance BDCM is used. If only a low inductance machine is available, then external inductances can be

inserted in series with the BDCM, but this will require increases of the V_{dc} because of the voltage drop in the external inductances, and it will also make the whole system bulky. Because of the voltage level sensitivity of the PHA method, its application for electrical vehicles is difficult

III.3 – DMIC driving a BDCM

The PHA method described in the previous section is not effective in driving a low inductance BDCM in the high speed, constant power range. The main problem with this method is the bypass diodes of the conventional VFI. Below base speed the voltage potential of the idling phase voltage is always smaller in absolute value than the positive or negative rails of the dc supply. Therefore, after the commutation period, the bypass diodes are reverse biased, and the transistors as well as the bypass diodes in the idling phase are off, which configures a single-phase operation. However, above base speed the voltage potential of the idling phase is greater in absolute value than either the positive rail or the negative rail of the dc supply. Consequently, the bypass diodes in the idling phase are forward biased. As a result, there is not an idling phase at any time, i.e., each phase current in the motor is contributing both motoring and regenerating power. If the motor inductance is low, then the current magnitude for both motoring and regenerating components are much larger than the rated current.

The DMIC controller works in the direction of avoiding the forward biasing of the bypass diodes [9], i.e., keeping the single-phase operation of the BDCM also above base speed. In order to achieve that, the converter configuration as well as the control (firing scheme) is different from those of the PHA controller. Figure 3.5 shows the inverter topology used by the DMIC.

The configuration of the converter in DMIC method is basically a standard VFI, connected to a thyristor-based ac voltage controller. The output of the thyristor-based ac voltage controller is then connected to the BDCM. The principal function of the thyristor-based ac voltage controller is to avoid the forward biasing of the bypass

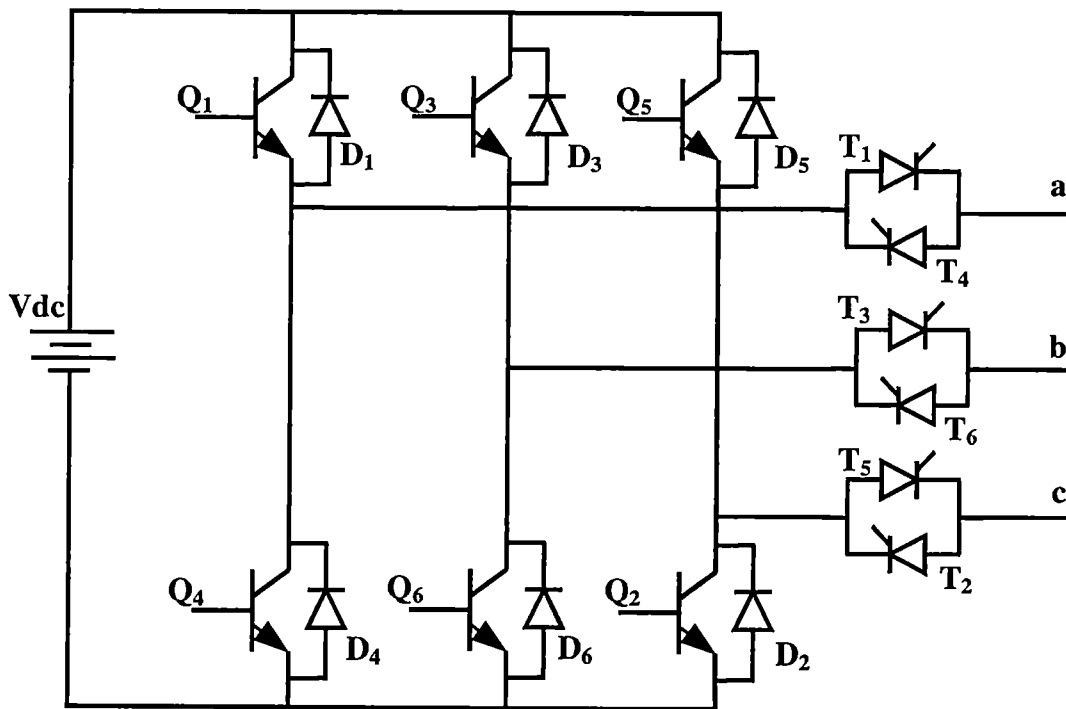


Fig. 3.5 Inverter Topology for the DMIC [9]

diodes, i.e., once the phase currents in the outgoing phase reach zero, the thyristor shuts off independent of the voltage potential of this phase. Therefore, there will be no regeneration through this phase, and the single-phase operation of the BDCM is assured.

Figure 3.6 shows the firing scheme for the motoring mode of the DMIC. The gate signals to fire the switches in phase a , i.e., transistors Q_1 and Q_4 , and thyristors T_1 and T_4 , are shown

Notice that in the DMIC a firing sequence is required for both transistors and thyristors. The firing sequence is similar to the sequence for PHA method, but the advance angle is defined relative to phase-to-phase back emf and dc supply voltage crossing point. In contrast to the PHA method, where each transistor always conducts 120° , in the DMIC the transistor conduction interval can vary from 120° to 180° . The conduction interval is controlled by the blanking angle θ_b . The main reason to use a variable conduction interval is to maximize the electrical to mechanical power conversion above base speed. This maximization is achieved because during the commutation time, the phase current in the outgoing phase may be large, but decreasing in magnitude because the back-emf is now higher than V_{dc} . But, although the phase current is decreasing, it is contributing in a large amount to motoring power (both, high current and voltage have the same sign). If the transistor is turned off, i.e. $\theta_b=60^\circ$, the current of the outgoing phase will commutate to the bypass diode of the opposite transistor and the opposite rail voltage will then be applied to the machine.

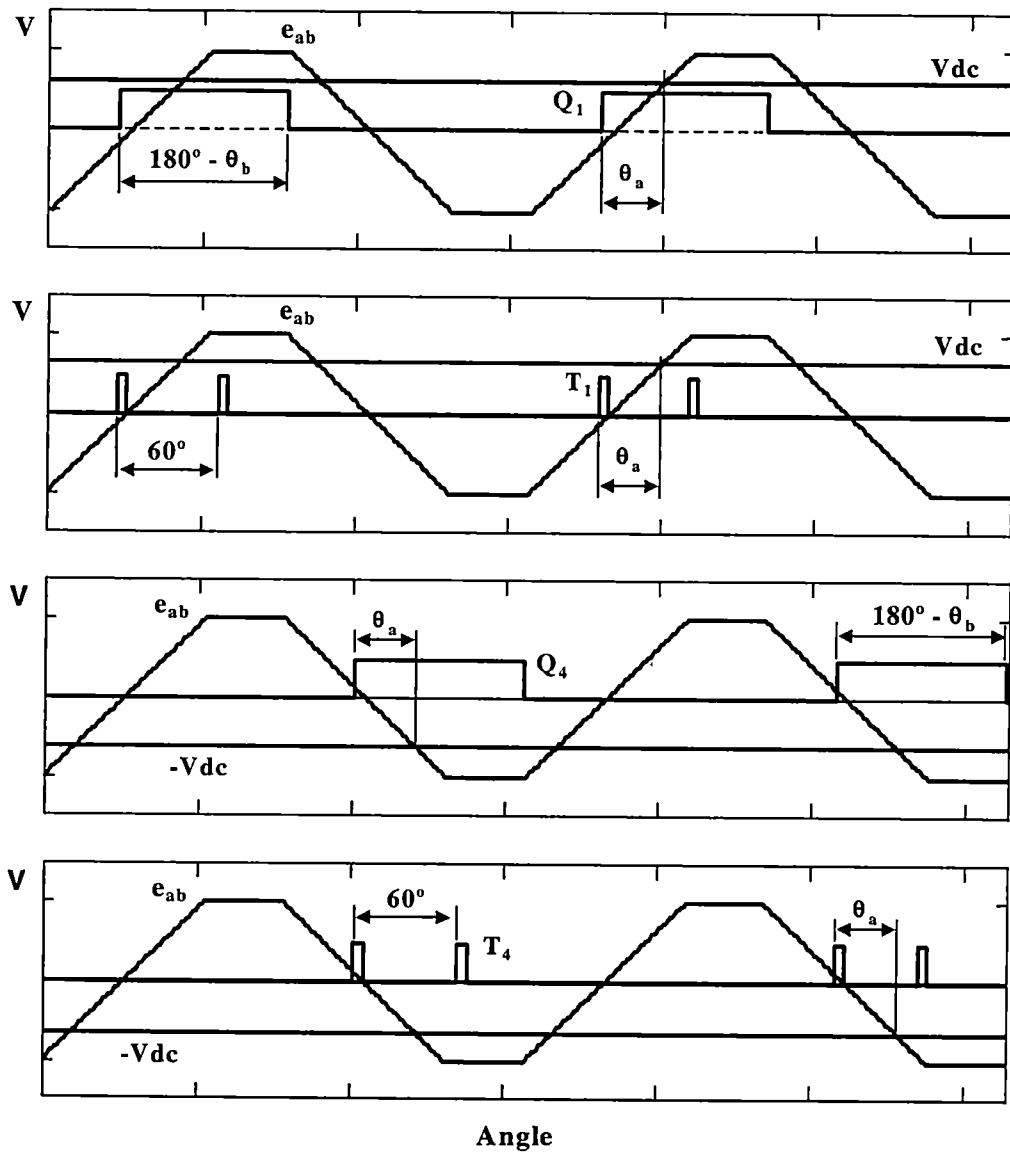


Fig 3.6 Firing scheme for motoring mode of DMIC driving a BDCM [9]

This commutation will make the voltage difference between the machine back-emf and the inverter voltage higher, and therefore current will decrease very fast. If the transistor is allowed to be on for a long period, i.e. $\theta_b < 60^\circ$, the same rail voltage will be applied to the machine, the voltage difference between the machine back-emf and the inverter voltage will be lower, and as a result, the phase current will decrease slower. Therefore, the period with high voltage and high current will be enlarged and the outgoing phase will contribute to the electrical to mechanical power conversion longer, increasing the overall performance of the system at a few rms amperes increasing cost. However, it is very important that at speeds slightly above base speed that the blanking angle does not decrease to very small values. At these speeds the back-emf is slightly bigger than V_{dc} and if the blanking angle is too small a commutation failure may occur, i.e., the current may not reach zero and commutation will not happen.

In order to compare DMIC with the PHA, the same drive system (Table 3.1) was simulated using DMIC at 5 times the base speed ($n=5$). Figure 3.7 shows the phase *a* current, phase *a* back-emf, current flowing through the transistors in phase *a*, and current flowing through the bypass diodes in phase *a*. Notice that in order to develop the rated power the phase *a* current peak is 271 A and the rms current is 191.6 A, while the rated peak and rms currents are 249 A and 203.3 respectively. The current through the diode is zero, i.e., the period with regenerating power was effectively avoided by the ac-voltage controller. Instantaneous total power and power developed in phase *a* are given in Figure 3.8.

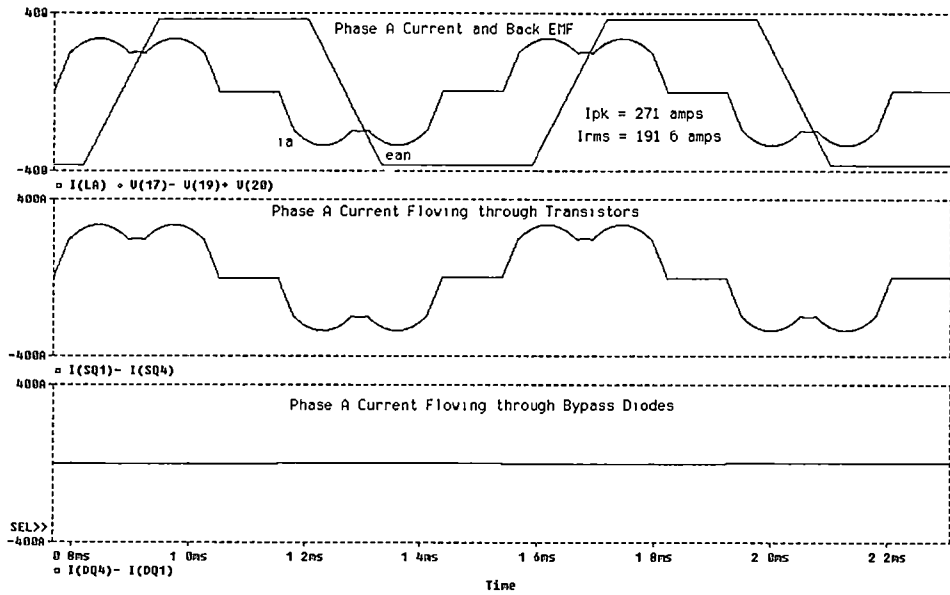


Fig 3.7 Current in phase a, transistor Q_1 and Q_4 and Diode D_1 and D_4

for $n=5$, $\theta_a = 36.6^\circ$, $\theta_b = 20^\circ$

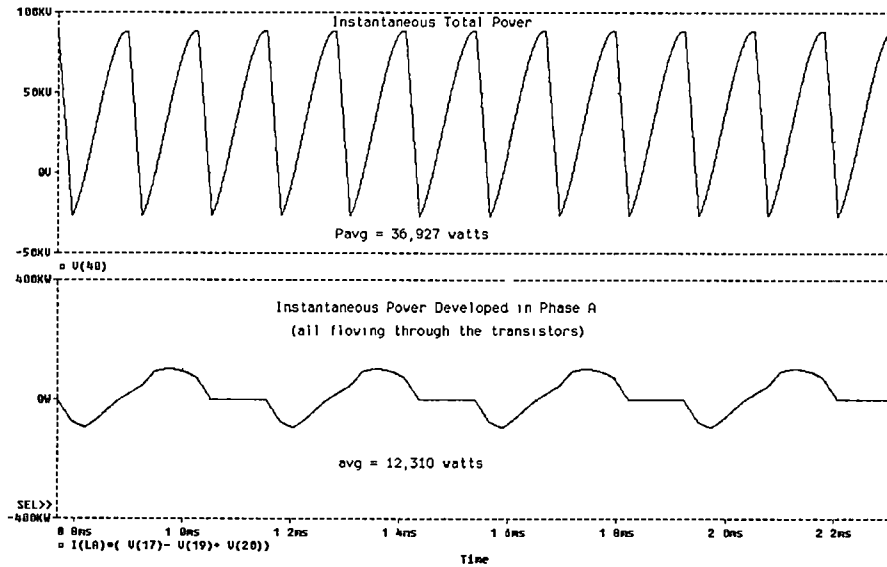


Fig. 3.8 Instantaneous total power, phase a power (transistors) for $n=5$, $\theta_a = 36.6^\circ$, θ_b

$= 20^\circ$

III.4 – DMIC driving a PMSM

In Section III 3, DMIC was proven to be effective driving a low inductance BDCM. It was shown in the previous section that three factors are vital for the DMIC effectiveness, two are related to the firing scheme and one is related to the inverter topology. The first related to the firing scheme is the advance angle, which allows current to be driven into the machine during the time the phase back-emf is smaller than DC link voltage V_{dc} . The second related to the firing scheme is the blanking angle, which maximizes the power conversion process by increasing the on time of the transistors and therefore slowing the rate of decrease of the current in the outgoing phase. The factor related to the inverter topology is the reversed blocking capability given by ac-voltage controller, which is used to avoid the regeneration when motoring is desired.

The aim of this section is to show that the same principle can be applied to Permanent Magnet Synchronous Machine (PMSM), which has sinusoidal back-emf, rather than trapezoidal back-emf like the BDCM. The biggest difference between these two machines, from the drive point of view, is that the BDCM operates at single-phase (120° conduction) below base speed and the PMSM operates at three-phase (180° conduction). Therefore, the DMIC philosophy for PMSM will be different than for the BDCM. The DMIC method keeps the single-phase operation (less than 180° conduction) also above base speed for BDCM. However, for PMSM,

the DMIC will change the three-phase operation below base speed to single-phase (less than 180° conduction) operation above base speed

The inverter topology for DMIC driving a PMSM is identical to that one driving the BDCM and is given in Figure 3.5. The firing scheme for DMIC driving a PMSM is given in Figure 3.9. The gate signals to fire the switches in phase a , i.e., transistors Q_1 and Q_4 , and thyristors T_1 and T_4 , are shown. In this scheme, as in DMIC driving a BDCM, the advance angle θ_a is measured relative to the phase-to-phase back-emf and DC supply voltage crossing point. The conduction angle starts at 180° at base speed, and slowly decreases toward 120° in such a way that the single-phase operation is reached and commutation failure is avoided. This control is made possible by controlling the blanking angle θ_b . The thyristor-based AC-voltage controller interfaces the standard VFI and the PMSM. Therefore, by shutting off as the current reaches zero, the thyristors avoid the current reversal and the resultant regeneration that occurs due to bypass diode conduction.

The DMIC/PMSM system was simulated in order to evaluate the DMIC efficacy driving a PMSM. The system is the same as the one given in Table 3.1. However, the machine is a PMSM, i.e., a sinusoidal back-emf type of machine, therefore, considering the same peak phase-to-neutral back-emf at base speed ($E_b=74.2$ volts), the equivalent rated power is 31,980 W and the rms current is 176 A. The machine simulated was then a PMSM, but with the same parameters for the BDCM as given in Table 3.1. The system was simulated at 5 times the base speed

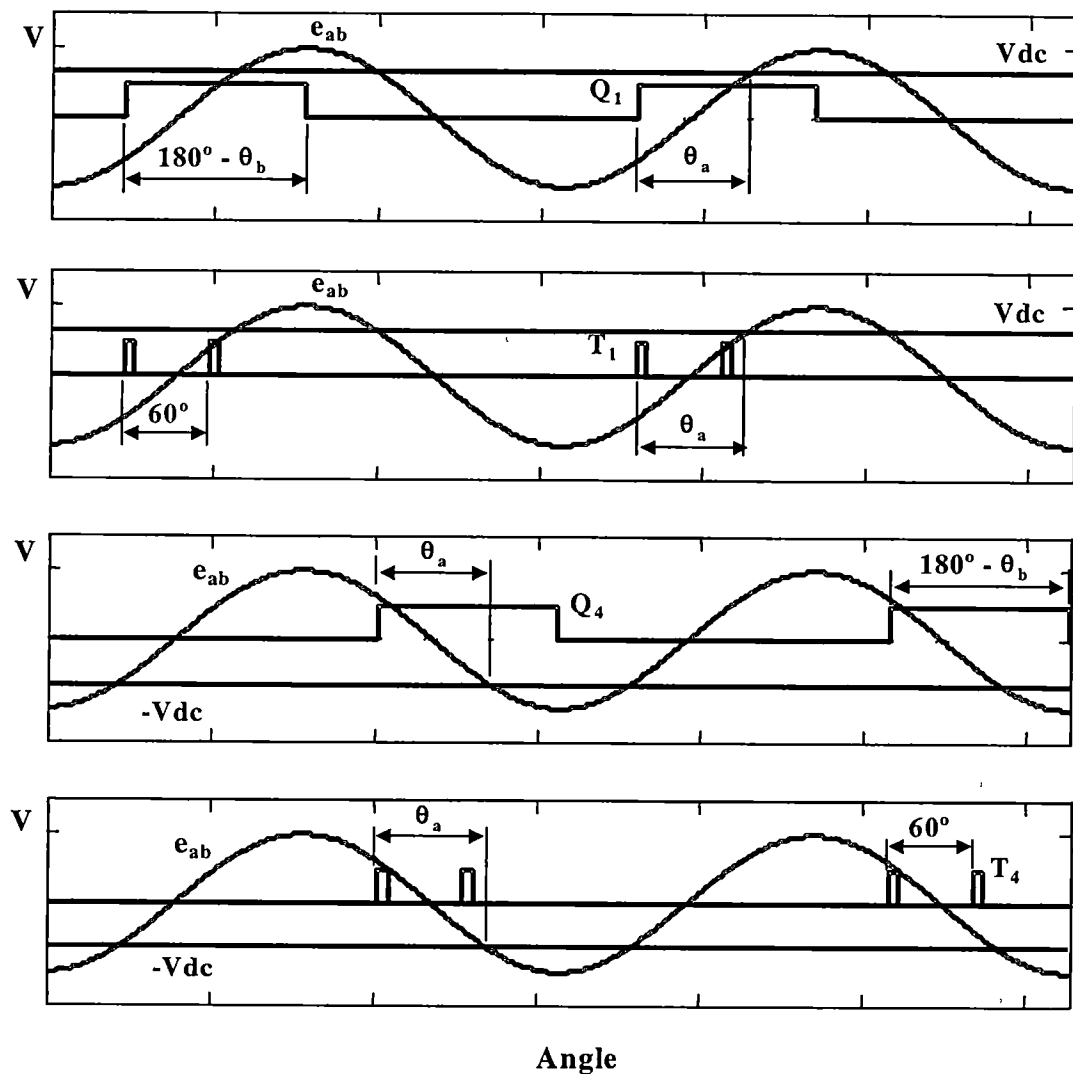


Fig 3 9 Firing scheme for motoring mode of DMIC driving a PMSM

($n=5$) Figure 3.10 shows the phase a current, phase a back-emf, current flowing through the transistors in phase a , and current flowing through the bypass diodes in phase a . Notice that in order to develop 36,800 W the phase a current peak is 277.7 A and the rms current is 187 A, while the rated peak and rms currents are 249 A and 176 A respectively. Therefore, the machine developed 15% more power at a cost of 11% and 6% more current than the rated peak and rms currents respectively. The current through the diode is zero, i.e., the period with regenerating power was effectively avoided by the ac-voltage controller. Instantaneous total power and power developed in phase a are given in Figure 3.11. However, the pulsating torque, which follows the pulsating power, is high, but it will be filtered out by the load/machine inertia.

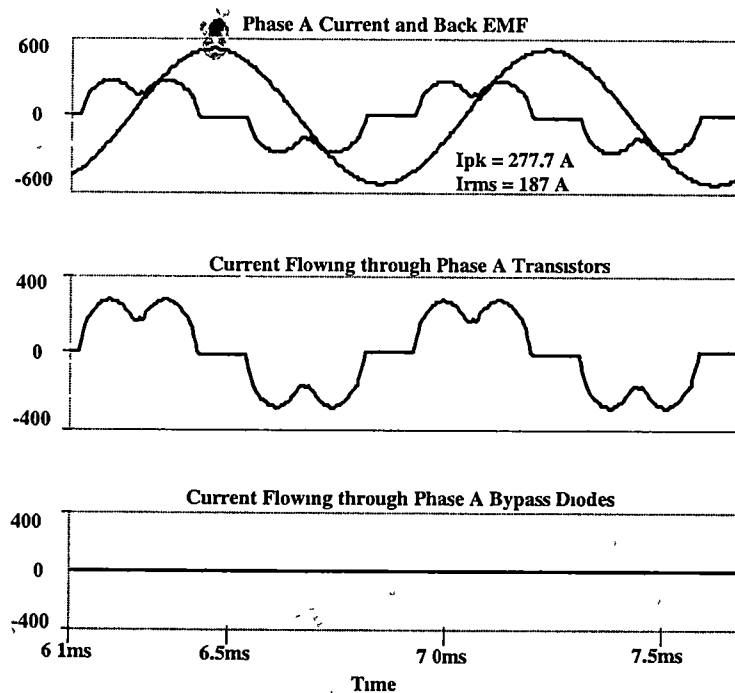


Fig. 3.10 Current in phase a , transistor Q_1 and Diode D_1 for $n=5$, $\theta_a = 42^\circ$, $\theta_b = 20^\circ$

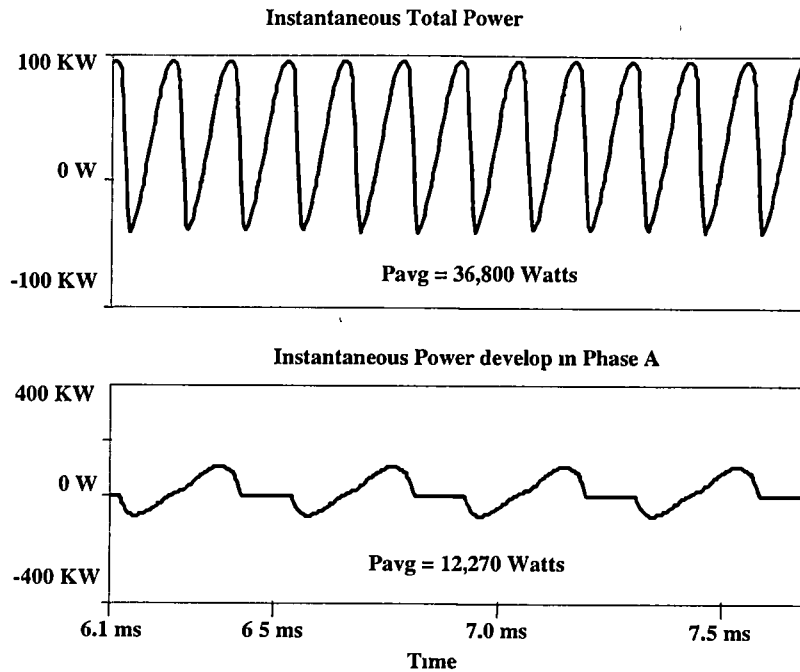


Fig. 3 11 Instantaneous total power, phase *a* power (all flowing through the transistors) for $n=5$, $\theta_a = 42^\circ$, $\theta_b = 20^\circ$

III.5 – Conclusion

The Phase Advance Angle (PHA) method driving a BDCM was described, and its inefficiency for low inductance machine was shown. The deficiency of this method was pointed out as being the conduction of the bypass diodes, which allowed regeneration when motoring action was desired. In sequence, the DMIC driving a BDCM was presented. The DMIC principle was then described. The main differences between DMIC and PHA were highlighted. It was discussed that the DMIC method is more effective in driving a low inductance BDCM mainly because of its capability of

CHAPTER IV

FIELD WEAKENING TECHNIQUE FOR PMSM

IV.1 - Introduction

The Vector Control (VC) technique is used to achieve DC machine like performance/dynamic response in AC machines [16], [17], [18]. In a DC machine, the field current and the armature (torque) current are orthogonal and therefore decoupled. In other words, the currents can be controlled independently, without one affecting the other. This decoupling allows fast dynamic response for DC machines.

The theory behind VC of AC machines relies on the dq-model of these machines. Therefore, the dq model of the PMSM will be used in order to describe the VC of PMSM. As discussed in chapter 2, the dq model of the PMSM leads to two equivalent electric circuits: the q-axis equivalent circuit and the d-axis equivalent circuit. The current i_q , in the q-axis equivalent circuit is the torque component of the stator current, and is analogous to the armature current in a DC machine. The current i_d , in the d-axis equivalent circuit is the field component of the stator current, and is analogous to the field current in a DC machine. In VC applications, these two current components are controlled independently, i.e., one control loop controls the torque component of the armature current and another controls the field component of the armature current.

The objective of this chapter is to review VC of PMSM. Initially the machine voltage equations are given and analyzed. The analysis of these equations is helpful to understand the effect of i_d and i_q in the machine. Then, the analysis of the machine operation regarding the current and voltage limits is given. This analysis allows understanding of how the current and voltage constraints define the range of the constant torque and constant power operation regions. Moreover, this analysis reveals the best strategy to control the i_d and i_q currents in order to make the constant power operation range as wide as possible. Finally, the PMSM drive system with VC that operates in both, constant torque and constant power operation regions is given and carefully described. Simulation results of this system are also given.

IV.2 - Vector Control of PMSM

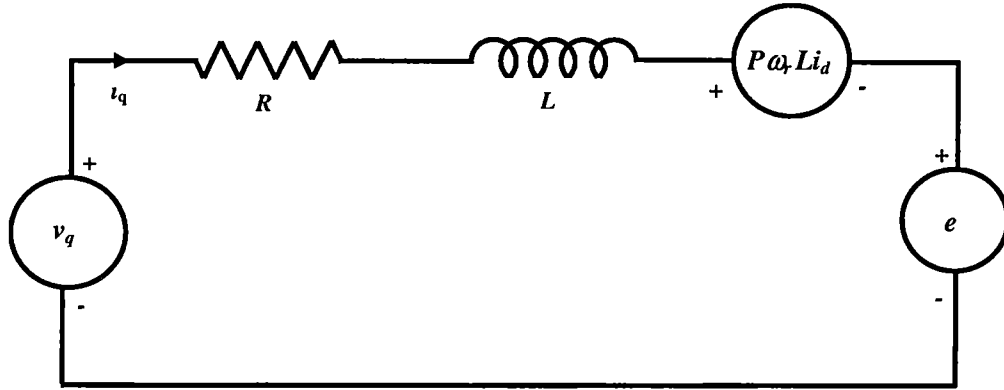
The Vector Control Technique uses the d-q model of the PMSM shown in Figure 4.1 (same as Figure 2.3).

The voltage equation for q-axis equivalent circuit is

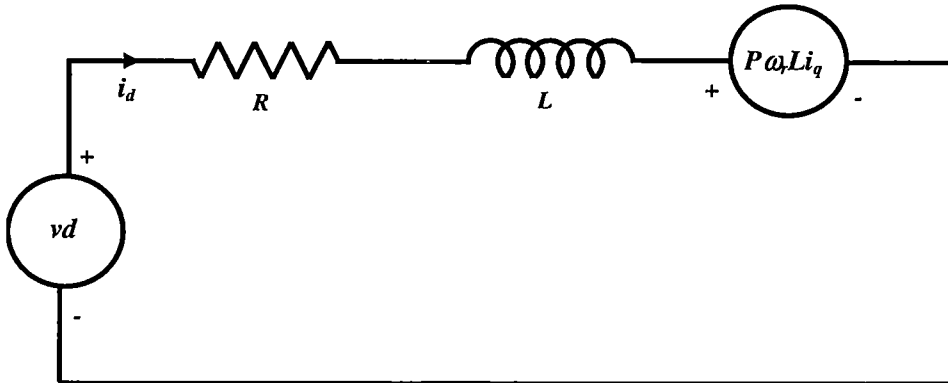
$$v_q = P\omega_r L i_d + R i_q + L \frac{di_q}{dt} + P\omega_r \phi_m = P\omega_r L i_d + R i_q + L \frac{di_q}{dt} + e \quad (4.1)$$

where

e - the back-emf, which is proportional to the speed ω_r and the rotor magnet flux ϕ_m ($e = P\omega_r \phi_m$)



(a) q-axis equivalent circuit



(b) d-axis equivalent circuit

Fig 4 1 d-q equivalent circuit in synchronously rotating frame (II)

$$\omega_r = \frac{\omega_e}{P} \text{ - rotor speed}$$

P – number of pole pairs

$$L = L_s + M$$

The voltage equation for *d*-axis equivalent circuit is

$$v_d = R i_d + L \frac{di_d}{dt} + P \omega_r L i_q \quad (4.2)$$

Figure 4.2 shows the phasor diagram representing the above equations. The *d*-axis is aligned with the rotor magnet flux ϕ_m .

The electromagnetic torque is then given by.

$$T_e = \frac{3}{2} P \phi_m i_q \quad (4.3)$$

As shown in Equation 4.3, the electromagnetic torque is proportional to the magnet flux ϕ_m and to the quadrature component of the stator current i_q .

In a PMSM, the field is provided by the permanent magnets and is constant; therefore no field component of the armature current is required. However, because the field is constant, as the rotor speed increases, the back-emf also increases, which makes it difficult to have electrical to mechanical power conversion with acceptable

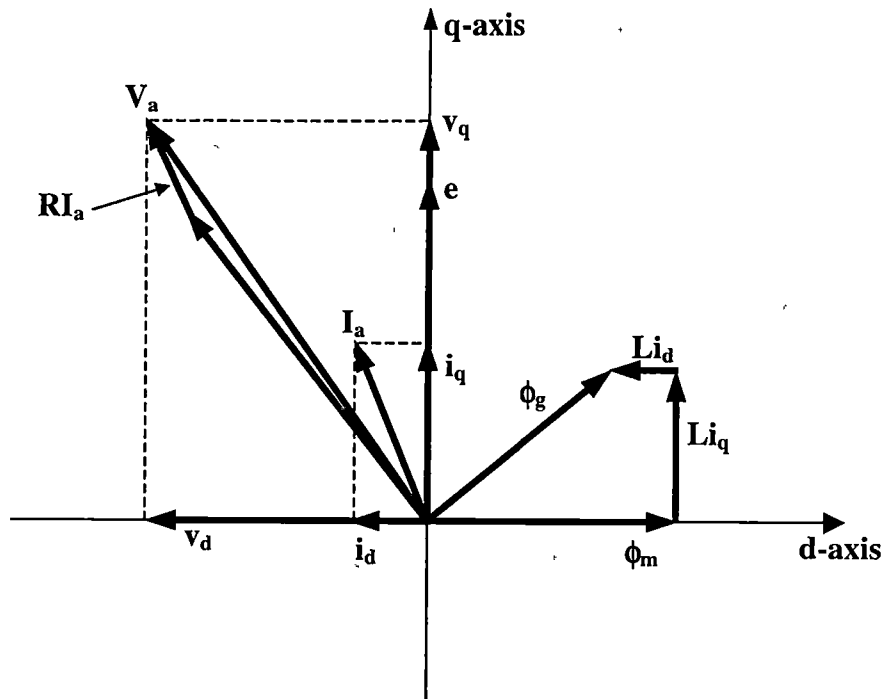


Fig. 4 2 Phasor diagram showing the variables of the d-q model of the PMSM

current level above a certain speed level. Therefore, the control of PMSM must be divided into two operation regions: Constant Torque Operation Region (CTOR) and Constant Power Operation Region (CPOR).

The constant torque operation region is defined as the region where the back-emf is lower or equal to the maximum output voltage that can be provided by the inverter and the DC link voltage. The speed at the end of this operation region, i.e. where the back-emf is equal to the maximum voltage provided by the inverter, is called Base Speed (ω_{tb}). Within this region the machine can provide up to rated torque, at any speed. In order to achieve optimum torque/ampere in this region, the

field component of the armature current i_d is held at zero, and the torque component of the armature current i_q is controlled according to the desired torque [19], [20], [21].

The idea behind vector control of the PMSM, which was qualitatively described above, can be easily understood by analyzing Equations 4.1, 4.2 and 4.3. In steady state, if optimum torque/current ratio is desired, then i_d is held at zero, and Equations 4.1, 4.2 and 4.3 become

$$v_q = R i_q + P \omega_r \phi_m \quad (4.4)$$

$$v_d = P \omega_r L i_q \quad (4.5)$$

$$T_e = \frac{3}{2} P \phi_m i_q \quad (4.6)$$

The v_d and v_q voltages are then controlled to provide the i_q necessary to develop the desired torque

However, as the speed increases the back-emf given by $P \omega_r \phi_m$ also increases. At the base speed, the inverter output voltage reaches its maximum value and therefore v_q and v_d cannot be increased further. This is the beginning of the Constant Power Operation Region. In this region, rated torque cannot be provided anymore, and the maximum developed torque decreases as speed increases. In order to oppose the effect of the constant flux provided by the permanent magnet, i_d is controlled to be

negative. The effect of i_d is to weaken the air gap flux, which was previously provided only by the permanent magnets. This is the reason that this region is called the Field Weakening Region.

The strategy of controlling i_d is what dictates the range of this region. If i_d is held to zero, as the speed increases the back-emf will also increase, making i_q decrease quickly, and therefore the operation range above base speed will be very narrow. Therefore a different strategy to control i_d and i_q is required to make this operation range wider [22]-[31].

In CPOR optimum torque/current ratio is not a priority anymore, i_d is different from zero and in steady state the machine voltage and torque equations become

$$v_q = P\omega_r L i_d + R i_q + P\omega_r \phi_m \quad (4.7)$$

$$v_d = R i_d + P\omega_r L i_q \quad (4.8)$$

$$T_e = \frac{3}{2} P \phi_m i_q \quad (4.9)$$

Notice in Equation 4.7 that if i_d is negative, then the component $P\omega_r L i_d$ will oppose the permanent magnet induced voltage $P\omega_r \phi_m$, allowing i_q to flow. From Equation 4.9, it may seem that there is no change in the torque as i_d becomes different

from zero. However, what this equation does not show is that as i_d increases in absolute value, i_q must decrease in order to obey the current constraint, which will in turn decrease the developed torque. Analysis regarding this constraint will be given in the next section.

IV.3 – Analysis of limits of operation of PMSM with Vector Control

The previous section described how to obtain DC machine-like performance of the PMSM. However, the operating limits of the VC of PMSM was not taken into consideration. Analysis of such limits will now be done. Although, there are many limits related to the DC link voltage (battery), inverter, machine, mechanical coupling, and so on, it is assumed that the most restrictive limits are imposed by the DC link voltage and current ratings of the inverter devices. The analysis of these limits will lead to power/torque-speed operating envelope of the PMSM.

IV.3.1 – Voltage and current limits

First, consider the current ratings of the inverter switches at maximum allowed machine stator current I_{max} . The maximum allowed current can then be represented in the synchronously rotating frame i_q-i_d plane as a circle centered at the origin and with radius I_{max} . Normalizing the maximum current to unity, the circle is then centered at zero with radius 1. The interior of this circle represents the locus where current regulators can generate any normalized current phasor without

exceeding the current limits of the drive system Figure 4 3 shows the current limit as well as a typical armature current phasor I operating within this limit.

The other operation limit that must be considered is the maximum output voltage provided by the inverter. The output voltage of the inverter is a function of the DC link voltage. In VC, the ability to control the stator current is critical. This ability to control the current is given by the PWM operation of the inverter, and it is lost if the inverter switches saturate. Therefore, the inverter must operate within the so-called undermodulation region of the PWM

In PWM operation, modulation index m can be defined as the ratio of the peak value of the fundamental voltage generated by the modulator and the peak value of

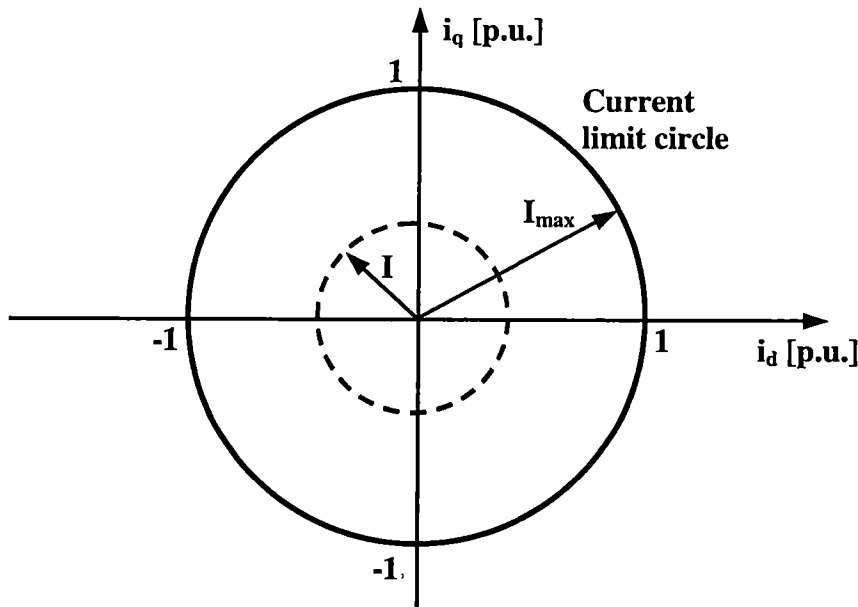


Fig 4 3 Normalized current limit circle in the synchronously rotating reference frame

the fundamental component of output voltage at square-wave operation [32], [33]

The modulation index is then given by Equation 4 10

$$m = \frac{V^*}{V_{1sw}} \quad (4 10)$$

$$V_{1sw} = \frac{2 * V_{dc}}{\pi} \quad (4 11)$$

where

V^* - Peak value of the fundamental voltage generated by the modulator

V_{1sw} – Peak valued of the fundamental voltage at square-wave
operation

Notice that with modulation index defined by Equation 4 10, its value varies from 0 to 1, 1 being the value for square wave operation. The maximum value of the modulation index that characterizes undermodulation region operation depends on the PWM algorithm. If sinusoidal PWM with the addition of triplen harmonics or if space vector PWM is used as the PWM algorithm, then the limit of the undermodulation region is given when the modulation index is [33], [37], [38]

$$m = \frac{\sqrt{3}\pi}{6} = 0.907 \quad (4 12)$$

Therefore, for VC of PMSM, the maximum peak value of the inverter output voltage as function of the DC link voltage is:

$$V_{\max} = \frac{\sqrt{3}V_{dc}}{3} \quad (4.13)$$

On the other hand, the machine terminal voltage amplitude is given by

$$V_a^2 = (PL\omega_r i_q + Ri_q)^2 + (P\omega_r \phi_m + PL\omega_r i_d + Ri_d)^2 \quad (4.14)$$

where V_a is the applied armature voltage

Neglecting the armature resistance and rearranging equation 4.14, it becomes

$$\left(\frac{V_a}{P\omega_r L} \right)^2 = (i_q)^2 + \left(\frac{\phi_m}{L} + i_d \right)^2 \quad (4.15)$$

Therefore, Equation 4.15 represents the voltage relations in terms of the currents i_d and i_q . This relation can then be represented in the synchronously rotating frame i_q - i_d plane as a circle centered at $\left(-\frac{\phi_m}{L}, 0 \right)$ and with radius $\frac{V_a}{P\omega_r L}$. The radius is proportional to the applied armature voltage V_a and inversely proportional to rotor

speed ω_r . It is important to notice that for a given V_a , the radius of the circle decreases as the speed increases

The operation limit established by the DC link voltage can be determined by substituting the applied armature voltage V_a in equation 4.15 by maximum peak value of the inverter output voltage from equation 4.13. This limit is given by

$$\left(\frac{\sqrt{3}V_{dc}}{3P\omega_r L} \right)^2 = (i_q)^2 + \left(\frac{\phi_m}{L} + i_d \right)^2 \quad (4.16)$$

Equation 4.16 represents the family of circles that limit the operation of the PMSM due to the DC link voltage constraint. In other words, for each speed there will be a voltage limit circle. Notice that as the speed increases, the circle shrinks. Figure 4.4 shows three examples of the voltage circle limit for speeds ω_{r1} , ω_{r2} , and ω_{r3} . Where ω_{r3} is bigger than ω_{r2} and ω_{r2} is bigger than ω_{r1} .

The two constraints discussed above must be combined in order to define the drive operation limits. Notice that since the two constraints must be satisfied, the drive operation limit will then be defined by the intersection of the two circles defined by the current and voltage limits.

Figure 4.5 shows the two constraints for PMSM drive system. The current limit circle and the voltage limit circle are given. In this figure, the shaded area represents the operation region where the machine can operate at speed ω_{r2} . I.e., any armature current vector can be generated by the controller within this area and

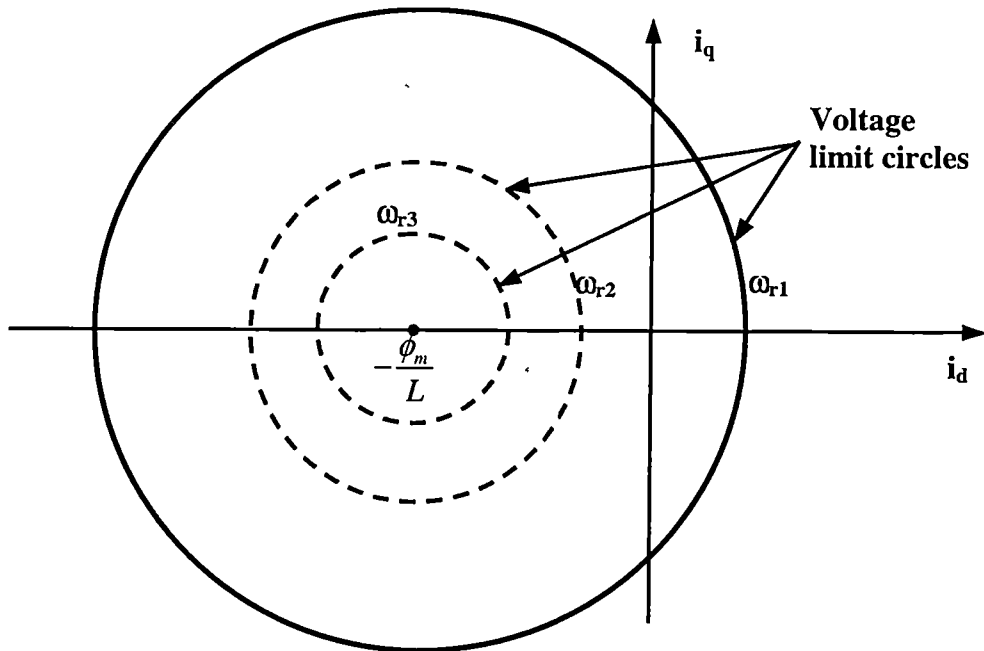


Fig 4 4 Voltage limit circles in the synchronously rotating reference frame

therefore any torque/speed associated with this current can be provided. The voltage limit circle in continuous line is the voltage limit circle for base speed ($\omega_{r1} = \omega_{rb}$)

In order to understand the operation of VC of PMSM drive system and its operation limits, the analysis will be divided into two parts, the constant torque region and the constant power region. Analysis of the best armature current vector trajectory will also be given.

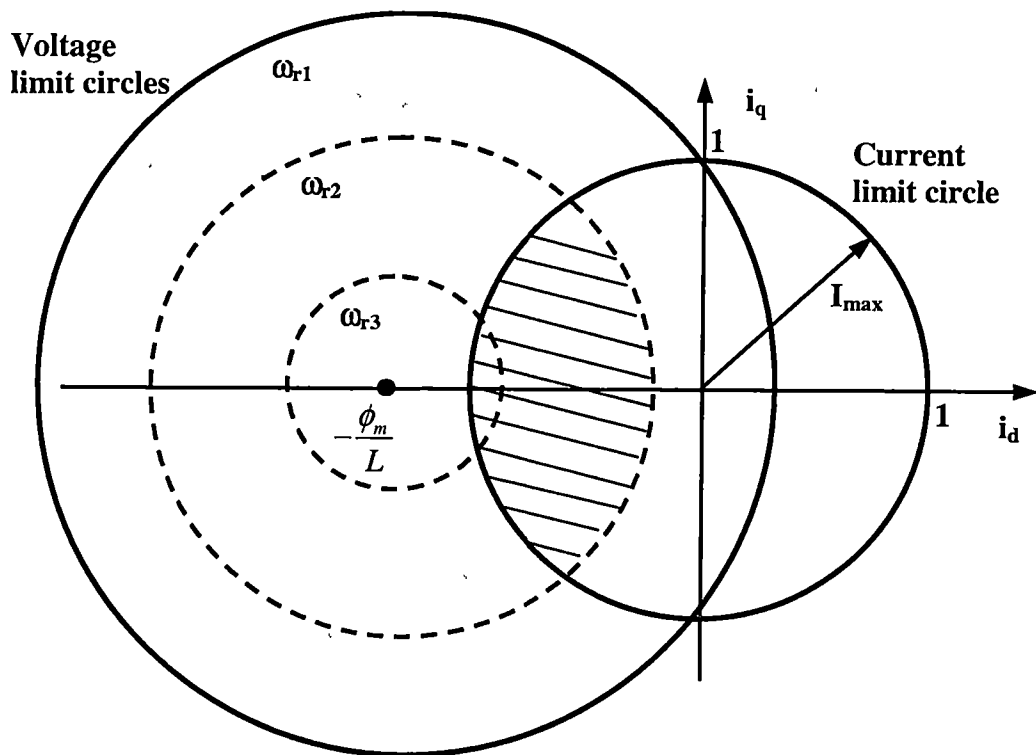


Fig 4.5 Current circle limit and voltage limit circle for PMSM drive system

IV.3.2 - Constant Torque Operation Region

In a PMSM, the magnetic field is provided by the permanent magnets, and therefore optimum torque/ampere ratio is obtained if the armature current is composed only of its torque component. In other words, the controller should control the machine in such a way that the i_d component of the armature current is zero, while the i_q component is proportional to the desired torque. This principle can be graphically observed by looking at Figure 4.6. The condition of maximum torque/ampere ratio

will be achieved by having the armature current trajectory along the i_q axis, as shown in the figure.

Figure 4.6 shows examples of armature current vector. The current I_1 is in the q -axis, and therefore i_d is zero. I_1 then represents a typical operation point where the voltage applied to the machine is V_1 , which is smaller than V_{max} . The armature current I_1 is smaller than I_{max} , and the machine is providing a torque T_1 at speed ω_{r1} . Notice that the same torque T_1 can be provided by the same current I_1 , but with different combinations of V_1 and ω_1 , i.e. lower or higher speeds can be reached by varying V_1 .

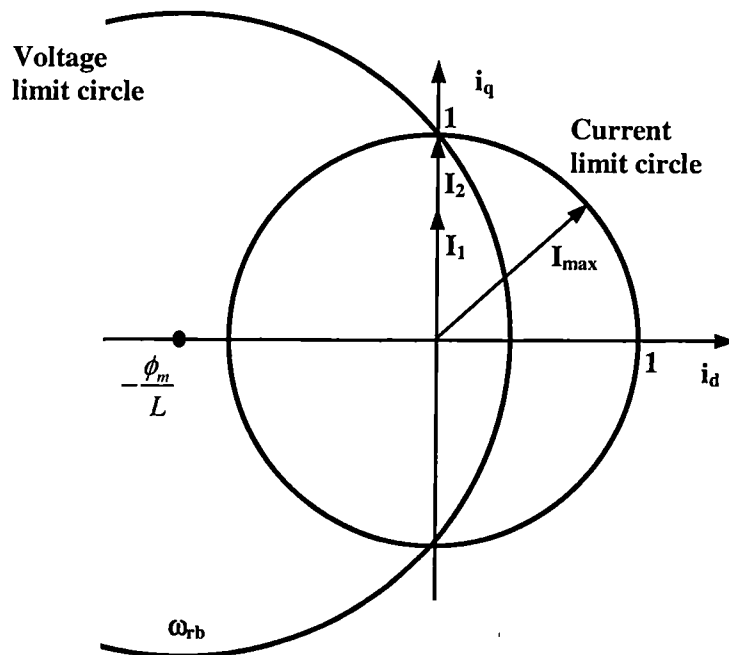


Fig. 4.6 Armature current trajectory for vector control of PMSM operating in CTOR

In the operating point I_2 , the machine is operating at maximum or rated torque. At this point any combination of the applied voltage V_2 and speed ω_2 can be used. However, there will be a speed that will allow the voltage limit circle to pass through the point where the current limit circle crosses the q-axis. This is the maximum speed where the rated torque can be developed. This speed is the aforementioned base speed ω_{rb} . The base speed is the limit of the constant torque operation range. Below this speed, the machine can provide the rated torque at any speed, but beyond this speed, the rated torque cannot be provided any longer, and this is the beginning of the constant power operation region. It is important to notice that in general the base speed is defined as the speed where the maximum circle voltage is provided by square-wave operation of the inverter. However, as mentioned before, at square-wave operation the inverter loses its ability to control the current, which is a requirement for VC and fast dynamic response of the system. Therefore, for vector control, the maximum voltage circle is defined in the limit of the undermodulation operation region of the inverter. The base speed for vector control will then be 9.3% smaller than the generally accepted base speed. Another important observation is that a well-designed PMSM drive system using VC will have the maximum voltage limit circle and the maximum circle current crossing at the same point on the q-axis. Any different design will be over designing the system either from the voltage or current point of view.

IV.3.3 - Constant Power Operation Region

As the speed increases beyond the maximum speed, the voltage limit circle passes through a point where the maximum current circle crosses the i_q axis, the voltage limit circle shrinks and the maximum torque can no longer be provided. It is important to emphasize that before this point the current command i_d was zero and the current command i_q was proportional to the desired torque. However, from this point on, although the current limit may not be violated, the controller cannot control the current in a way that the rated torque is provided, and the command currents i_d and i_q must be changed.

There are many different ways to control the i_d and i_q currents. For instance, consider that the current command will be controlled to be in the limit of the voltage limit circle, and inside the current limit circle; however, optimum torque/ampere ratio is desired and therefore i_d will be controlled to be zero. Figure 4.7 shows three operation points for speeds ω_{r1} , ω_{r2} , and ω_{r3} with this control strategy. Notice that as the speed increases from ω_{r1} to ω_{r2} , and from ω_{r2} to ω_{r3} , and the voltage limit circle shrinks, and therefore the maximum torque that can be developed also decreases. At speed ω_{r3} , the voltage limit circle is tangent to the i_q axis and the machine cannot provide any torque at this speed or higher. Therefore, if the current command trajectory is along the i_q axis, the range above base speed in which the machine can provide torque is very narrow.

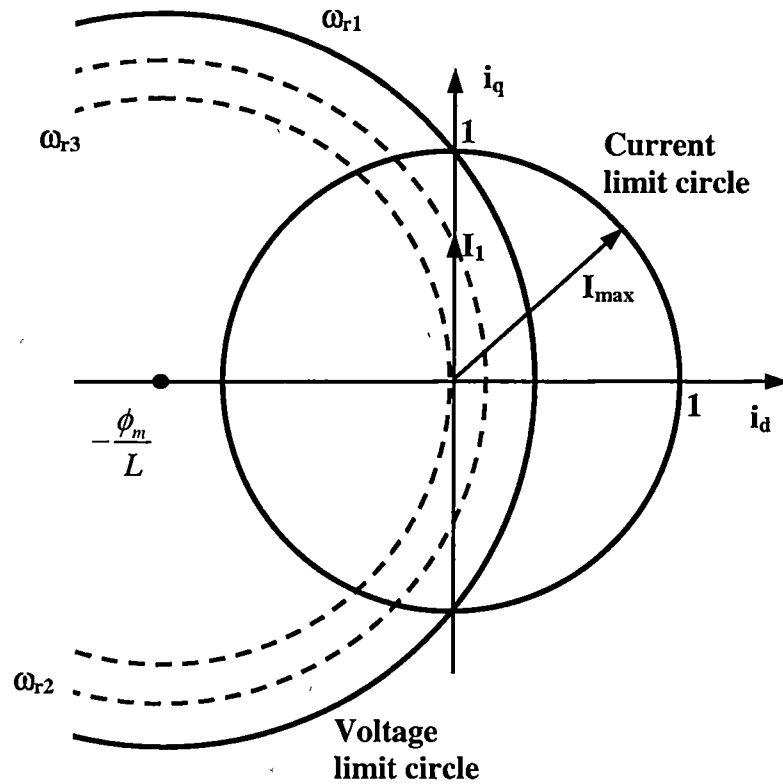


Fig. 4.7 Armature current trajectory for vector control of PMSM operating in CPOR
with $i_d=0$

Consider as an alternative for the previous current command trajectory, the trajectory that does not keep the i_d component of the command current zero. A possible current trajectory as the speed increases is along the current limit circle. Figure 4.8 shows this trajectory. In this trajectory, the i_d component of the current command increases negatively. In order to stay within the current limit circle, the i_q component must decrease, which causes the developed torque to decrease. However,

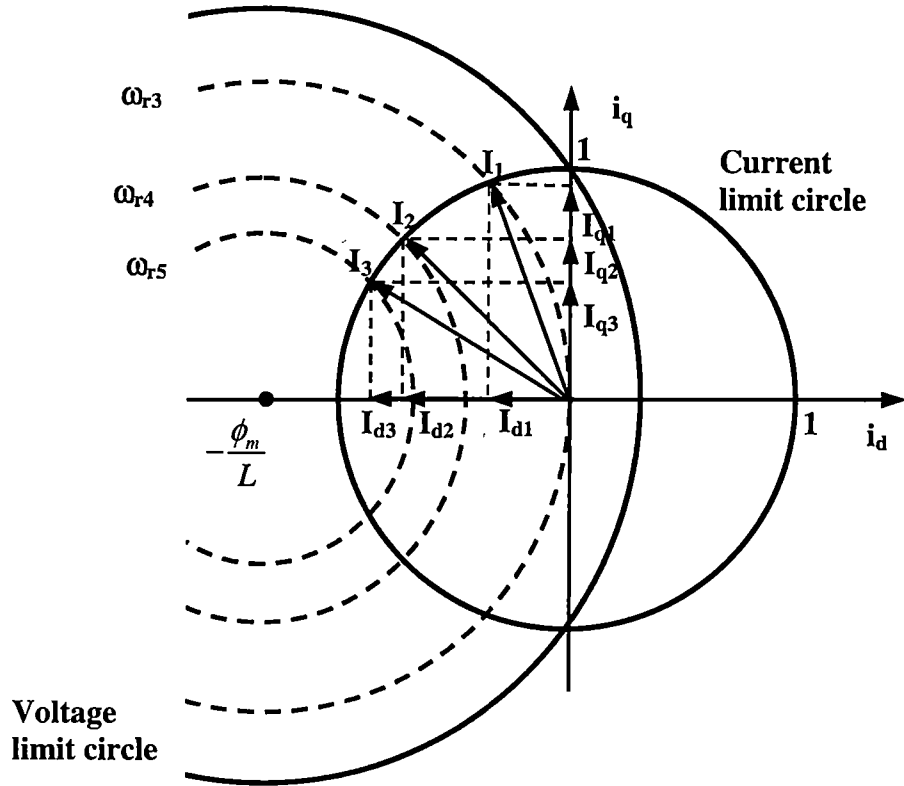


Fig. 4 8 Armature current trajectory for vector control of PMSM operating in CPOR with field weakening

in this way the decreasing rate of the torque as the speed increases is smaller, meaning that the range that the machine can operate above base speed is wider

The armature current vectors I_1 , I_2 , and I_3 are examples of the currents in this trajectory. Notice that they have nonzero i_d and i_q components, unlike the previous trajectory. In this case the optimum torque/ampere is not achieved anymore. However torque can be developed at higher speeds. For instance, as shown in Figure 4.7, if the machine is required to operate at speed ω_{r3} , by using the trajectory along the q-axis,

there would not be any i_q current, and therefore the machine would not be able to develop any torque. On the other hand, if the trajectory along the current limit circle is used, as shown in Figure 4.8, the i_q current would be I_{q3} and a considerable amount of torque would be developed.

The objective of the field weakening technique is then to control i_d and i_q current in such way that the machine can develop constant power. The power, speed and torque relation in the machine shaft is given by.

$$T_e = \frac{P_{rated}}{\omega_r} \quad (4.17)$$

In constant power operation region, the power is constant and thus, the torque profile as a function of speed is a hyperbola. If rated power in the constant power operation region is desired, then the current i_q should be controlled to provide torque as given in Equation 4.17, i.e., i_q must be controlled as

$$i_q = \frac{\omega_b}{\omega_r} I_{max} \quad (4.18)$$

Therefore, to keep the current satisfying the two constraints described above, the i_d current has to be controlled following Equation 4.19.

$$i_d = -\left(1 - \frac{\omega_b}{\omega_r}\right) \frac{\phi_m}{L} \quad (4.19)$$

Neglecting the losses, if the machine is operating at high speed at no-load condition, i_q current is required to be zero, however the flux still has to be weakened and the i_d current has to be controlled as follows:

$$i_d = -\frac{1}{L} \left(\phi_m - \frac{V_{\max}}{P\omega_r} \right) \quad (4.20)$$

Therefore, to attend the load and no-load operation conditions described above, the i_d current must be controlled as given in Equation 4.21.

$$i_d = -\frac{1}{L} \left(\phi_m - \frac{V_{\max}}{P\omega_r} \right) - \frac{i_q}{LI_{\max}} \left(\frac{V_{\max}}{P\omega_r} - \phi_m \right) \quad (4.21)$$

However, even if using the i_q and i_d currents given in Equations 4.18 and 4.21, the constant power operation region will have a maximum speed ω_{\max} . This speed will depend on the machine parameters. Analysis of Figure 4.8 gives a qualitative idea of the limit of the CPOR. The center of the voltage limit circle is $\left(-\frac{\phi_m}{L}\right)$. The radius of the voltage limit circle is $\frac{\sqrt{3}V_{dc}}{3P\omega_r L}$. As mentioned before, as the speed

increases, the radius of the voltage limit circle decreases. The radius then goes to zero when speed goes to infinity. Therefore, there will always be a voltage limit circle within which the machine can operate. However, as discussed previously, the current limit also must be satisfied, and therefore, the operating current vector locus is the area defined by the intersection of the two limit circles. Therefore, if $I_{\max} \geq \frac{\phi_m}{L}$, which means that the center of the voltage limit circle will be either in the current limit circle or inside of it, then the CPOR is theoretically infinite. On the other hand, if $I_{\max} < \frac{\phi_m}{L}$, then the intersection will vanish at finite value of ω_r . If the inductance is large enough, the constant power speed range can be infinite. There will be a maximum speed at which the machine can develop rated torque. This speed is called critical speed ω_{rc} and is the limit of the CPOR. Therefore, the constant power range then starts at ω_{rb} and ends at ω_{rc} . From Equations 4.18 and 4.19, and not exceeding the inverter current limit, the critical speed ω_{rc} is found as:

$$\omega_{rc} = \frac{\phi_m^2 + (LI_{\max})^2}{\phi_m^2 - (LI_{\max})^2} \omega_b \quad (4.22)$$

The analysis done in this section leads to the maximum torque-speed operating envelope shown in Figure 4.9.

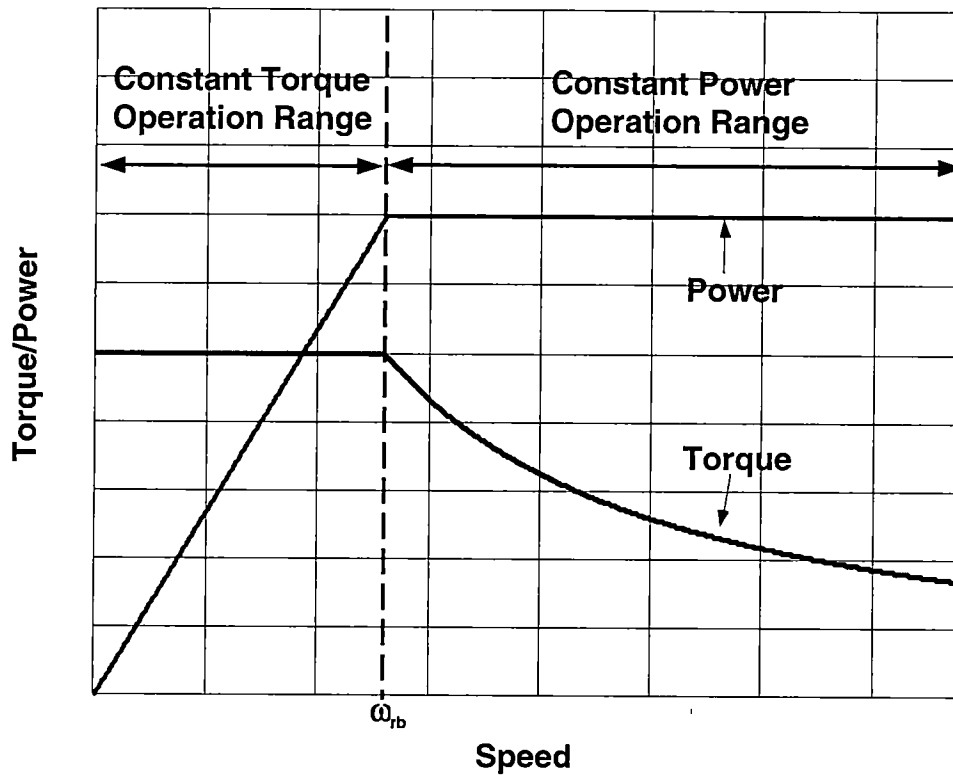


Fig 4 9 Maximum torque-speed and power-speed envelope

IV.4. – System Description of Vector Control of PMSM with Field Weakening Operation

The physical principle of the VC of PMSM operating at CTOR and CPOR with field weakening was addressed in the previous section. This section will describe how this system can be implemented. Figure 4.10 shows a typical block diagram of VC of PMSM with closed loop speed control. The system can be divided into two

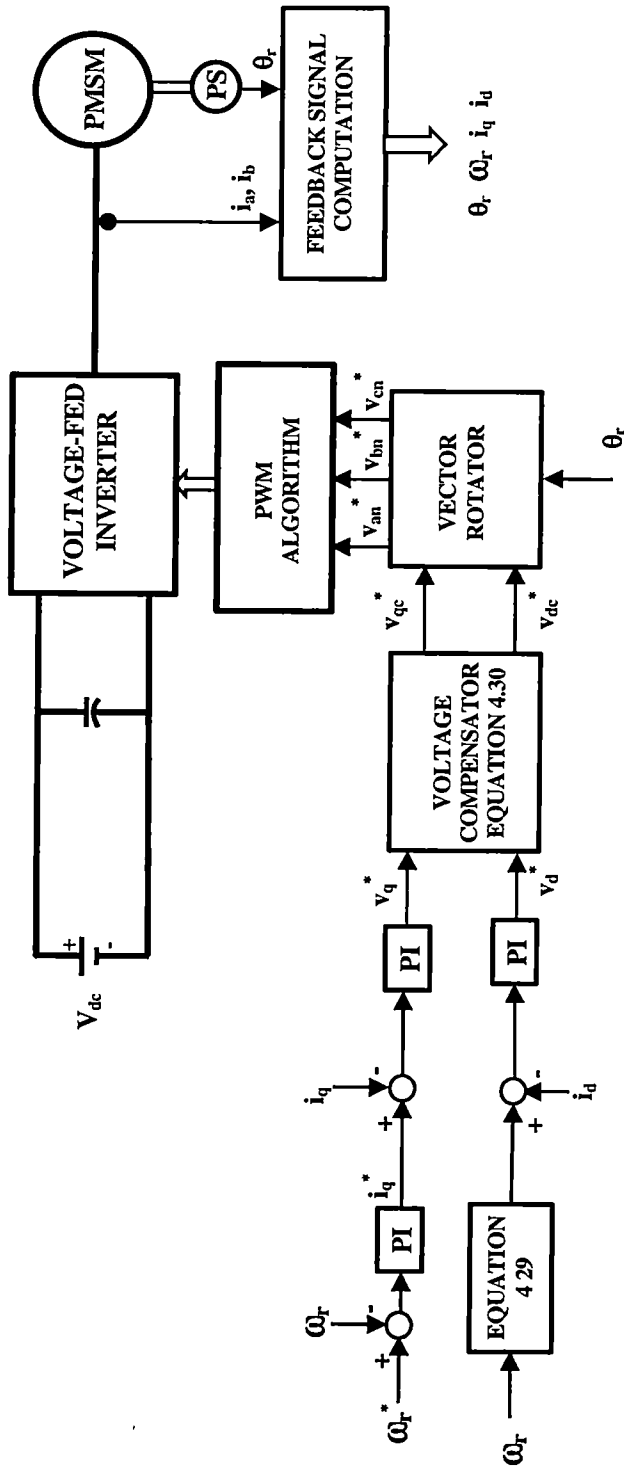


Fig 4 10 System description of VC of PMSM with closed loop speed control

parts, the power subsystem, which is composed of the PMSM, the VFI, and the DC link voltage (battery)

The other part is the signal subsystem, which is composed of a position sensor, feedback signal computation, PWM algorithm, current control loops, speed control loop, and vector rotator. Each element of the signal subsystem will be briefly described.

The phase currents i_a and i_b as well as the rotor position θ_r are sensed to be the inputs of the feedback signal computation block. Notice that because the machine has a neutral isolated connection, only two current sensors are required and the current i_c can be calculated as

$$i_c = -(i_a + i_b) \quad (4.23)$$

The currents i_d and i_q are then calculated using line currents i_a , i_b , i_c , and the rotor position θ_r through equation 4.24. This operation is called inverse Vector Rotation (VR^{-1}) and it maps the machine variables from three-phase stationary reference frame to the two-phase rotating reference frame. It needs high resolution of the rotor position.

$$\begin{bmatrix} i_q \\ i_d \\ i_0 \end{bmatrix} = \frac{2}{3} \begin{bmatrix} \cos \theta_r & \cos(\theta_r - 2\pi/3) & \cos(\theta_r + 2\pi/3) \\ \sin \theta_r & \sin(\theta_r - 2\pi/3) & \sin(\theta_r + 2\pi/3) \\ 1/2 & 1/2 & 1/2 \end{bmatrix} \begin{bmatrix} i_{an} \\ i_{bn} \\ i_{cn} \end{bmatrix} \quad (4.24)$$

Notice that because the machine has a neutral isolated connection the i_0 component will be zero

The speed ω_r is calculated using equation 4 25

$$\omega_r = \frac{d\theta_r}{dt} \quad (4 25)$$

The drive system shown in Figure 4 10 is sensor-based, it uses a position sensor to obtain the rotor position of the PMSM. In sensorless PMSM control, voltage sensors are used, instead of position sensor [32]. In such a case, the signal computation block uses the machine terminal voltages and currents to estimate the rotor position as well as the rotor speed. There are many different rotor and speed estimator algorithms proposed in literature. Although it is an interesting area, sensorless PMSM control is not in the scope of this work.

The feedback signals are used by the control loops. There are three control loops, the i_d current loop, the i_q current loop, and the speed loop, which is an outer loop of the i_q current loop. Equation 4 26 gives the output of the speed PI controller.

$$i_q^* = K_{\omega I} \int (\omega_r^* - \omega_r) dt + K_{\omega P} (\omega_r^* - \omega_r) \quad (4.26)$$

where

$K_{\omega I}$ – Integral constant for the rotor speed controller

ω_r^* – Rotor speed command

ω_r – Actual rotor speed

$K_{\omega P}$ – Proportional constant for the speed controller

Equation 4.27 gives the output of the i_q PI controller

$$v_q^* = K_{qI} \int (i_q^* - i_q) dt + K_{qP} (i_q^* - i_q) + v_{q0} \quad (4.27)$$

where

K_{qI} – Integral constant for the i_q controller

i_q^* – i_q command

i_q – Actual i_q

K_{qP} – Proportional constant for the i_q controller

$v_{q0} = P\omega_r\phi_m$ decoupling voltage

Equation 4.28 gives the output of the i_d PI controller.

$$v_d^* = K_{di} \int (i_d^* - i_d) dt + K_{dp} (i_d^* - i_d) + v_{d0} \quad (4.28)$$

where

K_{di} – Integral constant for the i_d controller

i_d^* – i_d command

i_d – Actual i_d

K_{dp} – Proportional constant for the i_d controller

$v_{d0} = -P\omega_r L i_q$ - decoupling voltage

The voltages v_{d0} and v_{q0} are called decoupling voltages. They are used to decouple the i_d and i_q control loops [10], i.e., they allow independent control of i_d and i_q currents

For operation with the field weakening operation the i_d command must be a function of the rotor speed ω_r . If the machine is operating below base speed, the i_d command must be zero, however, if the machine is operating above base speed, i_d command will follow equation 4.21. The i_d command is then given by equation 4.29.

if $\omega_r \leq \omega_{rb}$ then

$$i_d^* = 0$$

else

$$i_d^* = -\frac{1}{L} \left(\phi_m - \frac{V_{\max}}{P|\omega_r|} \right) - \frac{|i_q^*|}{L I_{\max}} \left(\frac{V_{\max}}{P\omega_b} - \phi_m \right)$$

(4.29)

The outputs of the controllers are the command voltages v_d and v_q . However, the amplitude of the vector defined by these two command voltages cannot exceed the maximum inverter output voltage. If this occurs, the current controllers will saturate. The saturation of the current controllers will mean coupling between them, and the system will lose the fast dynamic response. In order to avoid the saturation of the controller, the command voltages v_d and v_q are compensated. The compensated values of v_d and v_q are v_{dc} and v_{qc} . This compensation gives priority to the control of i_d rather than i_q . If the amplitude of the vector defined by command voltages exceeds the maximum inverter output voltage, the amplitude of the v_{dc} is made equal to v_d , and v_{qc} is the value that will make the amplitude of vector defined by v_{dc} and v_{qc} equal to the maximum inverter output voltage. The only condition that will make v_{dc} smaller than v_d is whenever the decoupling voltage v_{q0} is large, and the vector defined by v_d and v_{q0} has amplitude larger than the maximum inverter output voltage. In this case, v_{q0} has priority over v_d . Equation 4.30 uses if-then statements to explain the approach of the voltage command compensation discussed above.

$$\begin{aligned}
 & \text{if } v_d^{*2} + v_q^{*2} \leq V_{\max}^2 \text{ then} \\
 & \quad v_{dc}^* = v_d^* \quad \text{and} \quad v_{qc}^* = v_q^* \\
 & \text{elseif } v_d^{*2} + v_{q0}^{*2} \leq V_{\max}^2 \text{ then} \\
 & \quad v_{dc}^* = v_d^* \quad \text{and} \quad v_{qc}^* = \sqrt{V_{\max}^2 - v_d^{*2}} \\
 & \text{else} \\
 & \quad v_{dc}^* = \sqrt{V_{\max}^2 - v_{q0}^{*2}} \quad \text{and} \quad v_{qc}^* = v_{q0}^*
 \end{aligned} \tag{4.30}$$

The compensated command voltages are in d-q rotating frame and must be mapped to the abc stationary frame. The d-q rotating frame to abc stationary frame is done using the Vector Rotator (VR) given in Equation 4.31

$$\begin{bmatrix} v_{an}^* \\ v_{bn}^* \\ v_{cn}^* \end{bmatrix} = \begin{bmatrix} \cos \theta_r & \sin \theta_r & 1 \\ \cos(\theta_r - 2\pi/3) & \sin(\theta_r - 2\pi/3) & 1 \\ \cos(\theta_r + 2\pi/3) & \sin(\theta_r + 2\pi/3) & 1 \end{bmatrix} \begin{bmatrix} v_{qc}^* \\ v_{dc}^* \\ v_0^* \end{bmatrix} \quad (4.31)$$

The command voltages in abc stationary frame are then fed to a PWM algorithm to generate the gate signals for the VFI switches. There are many PWM algorithm options, among them, sinusoidal PWM and space vector PWM are the most popular. Description of this algorithm is not in the scope of this work, but it can be found in [34] – [40].

IV.5 – Simulation Results of Vector Control of PMSM with Field Weakening Operation

Vector control of PMSM with field weakening was described and analyzed in the previous sections. A SIMULINK model of the system described in section IV.4, Figure 4.10 is built (Appendix 1) [41], [42], [43]. The system parameters are given in Table 4.1. The PWM algorithm used is the space vector PWM. The motor parameters used are of a PMSM equivalent to the brushless DC motor used in Chapter 3 (Table

Table 4.1 – Drive system parameters - VCFW

DC-link voltage	$V_{dc} = 162 \text{ V}$
PWM Switching Frequency	$f_s = 10 \text{ kHz}$ ($T_s=100 \mu\text{s}$)
Brushless DC motor	$P_{rated} = 42.9 \text{ hp}$ (31,980 Watts), 12-pole Base Speed. $N_b = 2600 \text{ rpm}$ (260 Hz) Peak phase-to-neutral back-emf at N_b $E_b=74.2 \text{ V}$ Stator resistance $R_s = 0.0118 \Omega$ Stator inductance $L_s = 61.8 \mu\text{H}$ Stator mutual inductance. $M = 11.8 \mu\text{H}$ Rated peak current. $I_{rated (peak)} = 249 \text{ A}$ Rated rms current $I_{rated (rms)} = 176 \text{ A}$
System limits	Maximum voltage provided by the VFI $V_{max}=103 \text{ V}$ Maximum current $I_{max} = 245 \text{ A}$ Frequency limit of the CTOR: $f_b = 260 \text{ Hz}$ (2600 rpm) Frequency limit of the CPOR $f_c = 320 \text{ Hz}$ (3198 rpm)
Load	$T_L=k\omega_r^2$ Below base speed. $k = 1.58 \cdot 10^{-3}$ Above base speed $k = \frac{1.58 \cdot 10^{-3}}{\omega_r^3}$

3 1) The values of the proportional-integral controller constants were not tuned for the optimal operation because the objective of this work is to evaluate the "steady-state" performance of the system, not the dynamic response, although results showing the dynamic response of the system are also given. The aim, here, is to show the maximum speed at which the machine can provide rated power without exceeding the rated current.

The system was simulated and results at 5 different steady-state operating points were recorded and plotted. Figure 4.11, 4.12, 4.13 and 4.14 show the results for the machine providing rated power and rated torque at base speed. Figure 4.11 shows the commanded rotor speed and actual rotor speed. Figure 4.12 shows the load torque and the developed torque. The load was chosen in such way that the developed torque was the rated torque at base speed. Figure 4.13 shows the output power at the machine shaft. The machine is providing rated torque at base speed, therefore, as expected, the power is equal the rated power. Figure 4.14 shows the i_d and i_q components of the armature current. Notice that the maximum torque/ampere ratio strategy is used, since the i_d is zero and i_q is the rated current. The high frequency pulsating torque and power as well as the high frequency components of the i_q and i_d current are expected because of the PWM operation of the inverter.

The machine system was simulated at critical speed. As defined in the previous section, the critical speed is the maximum speed that the machine can develop rated power using VC with field weakening, i.e., the speed limit of the CPOR. The critical rotor speed, ω_{rc} for the PMSM in the study was calculated using

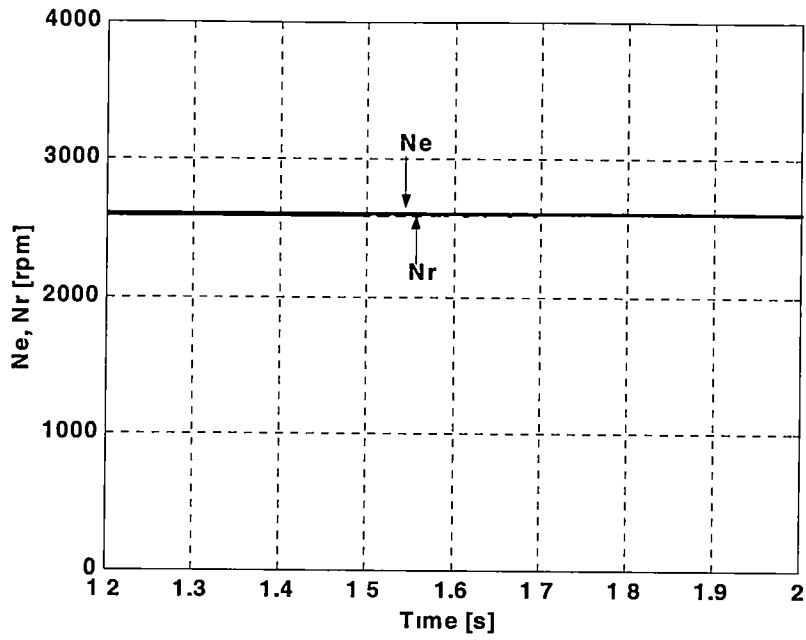


Fig 4 11 Command and actual rotor speeds at base speed (2600 rpm)

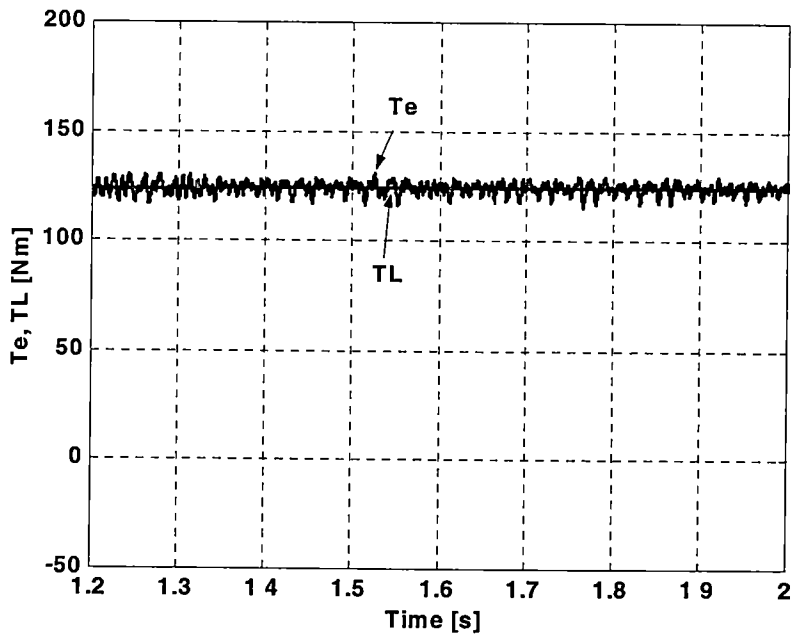


Fig 4 12 Load and developed torque at base speed (2600 rpm)

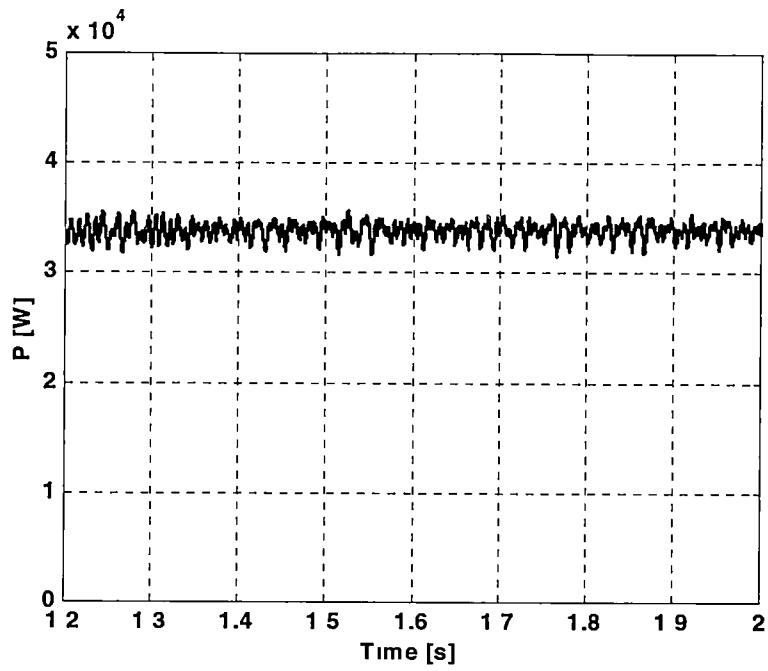


Fig 4 13 Machine output power at base speed (2600 rpm)

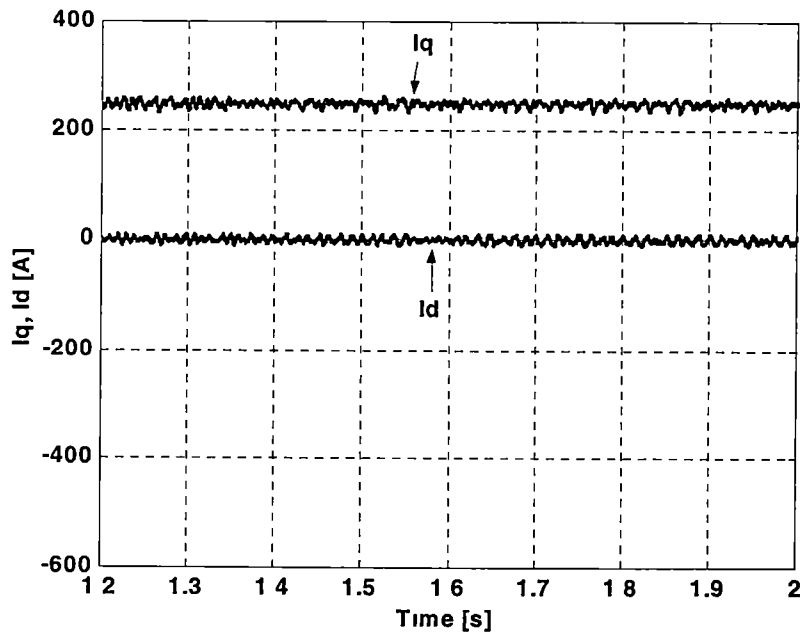


Fig 4 14 i_d and i_q components of the armature current at base speed (2600 rpm)

Equation 4.22 and it was found to be 23% higher than the base speed. Therefore, speed limit of the CTOR is 1632.8 rad/s and the speed limit of the CPOR is 2009.6 rad/s. Thus, the CPOR is very narrow for the example motor, meaning that this drive system cannot be used for high speed applications. This narrowness is due to the low inductance of the machine under study. Although low inductance machines have a wide CTOR, their CPOR are very narrow. On the other hand, high inductance machines have a low CTOR, but their CPOR is much wider than that for low inductance machines [19].

The results for machine operating at critical speed are given in Figures 4.15-4.18. Figure 4.15 shows the command and actual speed. Figure 4.16 shows the developed and load torques. Notice that the machine is operating at constant power region, therefore the developed torque is smaller than the rated torque. Figure 4.17 shows the developed power. As expected, the developed power equals to the rated power. Figure 4.18 shows the i_d and i_q currents. At this operating point, the i_d current is different from zero, and it is controlled to be negative in order to oppose the permanent magnet flux effect. In order to keep the total armature current equal to the maximum current, i_q is controlled to be smaller than the rated value. This is the speed limit at which the total current equals the maximum current limit if the machine is required to develop rated power. From this point on, in order to develop rated torque the current will increase above the maximum current.

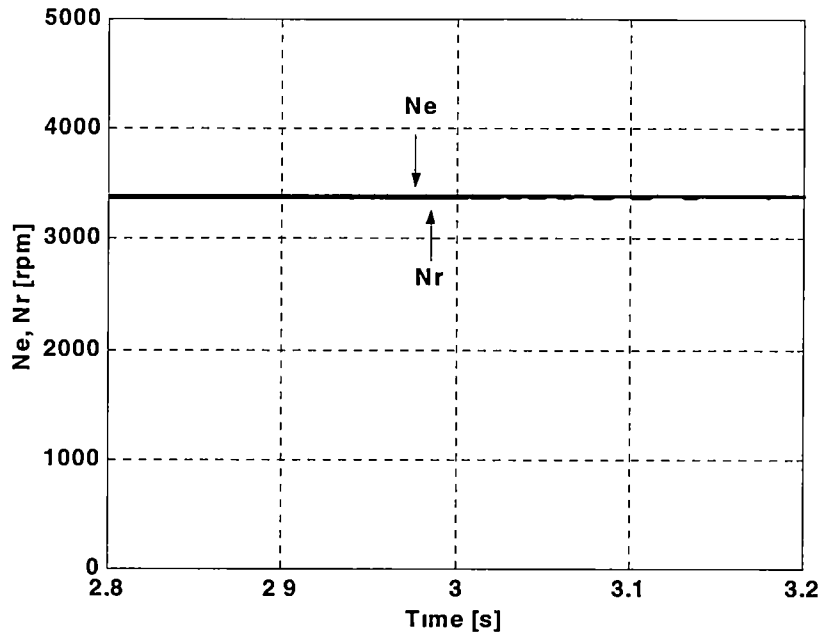


Fig 4.15 Command and actual rotor speeds at critical speed (3198 rpm)

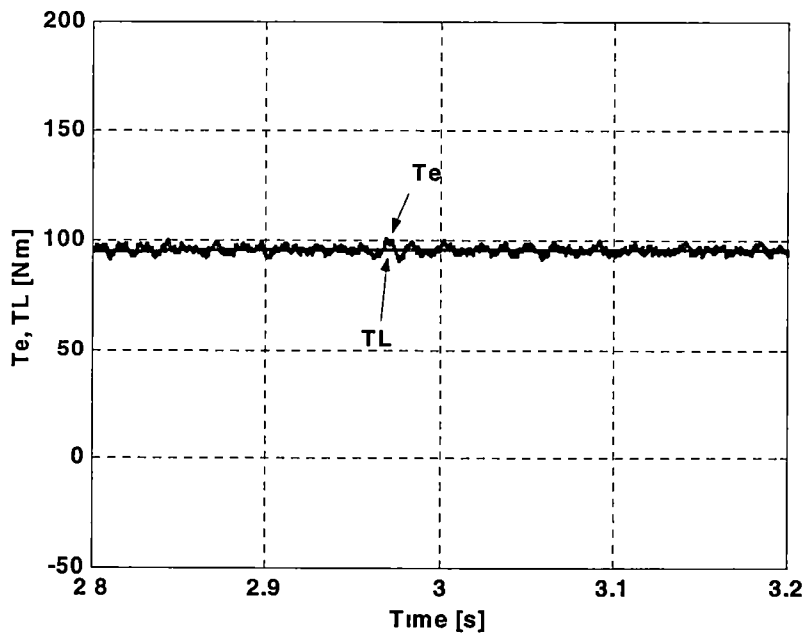


Fig 4.16 Load and developed torque at critical speed (3198 rpm)

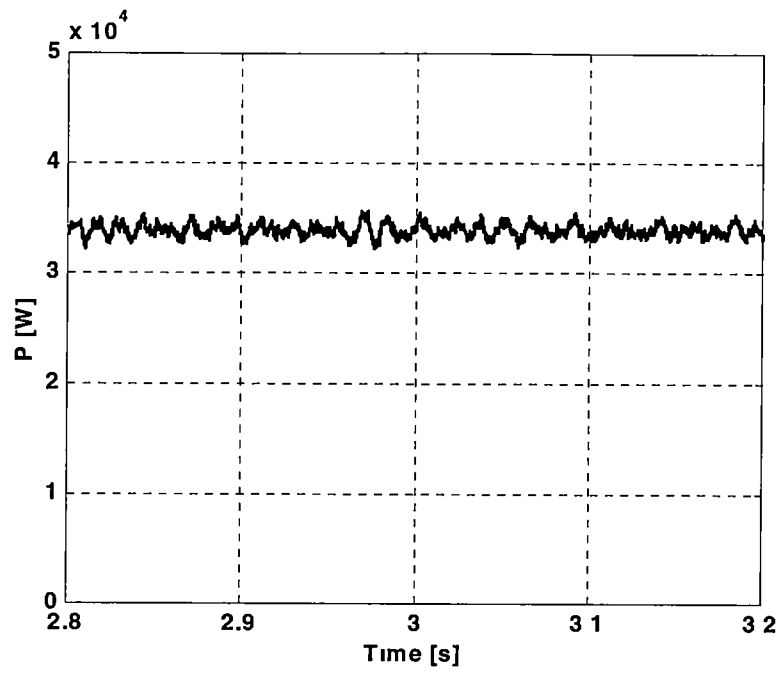


Fig. 4 17 Machine output power at critical speed (3198 rpm)

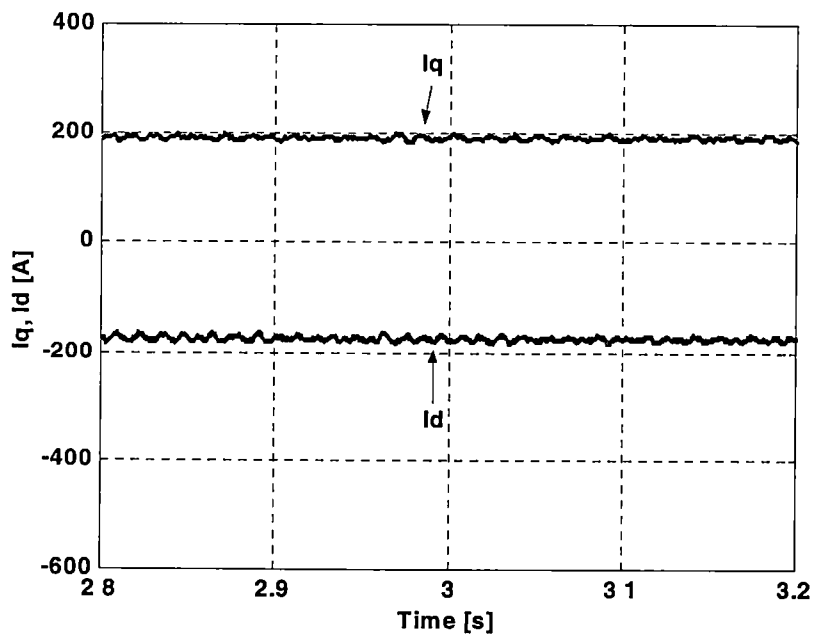


Fig 4 18 i_d and i_q components of the armature current at critical speed (3198 rpm)

In order to evaluate the poor performance of the vector control with field weakening at higher speeds, the system was simulated right above the critical speed and also at 3 times the base speed. Figure 4 19 through 4 22 show the results of the machine operating at 50% above base speed (3900 rpm), which is only 20% above critical speed ω_c . The objective is to keep the output power of the machine constant and evaluate the increase in the current amplitude. Figure 4 19 shows the command and actual rotor speeds. Figure 4 20 shows the developed and load torques. It is important to notice that the decrease in the developed torque is inversely proportional to the speed ($1/\omega_r$) in order to keep the machine output power constant. The load torque is controlled to match the developed torque at this operating point. Figure 4 21 shows that the output power of the machine is kept constant and Figure 4 22 shows the substantial increase in the total current necessary to achieve the rated output power. The i_q component is 165.8 A and the i_d component is -252 A. With these values of i_d and i_q components of the armature current, the total armature current is 301.65 A, against a maximum current of 250A. This increase in current is prohibited by the inverter switch rating, machine losses and heating of inverter and machine.

A simulation at 3 times the base speed was done to further explore the limitations of the VC with field weakening for low inductance PMSMs. However, because of the long computation time to reach this speed, the PWM waves were replaced by pure sine waves to increase the simulation speed. The effect of this procedure is just the elimination of the high frequency ripple, but the average values of the results stay the same. Figures 4 23 through 4 26 show such results. Figure 4 26

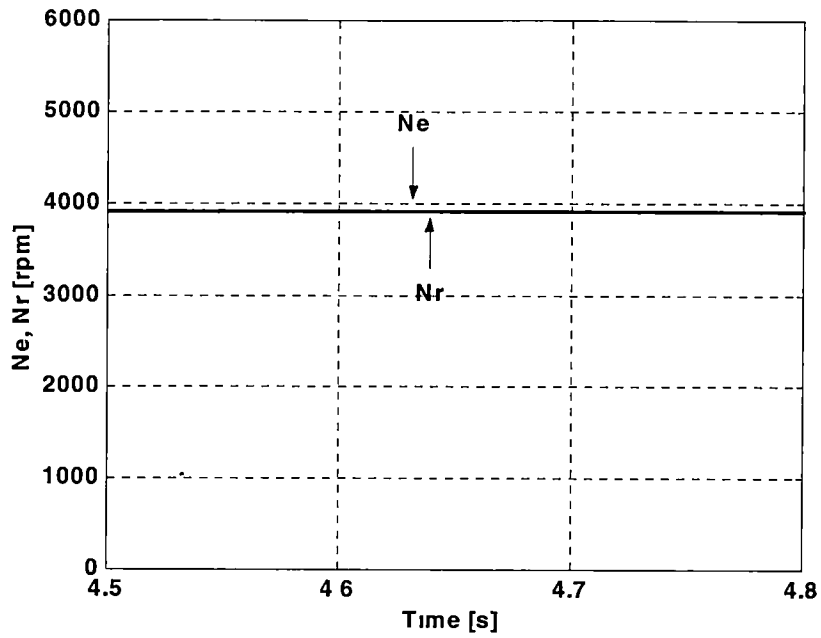


Fig. 4.19 Command and actual rotor speeds at 50% above base speed (3900 rpm)

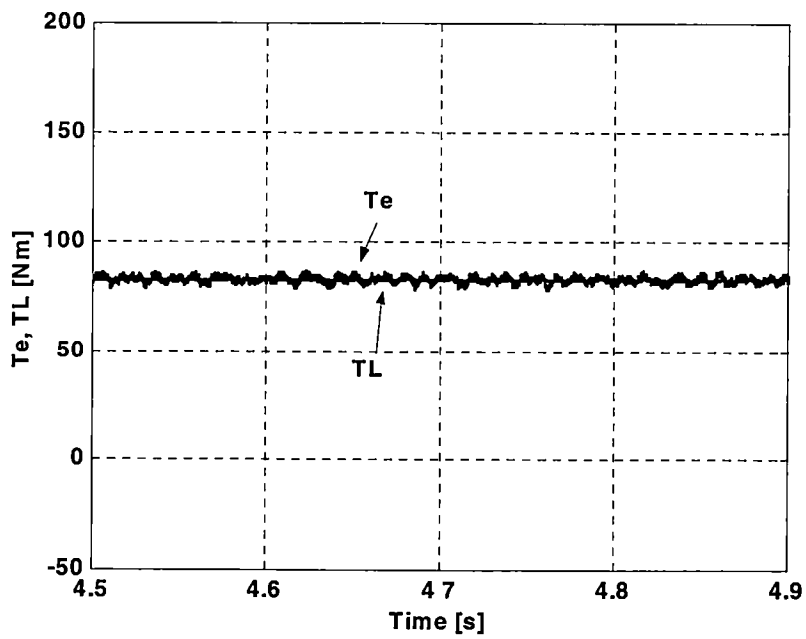


Fig 4 20 Load and developed torque at 50% above base speed (3900 rpm)

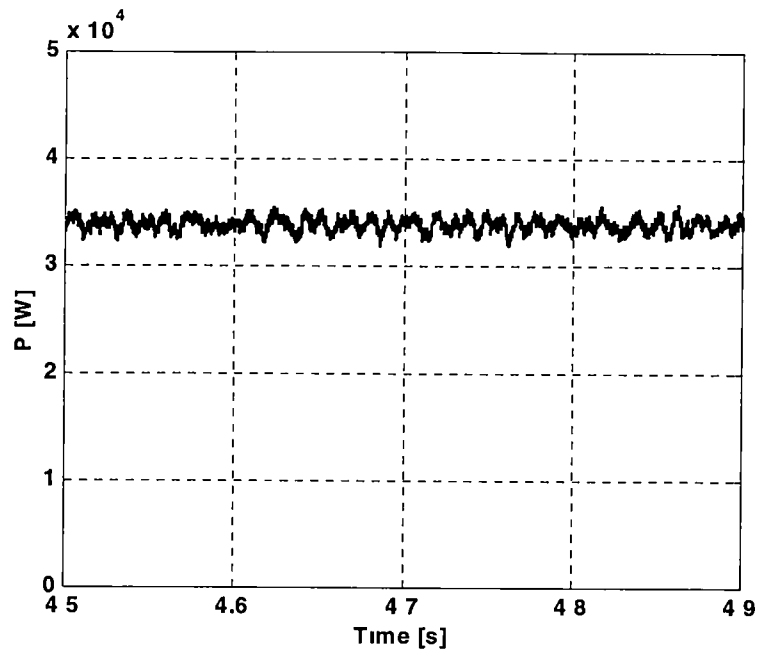


Fig. 4 21 Machine output power at 50% above base speed (3900 rpm)

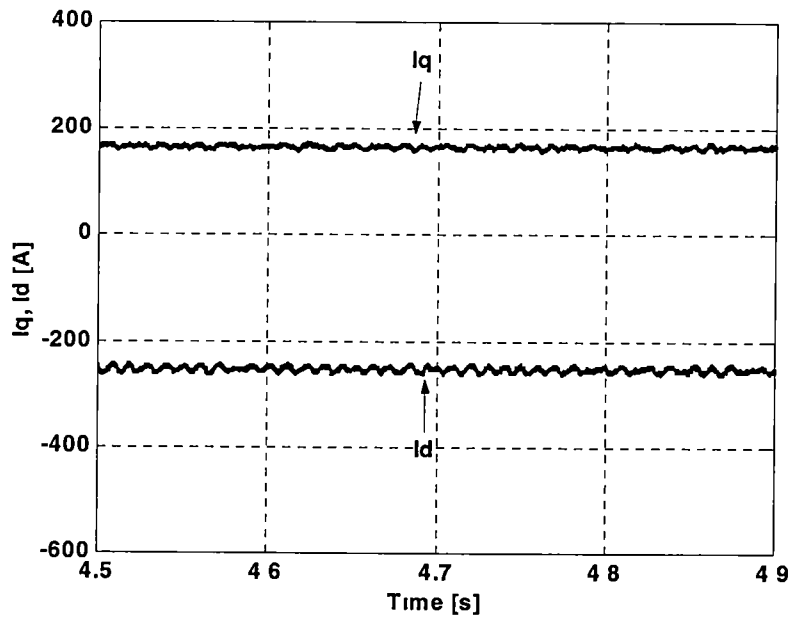


Fig. 4 22 i_d and i_q components of the armature current at 50% above base speed (3900 rpm)

shows the i_q and i_d currents. The i_q component is 83 A and i_d component is -503.6 A. Therefore the total current is 510.4 A, which is more than doubling of the current limit.

The results shown in Figures 4.11-4.26 were in steady-state operation of the system at different operating points. The system was also simulated in such a way that its dynamic response could be observed. In order to save simulation time, the dynamic results were also obtained using pure sine waves instead of the PWM waves.

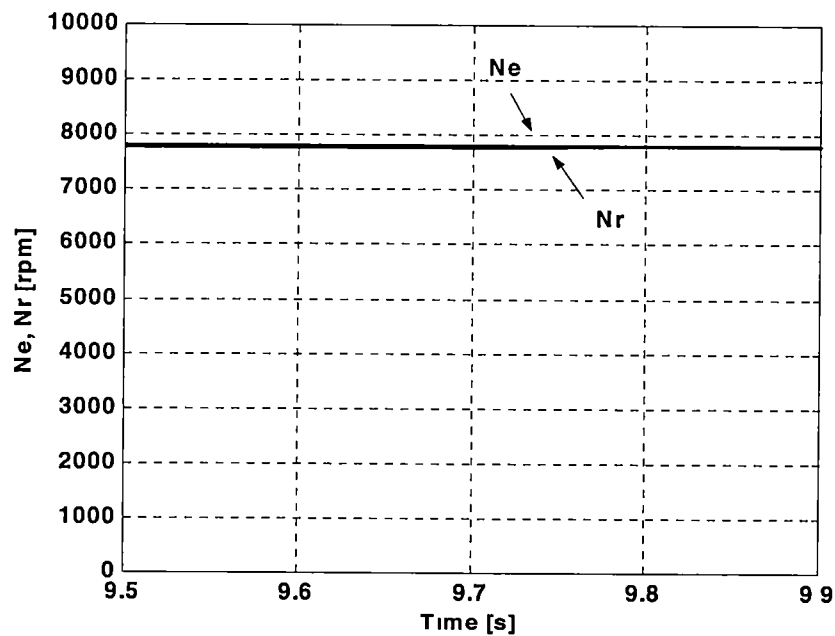


Fig. 4.23 Command and actual rotor speeds at 3 times base speed (7800 rpm)

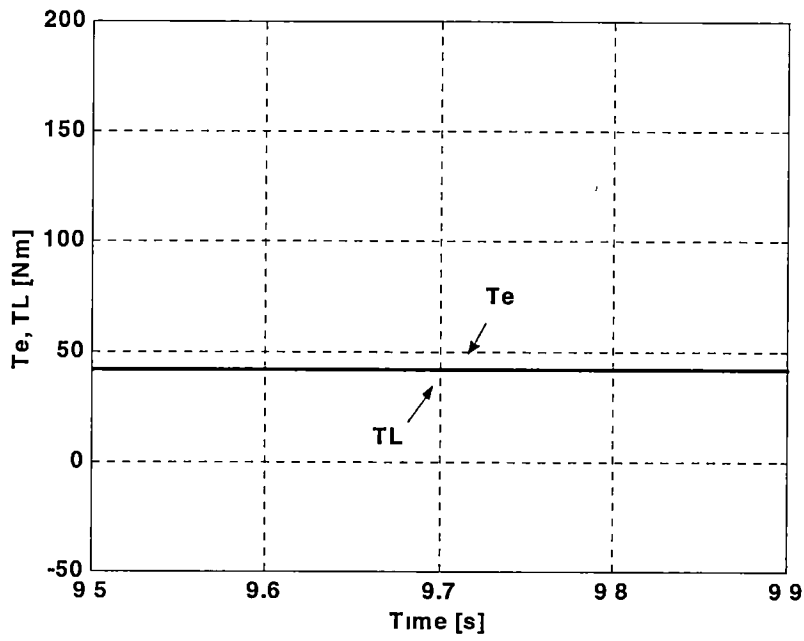


Fig 4 24 Load and developed torque at 3 times base speed (7800 rpm)

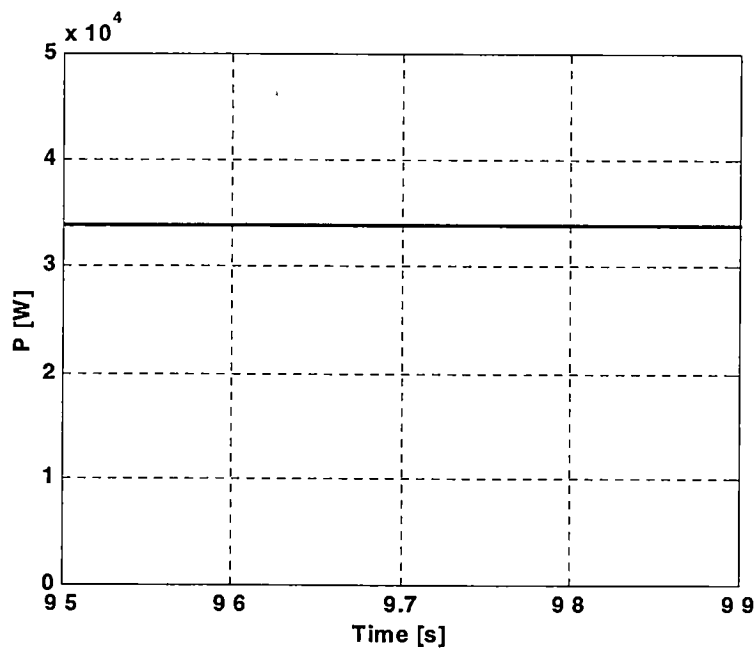


Fig 4 25 Machine output power at 3 times base speed (7800 rpm)

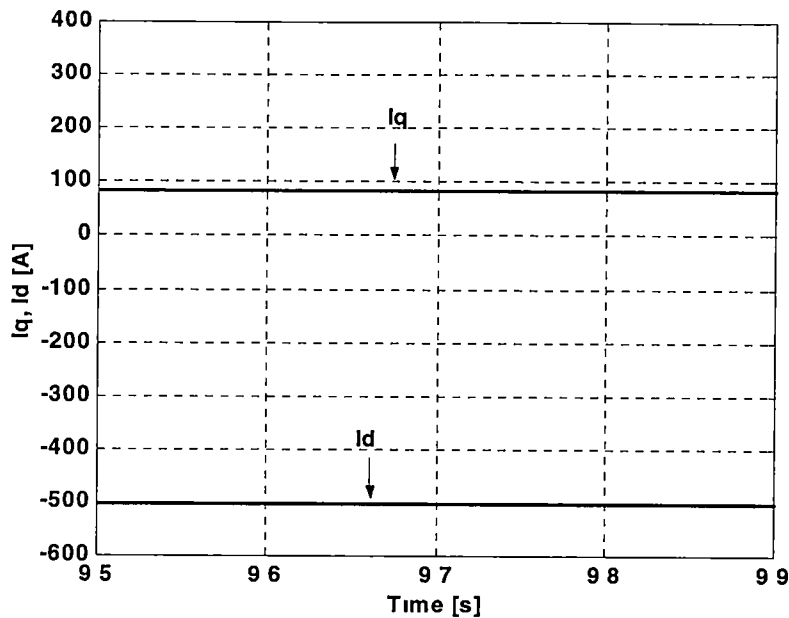


Fig 4.26 i_d and i_q components of the armature current at 3 times base speed (7800 rpm)

Figures 4.27 through 4.30 show the dynamic response of the system during acceleration. The command speed is such that the machine starts from zero speed, stays at base speed until it reaches steady state at that speed. In the sequence the machine is accelerated until the critical speed, and it is held at that speed until it reaches steady state. This acceleration and holding process is repeated for 1.5 and 3 times base speed. Figure 4.27 shows the command and actual rotor speeds. Notice that below base speed, the system has fast response, but as the machine speed goes above base speed, the system response is slow. The system response gets sluggish above base speed because the output voltage of the inverter has already reached its maximum value at base speed. Therefore the system lacks capacity to provide high

torque and fast speed response for the machine. Notice that as the speed increases, the system sluggishness increases because the torque decreases inversely proportional to speed. Figure 4 28 shows the developed torque behavior as speed increases. Figure 4 29 shows the output power of the machine. Notice that the power is held constant above base speed. Figure 4 30 shows the steady state and dynamic behavior of i_q and i_d for machine operating below and above base speed.

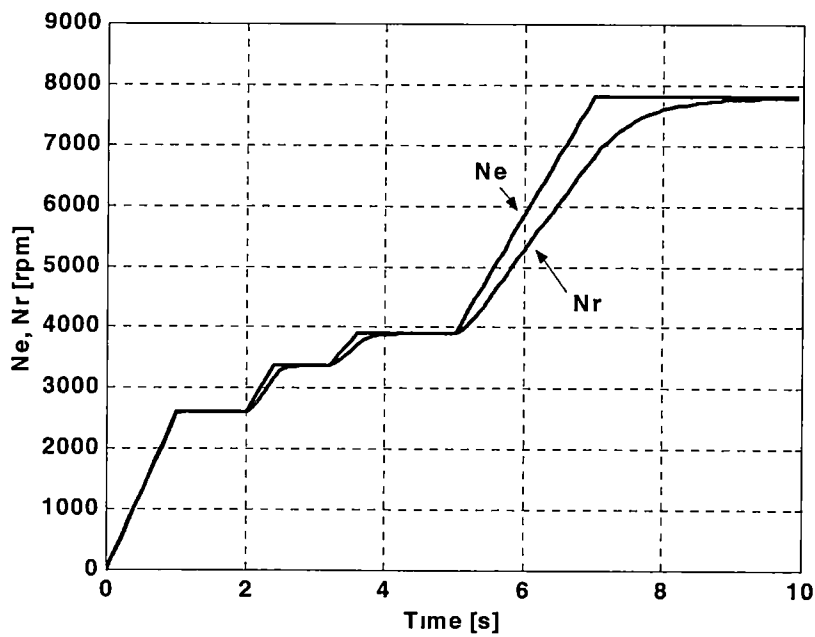


Fig 4 27 Rotor speed dynamic response of the system

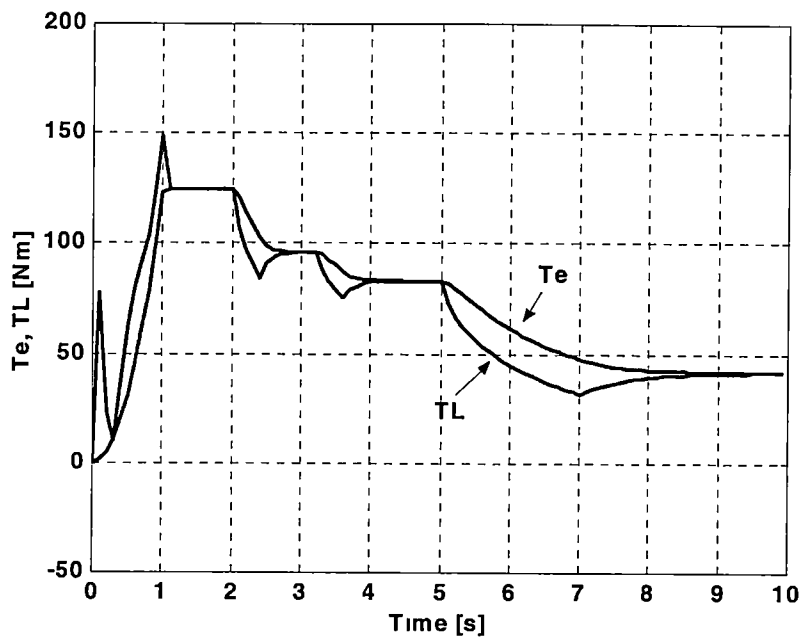


Fig. 4 28 Load and developed torque during machine acceleration

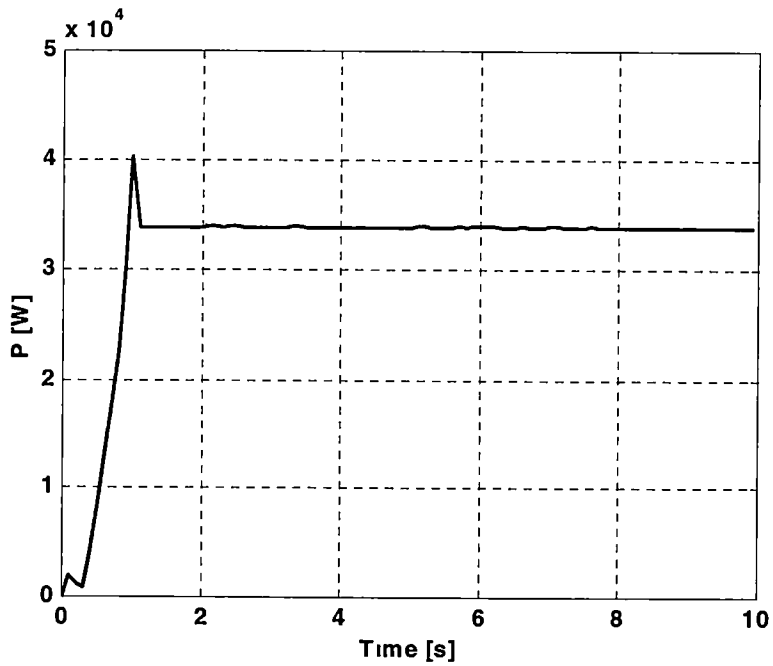


Fig 4 29 Machine output power during machine acceleration

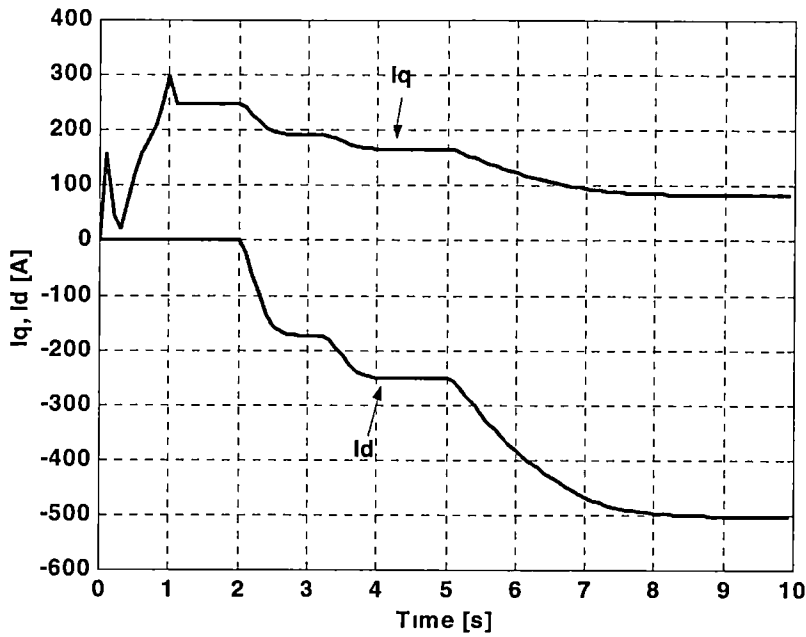


Fig 4.30 i_q and i_d behavior during machine acceleration

IV.6 – Conclusions

Vector control of PMSM with field weakening was described. Analysis of the operation limits of the system was done. This analysis considers the voltage and current limits. The result of this analysis showed that the constant power operation range of the PMSM when using VC with field weakening technique is narrow for low inductance machines. For the machine under study the CPOR is only 23% of the base speed.

In order to verify the analysis, a SIMULINK model of the system was built and the system was simulated. Steady state and dynamic results at base speed, critical speed and above critical speed were given. The results showed that in order to keep

the machine developing rated power above the base speed the current has to increase above the current limit, which is extremely pernicious to the system. However, if the armature current is kept under the current limit, the machine stops developing rated power at 23% above base speed. Therefore, this technique cannot be used for applications that require high-speed operation. In order to show that DMIC is a better option for these kind of applications, Chapter V will compare the performance of VCFW with DMIC in high speed operation and show that DMIC/PMSM system can develop rated power at high speed without exceeding the current limit, while VCFW/PMSM system cannot.

CHAPTER V

ANALYSIS OF DUAL MODE INVERTER CONTROL

V.1 – Introduction

The vector control technique with field weakening has its principles well explained from the machine perspective. The three-phase model of the machine cannot be used to explain it. It was developed after the advent of the three-phase stationary frame to two-phase rotating frame transformation. Therefore, the stator voltage/current required to drive the PMSM above base speed is obtained from the analysis of d-q machine model using the field weakening principle, as described in Chapter IV. The inverter is then controlled in such a way that it supplies the machine with the required voltage/current. In other words, the field weakening technique was developed based on the machine operation principle. The inverter was assumed to be able to satisfy the voltage/current machine requirement.

The DMIC, described in Chapter III, on the other hand, was developed using the three-phase model of the PMSM machine in adjunct with the inverter operation. The principle of the DMIC is to control the power flowing between the dc link and the machine through the inverter and to avoid regeneration through the bypass diodes when motoring operation is desired. Therefore, the DMIC is well understood using the DC link-machine power flow and the inverter/ac-voltage control; however, it is

not explained from the machine operation point of view. The coupling among the three phases given in the machine model makes it difficult to understand the machine behavior when it is driven by DMIC. Although, the machine is not in three-phase operation when driven by DMIC, it is still possible to apply the three-phase rotating frame to two-phase synchronous frame transformation. The analysis of the d-q model of the PMSM/DMIC system can help to explain DMIC from the machine perspective. The limit of the constant power speed range using DMIC can also be found from this analysis. Therefore, the objective of this work is to explain DMIC by analyzing DMIC driven PMSM using the d-q model of the PMSM.

V.2 – Analytical Equations of the PMSM Armature Phase Currents and Phase Voltages in DMIC/PMSM System

The DMIC driving a PMSM was described in Chapter III. However, there, only the description and simulation results were given. In this section, analytical expressions of the phase currents and phase voltages will be derived.

Above the base speed, the DMIC drives PMSM in two different modes: three-phase operation and single-phase operation. The three-phase operation occurs during commutation and the single-phase operation after commutation is over. The switching states change every 60 degrees, meaning that every 60 degrees there will be a commutation period and a post commutation period. An inverter can operate in 8 different states, six non-zero states and two zero states. This analysis is only

concerned about the six non-zero states. It would seem to be necessary to do the commutation and post commutation analysis for six 60 degree sub-intervals in order to get the analytical expression of the phase currents and voltages for a full cycle. However, the symmetry of the system allows analyzing only one 60 degree subinterval and to obtain the analysis for the next five sub-intervals by shifting and permuting the expressions derived for the first 60 degree sub-interval.

V.2.1 – Analytical Equations of the PMSM Armature Phase Currents

Figure 5.1 shows DMIC driving a PMSM. To derive the analytical expressions of the phase currents for the first 60° sub-interval, consider that in the previous 60° sub-interval the switches Q_5 , T_5 , Q_6 and T_6 were ON. Therefore the machine was operating on two phases, phase b and phase c . Phase b was connected to the negative terminal of the DC power supply and phase c was connected to the positive terminal of the DC power supply. Consider that at the end of that sub-interval the current in phase a was zero, current in phase b was $-I_0$ and current in phase c was I_0 . This is then the initial condition for the 60° sub-interval that will be analyzed, and at this instant the reference is set, i.e., t is zero ($\theta = 0$).

In the subinterval to be analyzed, the machine stops operating in phases c and b , and starts to operate in phases a and b . In other words, in this interval, phase c is the outgoing phase, and phase a is the incoming phase. Initially, when t is zero ($\theta =$

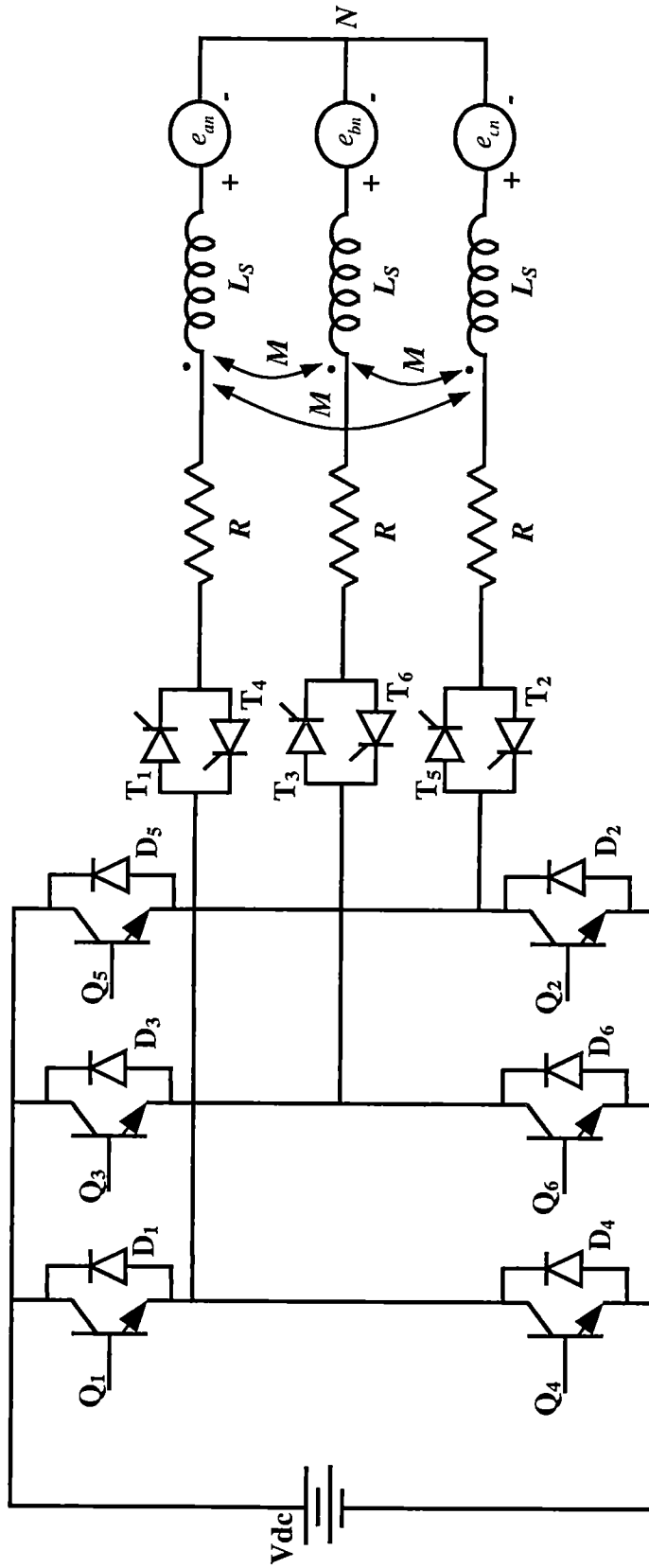


Fig 5.1 DMIC driving a PMSM

0), the switches Q_1 and T_1 are turned ON. The current in phase c commutates to phase a . Switch Q_5 is left ON, but conduction in phase c stops when the current reaches zero causing thyristor T_5 to snap off. Phase c is then isolated from the supply and commutation is complete. During the commutation period, the machine operates in three-phase mode. The commutation period starts at $\theta = 0$, and finishes at $\theta = \theta_c$, where θ_c is the commutation angle. Figure 5.2 shows the DMIC/PMSM circuit during the commutation period. The dark continuous line corresponds to elements that are part of the circuit during this interval, while the gray dashed line corresponds to the elements that are not part of the circuit.

The second order model of PMSM, as given in chapter II, is:

$$\frac{d}{dt} \begin{bmatrix} i_a(t) \\ i_c(t) \end{bmatrix} = \begin{bmatrix} -R/L & 0 \\ 0 & -R/L \end{bmatrix} \begin{bmatrix} i_a(t) \\ i_c(t) \end{bmatrix} + \frac{1}{3L} \begin{bmatrix} 2 & -1 \\ -1 & 2 \end{bmatrix} \begin{bmatrix} v_{ab}(t) - e_{ab}(t) \\ v_{cb}(t) - e_{cb}(t) \end{bmatrix} \quad (5.1)$$

Making the following change of variable

$$\theta = n\omega_b t \quad (5.2)$$

where

ω_b – base speed

n – rotor speed ω_r to base speed ω_b ratio;

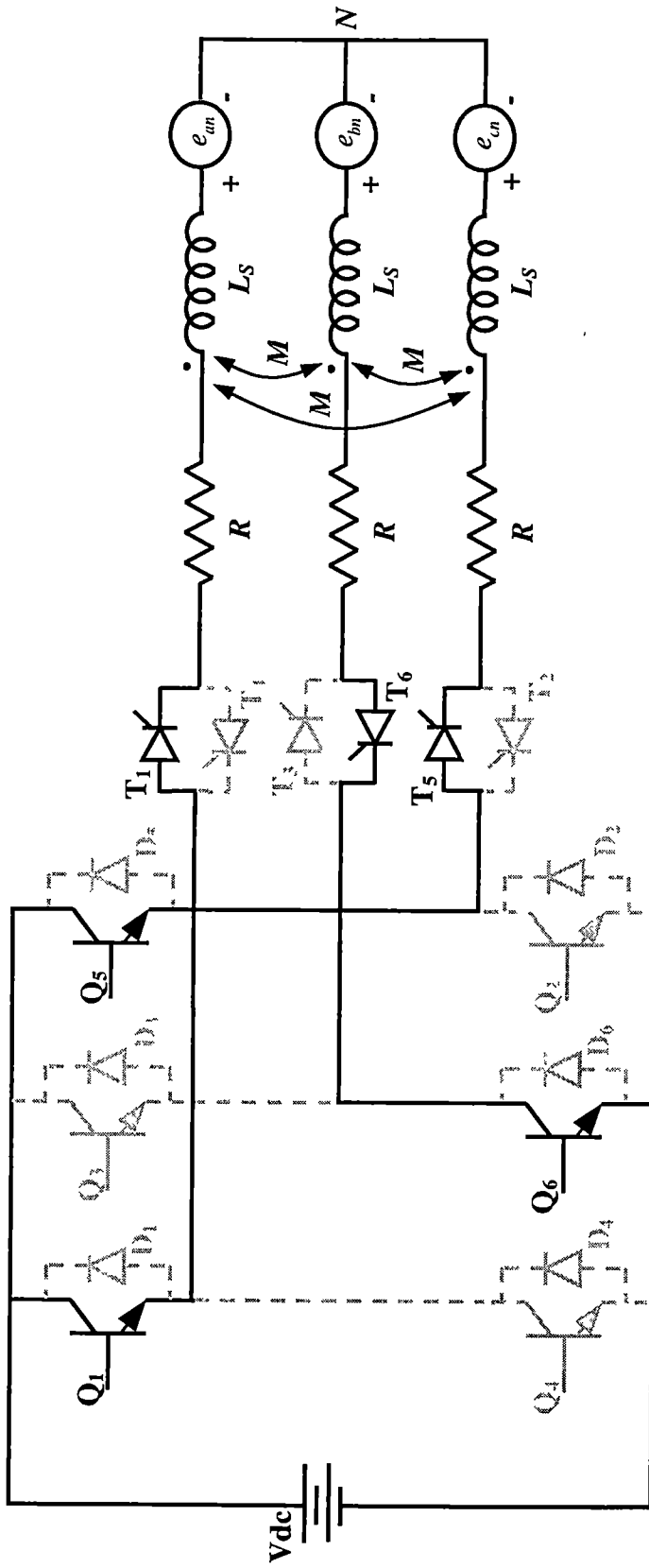


Fig 5 2 DMIC driving a PMSM during commutation period

Substituting Equation 5.2 in 5.1, it results:

$$\frac{d}{d\theta} \begin{bmatrix} i_a(\theta) \\ i_c(\theta) \end{bmatrix} = \frac{1}{n\omega_b} \begin{bmatrix} -R/L & 0 \\ 0 & -R/L \end{bmatrix} \begin{bmatrix} i_a(\theta) \\ i_c(\theta) \end{bmatrix} + \frac{1}{3n\omega_b L} \begin{bmatrix} 2 & -1 \\ -1 & 2 \end{bmatrix} \begin{bmatrix} v_{ab}(\theta) - e_{ab}(\theta) \\ v_{cb}(\theta) - e_{cb}(\theta) \end{bmatrix} \quad (5.3)$$

From the description of DMIC driving a PMSM, in Chapter 3, the switches Q_1 and T_1 are turned ON θ_a degrees before the line-to-line back-emf e_{ab} crosses the DC link voltage value. If the reference $t = 0$ ($\theta=0$) is set in the instant that Q_1 and T_1 are turned on, then Figure 5.3 shows the line-to-line back emf e_{ab} waveform with respect to the reference.

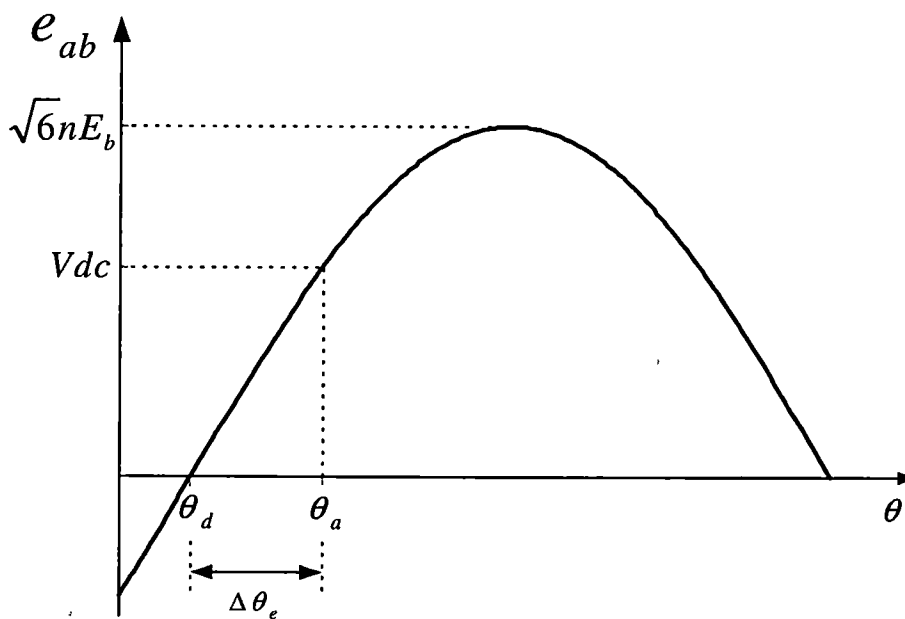


Fig 5.3 Line-to-line Back emf waveform with respect to the reference at

DMIC/PMSM system

From Figure 5 3, the PMSM line-to-line back emfs $e_{ab}(\theta)$ and $e_{cb}(\theta)$ can be described as:

$$e_{ab}(\theta) = \sqrt{6}nE_b \sin(\theta - \theta_d) \quad (5.4)$$

$$e_{cb}(\theta) = \sqrt{6}nE_b \sin\left(\theta - \theta_d + \frac{\pi}{3}\right)$$

In Figure 5 3, θ_a is the advance angle, the angle in advance of the instant that e_{ab} equals V_{dc} where Q_1 and T_1 are fired. Angle θ_d is the delay angle. θ_d is the angle after firing Q_1 and T_1 at which e_{ab} crosses zero. The angle $\Delta\theta_e$ is the difference between θ_a and θ_d and is given by.

$$\Delta\theta_e = \theta_a - \theta_d = \sin^{-1}\left(\frac{V_{dc}}{\sqrt{6}nE_b}\right) \quad (5.5)$$

In this discussion we consider only commutation option 1, and the applied machine armature voltages v_{ab} and v_{cb} during commutation are

$$v_{ab} = v_{cb} = V_{dc} \quad (5.6)$$

Therefore, for $0 \leq \theta \leq \theta_c$, disregarding the winding resistance R , the state model of the circuit shown in Figure 5 2 is:

$$\frac{d}{d\theta} \begin{bmatrix} i_a(\theta) \\ i_c(\theta) \end{bmatrix} = \frac{1}{3n\omega_b L} \begin{bmatrix} 2 & -1 \\ -1 & 2 \end{bmatrix} \begin{bmatrix} V_{dc} - e_{ab}(\theta) \\ V_{dc} - e_{cb}(\theta) \end{bmatrix} \quad (5.7)$$

The first order differential equations above were solved with the following boundary values

$$\begin{aligned} i_a(0) &= 0 & i_a(\theta_c) &= I_1 \\ i_b(0) &= -I_0 & i_b(\theta_c) &= -I_1 \\ i_c(0) &= I_0 & i_c(\theta_c) &= 0 \end{aligned} \quad (5.8)$$

The analytical expressions of phase currents during the commutation period are:

$$\begin{aligned} i_a(\theta) &= \frac{1}{3n\omega_b L} \left(V_{dc}\theta - 3\sqrt{2}nE_b \sin\left(\theta - \theta_d - \frac{2\pi}{3}\right) - 3\sqrt{2}nE_b \sin\left(\theta_d + \frac{2\pi}{3}\right) \right) \\ i_b(\theta) &= -\frac{1}{3n\omega_b L} \left(2V_{dc}\theta - 3\sqrt{2}nE_b \sin\left(\theta - \theta_d - \frac{2\pi}{3}\right) - 3\sqrt{2}nE_b \sin(\theta - \theta_d) - \right. \\ &\quad \left. 3\sqrt{2}nE_b \sin\left(\theta_d + \frac{2\pi}{3}\right) - 3\sqrt{2}nE_b \sin(\theta_d) \right) - I_0 \\ i_c(\theta) &= \frac{1}{3n\omega_b L} \left(V_{dc}\theta - 3\sqrt{2}nE_b \sin(\theta - \theta_d) - 3\sqrt{2}nE_b \sin(\theta_d) \right) + I_0 \end{aligned} \quad (5.9)$$

where I_0 and I_1 are given by

$$I_0 = -\frac{1}{3n\omega_b L} \left(V_{dc} \theta_c - 3\sqrt{2}nE_b \sin(\theta_c - \theta_d) - 3\sqrt{2}nE_b \sin(\theta_d) \right) \quad (5.10)$$

$$I_1 = \frac{1}{3n\omega_b L} \left(V_{dc} \theta_c - 3\sqrt{2}nE_b \sin\left(\theta_c - \theta_d - \frac{2\pi}{3}\right) - 3\sqrt{2}nE_b \sin\left(\theta_d + \frac{2\pi}{3}\right) \right)$$

After the commutation period is over, the phase c current reaches zero and thyristor T_5 turns OFF. From this point on, the machine starts to operate in single-phase, i.e., on two phases a and b . Figure 5.4 shows the active circuit between the instant that the commutation is over and the end of the 60° sub-interval. Therefore this circuit is valid for θ between θ_c and $\pi/3$.

Equation 5.11 gives the first order model of the circuit in two-phase operation.

$$\frac{di_a(t)}{dt} = \frac{1}{2L} (v_{ab}(t) - e_{ab}(t)) \quad (5.11)$$

The boundary values for the first order differential equation above are

$$\begin{aligned} i_a(\theta_c) &= I_1 & i_a\left(\frac{\pi}{3}\right) &= I_0 \\ i_b(\theta_c) &= -I_1 & i_b\left(\frac{\pi}{3}\right) &= -I_0 \\ i_c(\theta_c) &= 0 & i_c\left(\frac{\pi}{3}\right) &= 0 \end{aligned} \quad (5.12)$$

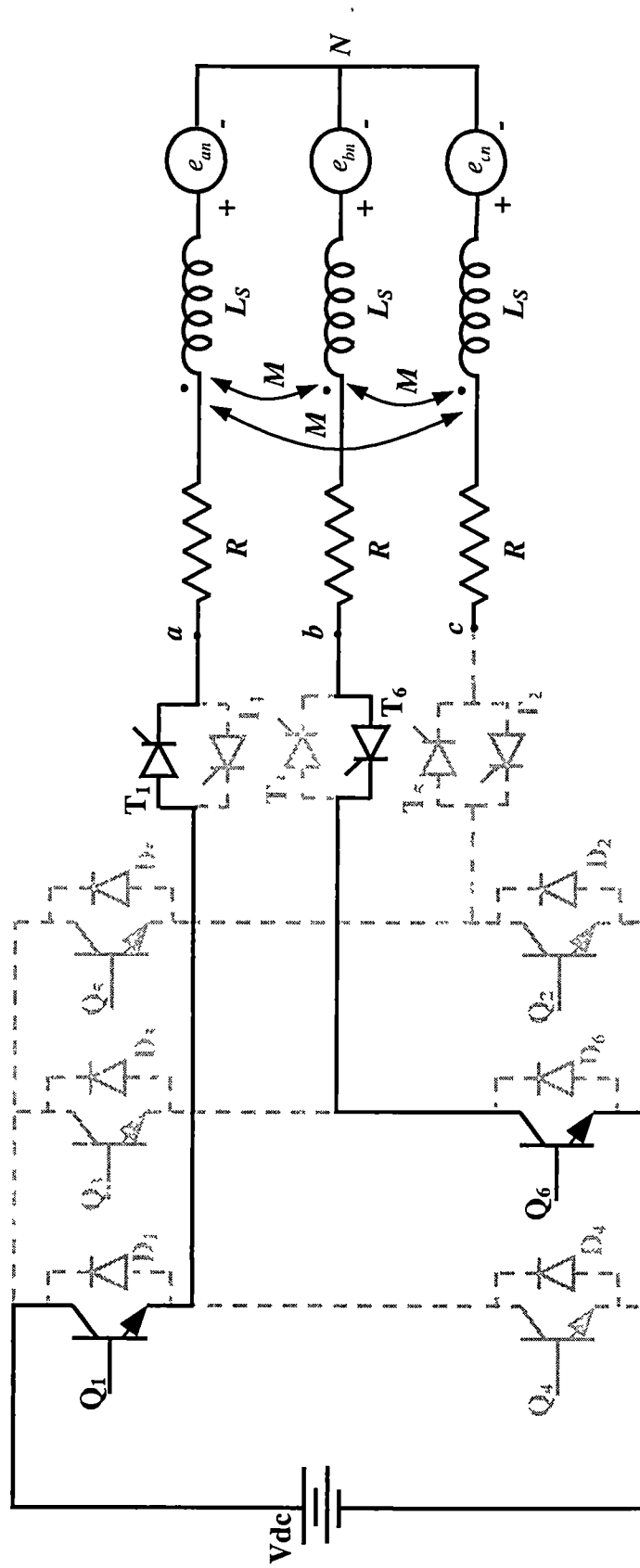


Fig 5 4 DMIC driving a PMSM after commutation period

Equation 5.13 gives the phase currents obtained solving Equation 5.11 subject to the boundary values given in Equation 5.12.

$$i_a(\theta) = \frac{1}{2n\omega_b L} \left(V_{dc} (\theta - \theta_c) - \sqrt{6}nE_b \sin\left(\theta - \theta_d - \frac{\pi}{2}\right) + \sqrt{6}nE_b \sin\left(\theta_c - \theta_d - \frac{\pi}{2}\right) \right) + I_1$$

$$i_b(\theta) = -\frac{1}{2n\omega_b L} \left(V_{dc} (\theta - \theta_c) - \sqrt{6}nE_b \sin\left(\theta - \theta_d - \frac{\pi}{2}\right) + \sqrt{6}nE_b \sin\left(\theta_c - \theta_d - \frac{\pi}{2}\right) \right) - I_1 \quad (5.13)$$

$$i_c(\theta) = 0$$

Equations 5.9, 5.10, and 5.13 completely describe the phase currents in the 60° sub-interval under consideration as functions of the system parameters and the commutation angle θ_c . The commutation angle θ_c can be found from Equation 5.14

$$\frac{\pi V_{dc}}{3nE_b} + \sqrt{2} \sin\left(\theta_d - \frac{\pi}{3}\right) + \frac{V_{dc}}{3nE_b} \theta_c - \sqrt{2} \sin(\theta_c - \theta_d) = 0 \quad (5.14)$$

Equation 5.14 is an implicit equation of θ_c and the system parameters. Therefore, the phase current equations cannot be found explicitly only as function of the system parameters. An approximation of Equation 5.14 could be found, but this would give some errors in the results. The choice then is to numerically solve Equation 5.14, to find θ_c , and to use the value of θ_c in Equations 5.9, 5.10, and 5.13. Then the phase current equations will be only functions of the system parameters.

To test the equations, a MATLAB code was written, and the same system parameters given in Table 4.1 were used. Figure 5.5 shows the phase currents i_a , i_b and i_c for the machine operating at 5 times base speed. The current waveforms are similar to those current waveforms in Figure 3.10. The difference in the peak value is because that, unlike the PSpice simulator where all machine parameters were considered, in the present analytical equations the winding resistance was disregarded. The winding resistance causes the peak value of the phase currents from the PSpice simulation to be smaller, since it increases the machine impedance.

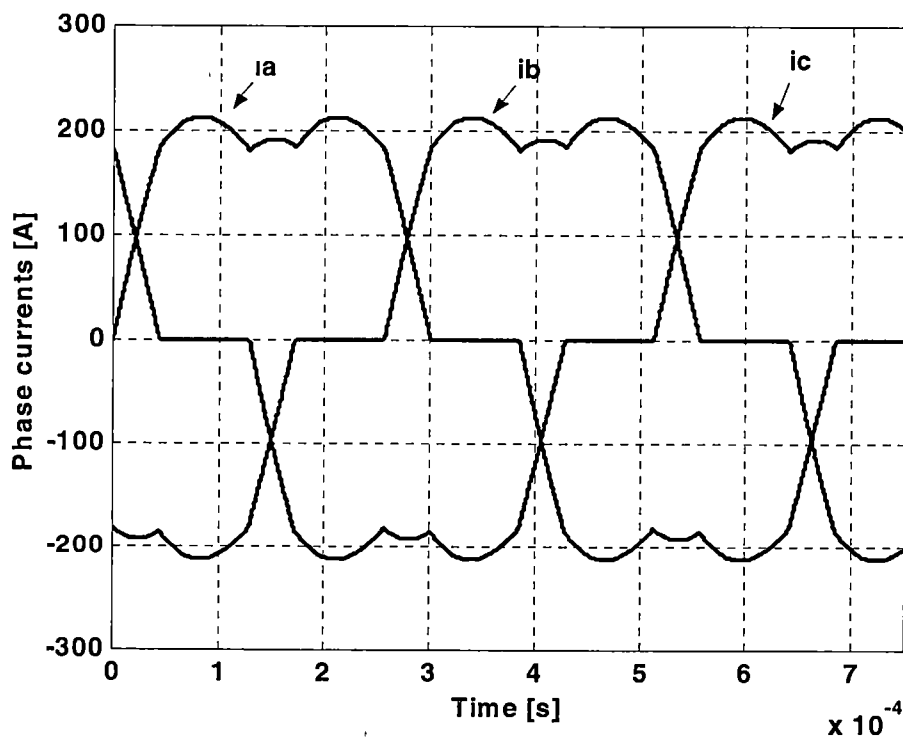


Fig 5.5 Armature phase currents for the machine operating at 5 times base speed

The current waveforms in Figure 5.5 does not help to explain the DMIC principles from the machine point of view. The next sections of this chapter will explain it using the d-q current components.

V.2.2 – Analytical Equations of the PMSM Phase Voltages

During the commutation period, because each phase has a thyristor conducting, the phase voltages at the PMSM armature are the phase voltages at the output of the VFI. The armature phase voltage during this interval is then given in Equation 5.15

$$\begin{aligned}
 v_{an} &= \frac{V_{dc}}{3} \\
 v_{bn} &= -\frac{2V_{dc}}{3} \\
 v_{cn} &= \frac{V_{dc}}{3}
 \end{aligned}
 \tag{5.15}$$

After the commutation is over, because both thyristors in one phase are OFF, the phase voltages at the PMSM armature are not the same as the phase voltage at the output of the VFI. In fact, the expressions of the PMSM armature phase voltages are not so obvious to obtain for this interval. During this interval, the DMIC/PMSM system is in two-phase operation. The difference of potential between the machine neutral point and a fictitious center tap of the DC link voltage v_{n0} is not one third of

the sum of the three phase-to-middle point of DC link voltages v_{a0} , v_{b0} , and v_{c0} . Therefore, the equations generally used to obtain the phase-to-neutral voltages are not valid. For this operation, the mesh analysis of the circuit must be done. Equation 5.16 shows the equation to be solved in order to obtain the expressions of phase-to-neutral PMSM armature voltages. These equations were derived based on the circuit shown in Figure 5.4.

$$\begin{aligned}
 v_{an} &= L_s \frac{di_a}{dt} + e_{an} \\
 v_{bn} &= L_s \frac{di_b}{dt} + e_{bn} \\
 v_{cn} &= e_{cn}
 \end{aligned} \tag{5.16}$$

Using expressions of the phase currents given in Equation 5.13 to solve Equation 5.16, the following expressions for PMSM armature phase voltages are found

$$\begin{aligned}
 v_{an} &= \frac{V_{dc}}{2} - \frac{\sqrt{6}E_b n}{2} \cos\left(n\omega_b t - \theta_d - \frac{\pi}{2}\right) + \sqrt{2}E_b n \sin\left(n\omega_b t - \theta_d - \frac{\pi}{6}\right) \\
 v_{bn} &= -\frac{V_{dc}}{2} - \frac{\sqrt{6}E_b n}{2} \cos\left(n\omega_b t - \theta_d - \frac{\pi}{2}\right) + \sqrt{2}E_b n \sin\left(n\omega_b t - \theta_d - \frac{\pi}{6}\right) \\
 v_{cn} &= \sqrt{2}E_b n \sin\left(n\omega_b t - \theta_d + \frac{\pi}{2}\right)
 \end{aligned} \tag{5.17}$$

Figure 5.6 shows the phase voltages for a full cycle. This figure was plotted using a MATLAB code that implemented Equations 5.16 and 5.17.

The voltage waveforms shown in Figure 5.6 do not give much information about the power conversion process in the DMIC/PMSM drive system. However, they show that the voltages assume higher amplitudes than the square-wave operation case of the standard VFI.

V.3 – Equations of the dq Components of the Armature Current and Voltage

The analytical equations of phase currents and voltages of the PMSM when

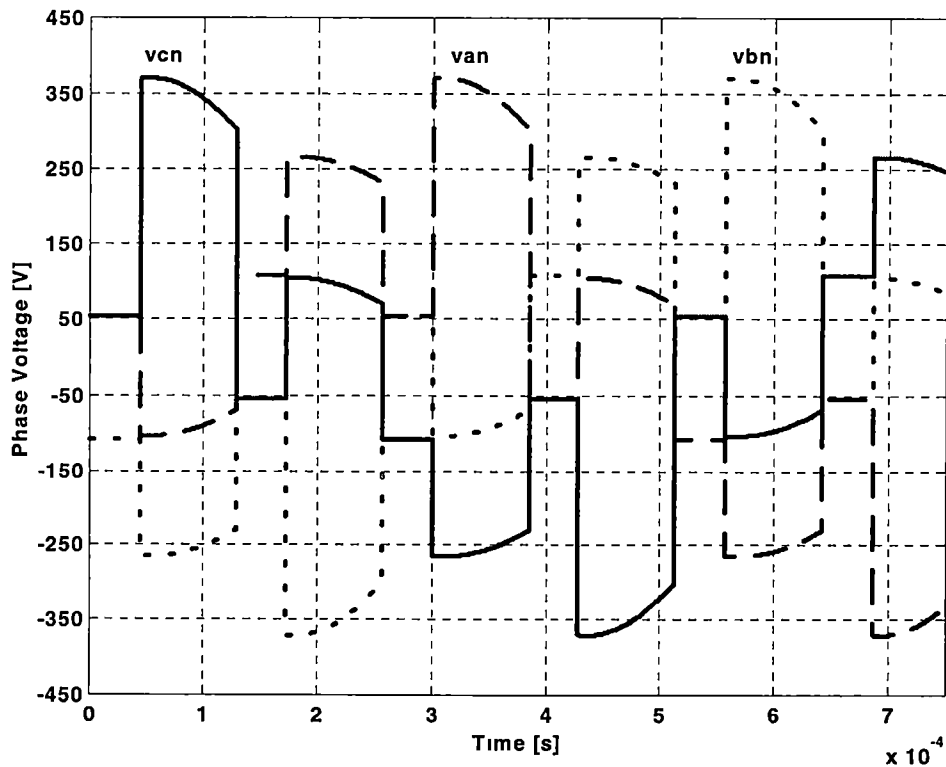


Fig 5.6 Armature phase voltages for the machine operating at 5 times base speed

PMSM is driven by DMIC were derived in the previous section. However, these equations do not explain why the PMSM can develop rated power at speeds as high as 5 times base speed without exceeding the current limit. In this section, analytical expressions of i_d , i_q , v_d , and v_q are derived. These expressions and the dq model of the PMSM will be used to explain the capability of the DMIC to drive PMSM at high speeds. The i_d , i_q , v_d , and v_q expressions are obtained by applying the abc to dq transformation to the phase current and voltage equations obtained in the previous sections.

V.3.1 – Equations of the dq Components of the Armature Current

As shown in Figure 5.1, the PMSM is wye connected, therefore, Equation 5.18 gives the abc to d-q transformation of the current

$$\begin{bmatrix} i_q \\ i_d \end{bmatrix} = \frac{2}{3} \begin{bmatrix} \cos \theta & \cos(\theta - 2\pi/3) & \cos(\theta + 2\pi/3) \\ \sin \theta & \sin(\theta - 2\pi/3) & \sin(\theta + 2\pi/3) \end{bmatrix} \begin{bmatrix} i_a \\ i_b \\ i_c \end{bmatrix} \quad (5.18)$$

As it was done for the phase current, the derivation of i_d and i_q currents will be done initially for 60° sub-interval, and the results will be shifted and permuted in order to obtain the whole 360° cycle. The transformation given in Equation 5.18 is applied in one 60° sub-interval. Within the 60° subinterval, the transformation must

be applied twice, during the commutation period and after the commutation period is over.

Equation 5 19 shows i_d and i_q equations of the PMSM armature current during the commutation period.

$$i_q = \frac{KVdc}{\sqrt{6}E_b} t \sin\left(n\omega_b t - \theta_d + \frac{\pi}{6}\right) - \frac{K}{\omega_b} \sin\left(\theta_d + \frac{2\pi}{3}\right) \sin(n\omega_b t - \theta_d) - \frac{KVdc}{3\sqrt{2}E_b} t_c \sin\left(n\omega_b t - \theta_d + \frac{\pi}{3}\right) + \frac{K}{\omega_b} \sin(\theta_c - \theta_d) \sin\left(n\omega_b t - \theta_d + \frac{\pi}{3}\right) \quad (5 19)$$

$$i_d = \frac{KVdc}{\sqrt{6}E_b} t \sin\left(n\omega_b t - \theta_d - \frac{\pi}{3}\right) - \frac{3K}{2\sqrt{3}\omega_b} + \frac{K}{\omega_b} \sin\left(\theta_d + \frac{2\pi}{3}\right) \sin\left(n\omega_b t - \theta_d + \frac{\pi}{2}\right) - \frac{KVdc}{3\sqrt{2}E_b} t_c \sin\left(n\omega_b t - \theta_d - \frac{\pi}{6}\right) + \frac{K}{\omega_b} \sin(\theta_c - \theta_d) \sin\left(n\omega_b t - \theta_d - \frac{\pi}{6}\right)$$

where $K = \frac{2\sqrt{6}E_b}{3L}$

$n = \frac{\omega_r}{\omega_{rb}}$ - actual and base speed ratio

$t_c = \frac{\theta_c}{n\omega_b}$ - commutation period

After commutation is over, the equations for i_d and i_q currents are.

$$\begin{aligned}
i_q(t) = & \frac{KVdc}{6\sqrt{2}E_b}(3t-t_c)\sin(n\omega_b t - \theta_d) + \frac{\sqrt{3}K}{4\omega_b}\sin(2(n\omega_b t - \theta_d)) + \\
& \frac{\sqrt{3}K}{2\omega_b}\sin\left(\theta_c - \theta_d - \frac{\pi}{2}\right)\sin(n\omega_b t - \theta_d) - \frac{K}{\omega_b}\sin\left(\theta_c - \theta_d - \frac{2\pi}{3}\right)\sin(n\omega_b t - \theta_d) - \\
& \frac{K}{\omega_b}\sin\left(\theta_d + \frac{2\pi}{3}\right)\sin(n\omega_b t - \theta_d)
\end{aligned} \tag{5 20}$$

$$\begin{aligned}
i_d(t) = & \frac{KVdc}{6\sqrt{2}E_b}(3t-t_c)\sin\left(n\omega_b t - \theta_d - \frac{\pi}{2}\right) - \frac{\sqrt{3}K}{4\omega_b} + \frac{\sqrt{3}K}{4\omega_b}\sin\left(2(n\omega_b t - \theta_d) - \frac{\pi}{2}\right) + \\
& \frac{\sqrt{3}K}{2\omega_b}\sin\left(\theta_c - \theta_d - \frac{\pi}{2}\right)\sin\left(n\omega_b t - \theta_d - \frac{\pi}{2}\right) - \frac{K}{\omega_b}\sin\left(\theta_c - \theta_d - \frac{2\pi}{3}\right)\sin\left(n\omega_b t - \theta_d - \frac{\pi}{2}\right) - \\
& \frac{K}{\omega_b}\sin\left(\theta_d + \frac{2\pi}{3}\right)\sin\left(n\omega_b t - \theta_d - \frac{\pi}{2}\right)
\end{aligned}$$

Therefore, equations 5 19 and 5 20 are the analytical expressions of i_d and i_q over a 60° interval Figure 5.7 shows the i_d , and i_q currents for the machine operating at 5 times base speed This is the same operating point as the one for the phase currents shown in Figure 5 5

As we can see from Figure 5 7, the currents i_d and i_q repeat at all six 60° sub-intervals It means that i_d and i_q are periodic functions of the time, and the period is six times smaller than the fundamental period of the three-phase currents In other words, the frequency of the i_d and i_q currents is 6 times the fundamental frequency Therefore, equations 5.19 and 5 20 fully describe the behavior of i_d and i_q when PMSM is driven by DMIC.

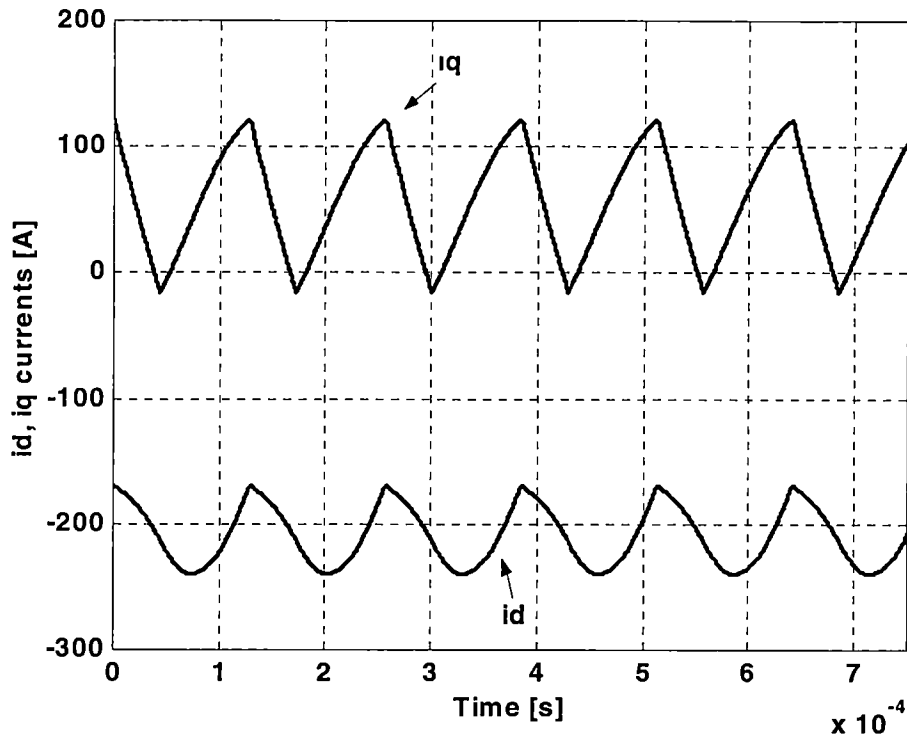


Fig 5.7 i_d and i_q currents for the machine operating at 5 times base speed

V.3.2 – Equations of the dq Components of the Armature Voltage

Equation 5.21 gives the abc to dq transformation of the armature voltages.

$$\begin{bmatrix} v_q \\ v_d \end{bmatrix} = \frac{2}{3} \begin{bmatrix} \cos \theta & \cos(\theta - 2\pi/3) & \cos(\theta + 2\pi/3) \\ \sin \theta & \sin(\theta - 2\pi/3) & \sin(\theta + 2\pi/3) \end{bmatrix} \begin{bmatrix} v_{an} \\ v_{bn} \\ v_{cn} \end{bmatrix} \quad (5.21)$$

Following the same strategy done for the currents, the dq expressions of the voltages were found Equation 5 22 shows the expressions of v_d and v_q voltages during the commutation period

$$v_q = \frac{2V_{dc}}{3} \sin\left(\theta - \theta_d + \frac{\pi}{6}\right)$$

$$v_d = \frac{2V_{dc}}{3} \sin\left(\theta - \theta_d - \frac{\pi}{3}\right)$$
(5 22)

Equation 5 23 shows the expressions of v_d and v_q voltages after the commutation period is over

$$v_q = \frac{\sqrt{3}V_{dc}}{3} \sin(n\omega_b t - \theta_d) + \sqrt{2}E_b n \cos^2(n\omega_b t - \theta_d)$$

$$v_d = -\frac{\sqrt{3}V_{dc}}{3} \sin(n\omega_b t - \theta_d) + \frac{\sqrt{2}E_b n}{2} \sin(2(n\omega_b t - \theta_d))$$
(5.23)

Equations 5 22 and 5.23 are the analytical expressions of v_d and v_q over a 60° interval Figure 5 8 shows v_d and v_q for full cycle They are the v_d and v_q equivalent voltages to v_{an} , v_{bn} , and v_{cn} shown in Figure 5 6 Because v_d and v_q are pulsating, it is difficult to understand their effect in the PMSM operation The effect of the d-q voltages and currents given in this section for the PMSM operation is given in the next sections using the average values of the d-q voltages and currents.

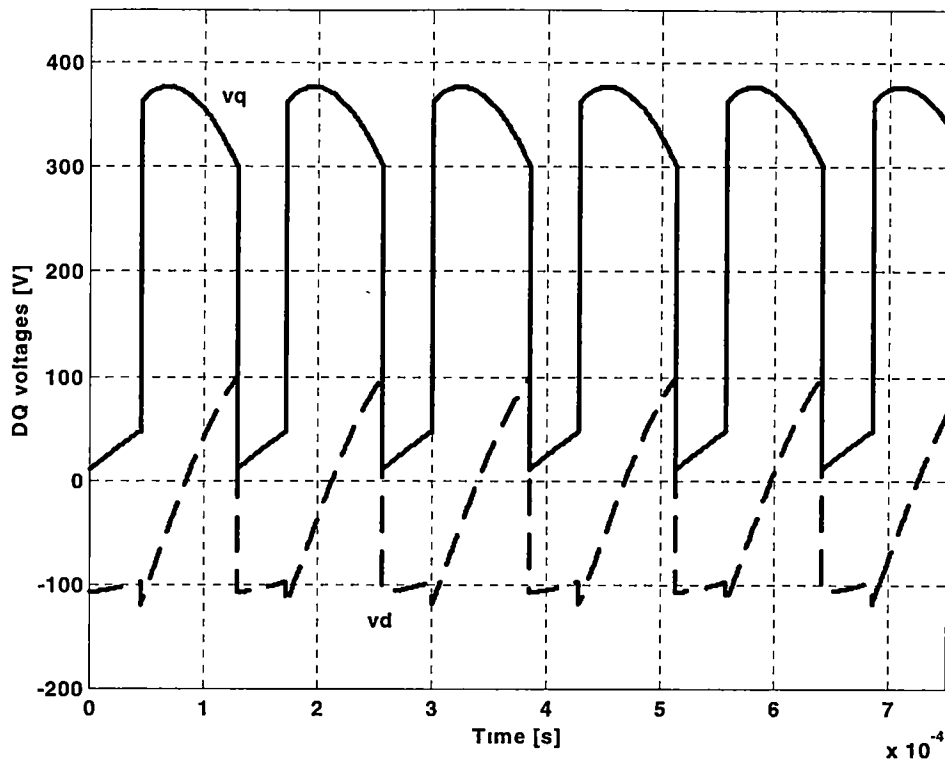


Fig 5.8 v_d and v_q voltages for the machine operating at 5 times base speed

V.4 – Analysis of PMSM Driven by DMIC Using the PMSM dq Model.

The analytical expressions of dq equivalent currents and voltages as functions of the system parameters were derived in section V.3. Therefore, now, the PMSM driven by DMIC can be analyzed using the dq theory. In other words, the same analysis in the dq plane that was done for VC with field weakening (VCFW) will be done for DMIC

However, the analysis in dq plane must be done with DC values, while for DMIC, i_d , i_q , v_d , and v_q , as shown in section V.3, are pulsating. Therefore, the analysis has to be done considering the average values of these variables. The analysis of the

average values of i_d , i_q , v_d , and v_q is a valid approach since we are concerned about the average power developed by the machine and also because the peak values of the equivalent phase currents and voltages at the inverter are monitored not to exceed the switches ratings.

The i_d , i_q expressions are obtained using the definition of average value, as given in (5.24).

$$I_q = \frac{1}{\pi/3} \int_0^{\pi/3} i_q(\theta) d\theta = \frac{3}{\pi} \left[\int_0^{\theta_c} i_{q1}(\theta) d\theta + \int_{\theta_c}^{\pi/3} i_{q2}(\theta) d\theta \right] \quad (5.24)$$

$$I_d = \frac{1}{\pi/3} \int_0^{\pi/3} i_d(\theta) d\theta = \frac{3}{\pi} \left[\int_0^{\theta_c} i_{d1}(\theta) d\theta + \int_{\theta_c}^{\pi/3} i_{d2}(\theta) d\theta \right]$$

where.

$i_{q1}(\theta)$ – instantaneous i_q current during commutation interval (Equation 5.19)

$i_{d1}(\theta)$ – instantaneous i_d current during commutation interval (Equation 5.19)

$i_{q2}(\theta)$ – instantaneous i_q current after commutation is over (Equation 5.20)

$i_{d2}(\theta)$ – instantaneous i_d current after commutation is over (Equation 5.20)

The final expressions of the average value of i_d and i_q are very complex and do not give any explicit information about their behavior as functions of speed. For this reason, they are not given.

The expressions of the average values of v_d and v_q were obtained following the steps used for i_d and i_q . However, the expressions for the average value of v_d and v_q are not complicated and they are given by

$$V_q = \frac{3}{\pi} \left[\frac{2V_{dc}}{3} \cos\left(\frac{\pi}{6} - \theta_d\right) - \frac{2V_{dc}}{3} \cos\left(\theta_c - \theta_d + \frac{\pi}{6}\right) + \frac{\sqrt{2}E_b}{2} n \left(\frac{\pi}{3} - \theta_c\right) + \frac{\sqrt{3}V_{dc}}{3} \cos(\theta_c - \theta_d) - \frac{\sqrt{3}V_{dc}}{3} \cos\left(\frac{\pi}{3} - \theta_d\right) + \frac{\sqrt{2}E_b}{4} n \sin\left(\frac{2\pi}{3} - \theta_d\right) - \frac{\sqrt{2}E_b}{4} n \sin(\theta_c - \theta_d) \right] \quad (5.25)$$

$$V_d = \frac{3}{\pi} \left[-\frac{2V_{dc}}{3} \cos\left(\theta_c - \theta_d - \frac{\pi}{3}\right) + \frac{2V_{dc}}{3} \cos\left(-\theta_d - \frac{\pi}{3}\right) - \frac{\sqrt{2}E_b}{4} n \cos\left(\frac{2\pi}{3} - 2\theta_d\right) + \frac{\sqrt{2}E_b}{4} n \cos(2\theta_c - 2\theta_d) \right]$$

The equations of average values of i_d , i_q , v_d and v_q do not result in conclusions about their behavior as functions of speed. However, in Equation 5.25, the factor n , which is the ratio of actual speed to base speed, multiplies some terms of the equation. This implies that the absolute value of the average values of the armature voltages increase as speed increases.

In order to see the behavior of the average values of the currents and voltages as functions of speed, a MATLAB code was written and the average values of the quadrature current I_q , direct current I_d , total armature current I_T , quadrature voltage V_q , direct voltage V_d , and total armature voltage V_T were calculated for the example

motor. Table 5.1 shows these values for speeds varying from 2 to 10 times base speed. These values were obtained for the machine developing rated power and the peak and rms values of the armature phase currents below the limit. Column eight is the voltage circle limit radius calculated using the average values of the voltages for DMIC. Column nine is the voltage circle limit radius for VCFW. This radius is calculated using the maximum output voltage of the VFI.

The results shown in Table 5.1 are meaningful. Table 5.1 shows that the value of the d and q components of the armature current varies, but the total current, which is the magnitude of the vector defined by these components, is almost constant and its value is around the value of current limit 215A. Notice that the current i_q decreases as

Table 5.1 – Average Values of Voltages and Currents

n	I_q (A)	I_d (A)	I_T (A)	V_q (V)	V_d(V)	V (V)	V_{R-DMIC}	V_{R-VCFW}
2	143.74	-160.61	215.54	109.76	-34.55	115.08	478.54	428.88
3	95.87	-194.28	216.65	152.51	-34.55	156.37	433.51	285.92
4	71.89	-204.47	216.75	198.44	-34.50	201.42	418.81	214.44
5	57.62	-209.43	217.21	245.08	-34.59	247.51	411.71	171.55
6	47.95	-211.43	216.84	292.66	-34.45	294.68	408.48	142.96
7	40.94	-212.34	216.25	340.66	-34.45	342.40	406.82	122.54
8	35.81	-212.75	215.75	388.96	-34.25	390.46	405.94	107.22
9	32.00	-215.00	217.36	435.10	-34.69	436.48	403.36	95.31
10	28.78	-214.94	216.85	483.55	-34.47	436.48	403.19	85.78

speed increases following the $\frac{1}{n}$ rule, which assures that the machine develops average power equal to the rated power. On the other hand, the voltages have an interesting behavior. The q component of the voltage increases as the speed increases, but the d component remains constant. Therefore, the total armature voltage increases as speed increases.

In order to understand the influence of the current and voltage behavior on the machine operation, the analysis using the i_q - i_d plane must be done. This is the same analysis as that done for VC with field weakening in Chapter IV. The current limit circle is the same, thus, the voltage limit circle will change. In VCFW, the maximum PMSM armature voltage is the maximum output voltage that the VFI can provide. In the DMIC, the PMSM is not connected to the three-phase output of the VFI, but only to two of them. The third phase is floating and therefore the armature voltage is not the three-phase voltages provided by the VFI, but the voltages given in Equations 5.16 and 5.17. This operating condition, which is guaranteed by the thyristor turning off to avoid regeneration, provides a total armature voltage to the machine that is higher than the output voltage a VFI can provide. Moreover, as shown in Table 5.1, this voltage increases as the speed increases. To better illustrate this phenomenon, waveforms of the three different operating conditions of the PMSM using DMIC and VCFW are plotted.

Figure 5.9 shows a plot of the current and voltage limits of the PMSM using DMIC and VCFW for machine operating at twice the base speed. The current vectors for both drive systems are also shown in this figure. Notice that the current limit

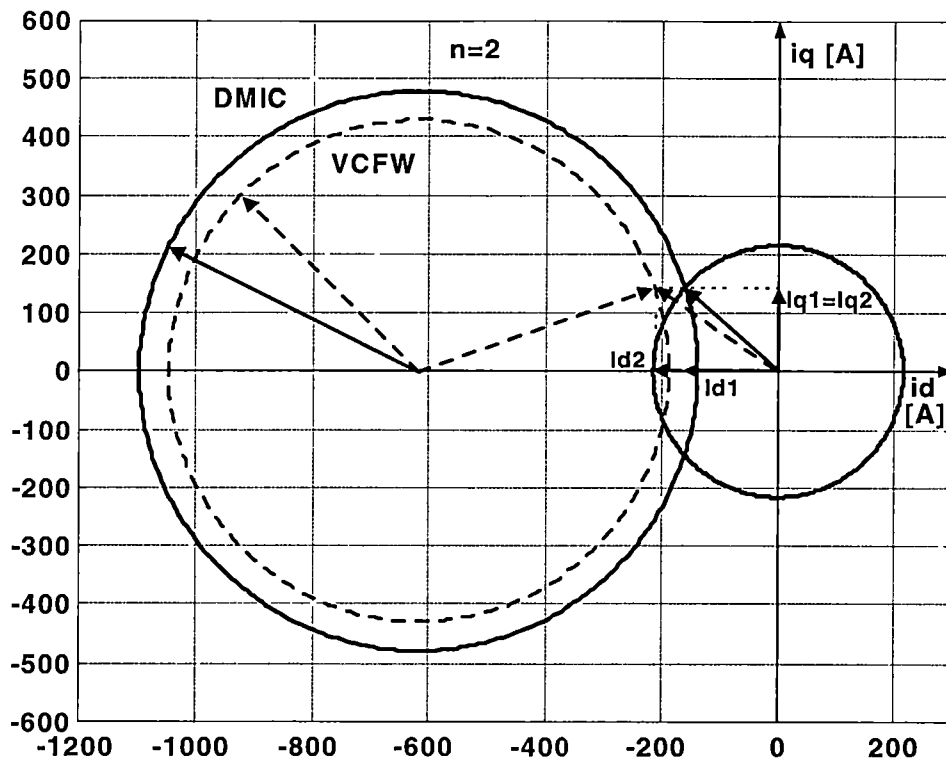


Fig. 5.9 Current and voltage limits of the PMSM using DMIC and VCFW for machine operating at twice the base speed

circle is the same for both techniques, however the voltage limit circle is bigger for DMIC than for VCFW. If i_q is controlled to vary following the $\frac{I_{max}}{n}$ rule, then the machine is assured to be developing rated power. For DMIC driving the machine, the current vector is inside of the intersection of the two circles defined by the current and voltage limits. However, if VCFW is used, the current vector will be either violating the current limit or smaller than what is required to develop rated power.

The capability of the DMIC to drive PMSM above the base speed against the ineffectiveness of VCFW becomes yet more apparent when speed increases. Figure 5 10 shows the plot of i_d - i_q plane for the machine operating at 5 times the base speed. Again notice that in order to develop rated power, the machine when driven by DMIC operates without violating the voltage and current constraints, while when it is driven by VCFW one of the constraints must be violated. It is clear from this figure that the voltage limit shrinks for both techniques, however, it shrinks faster for VCFW than for DMIC

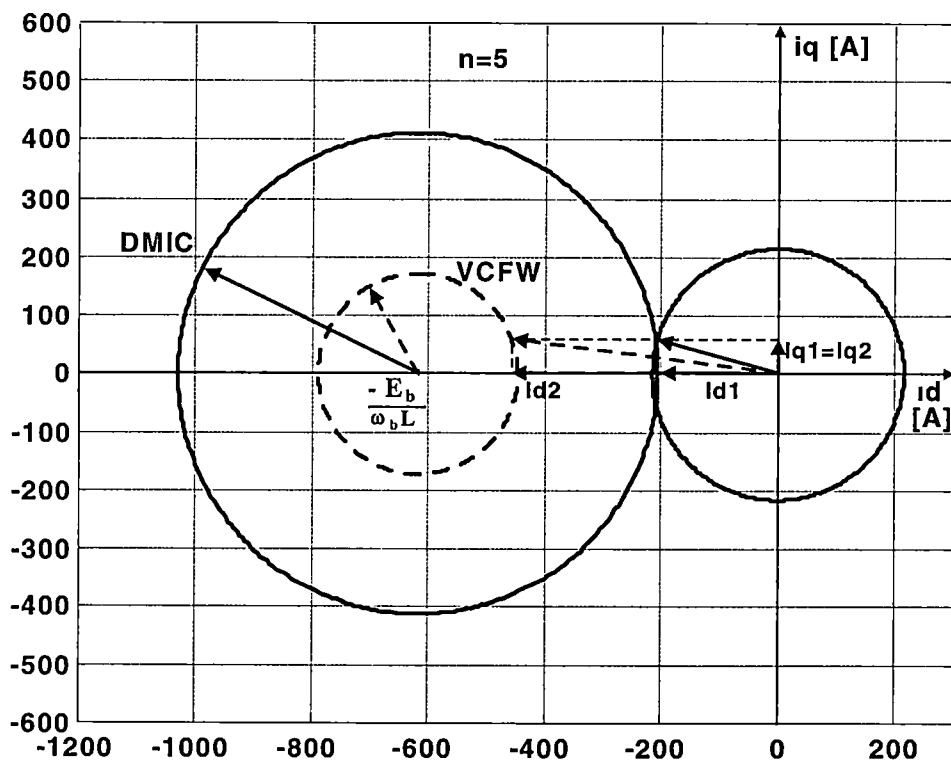


Fig 5 10 Current and voltage limit of the PMSM using DMIC and VCFW for machine operating 5 times base speed

Finally, to show the the superiority of DMIC compared to VCFW more effectively, Figure 5 11 shows the plot of i_d-i_q plane for the machine operating at 9 times the base speed

V.5 – Limit of Constant Power Operation Range of the PMSM Driven by DMIC

The differences between DMIC and VCFW from the machine point of view were identified and analyzed in section V 4 The superiority of DMIC over VCFW in allowing the machine to develop rated power at high speed was pointed out

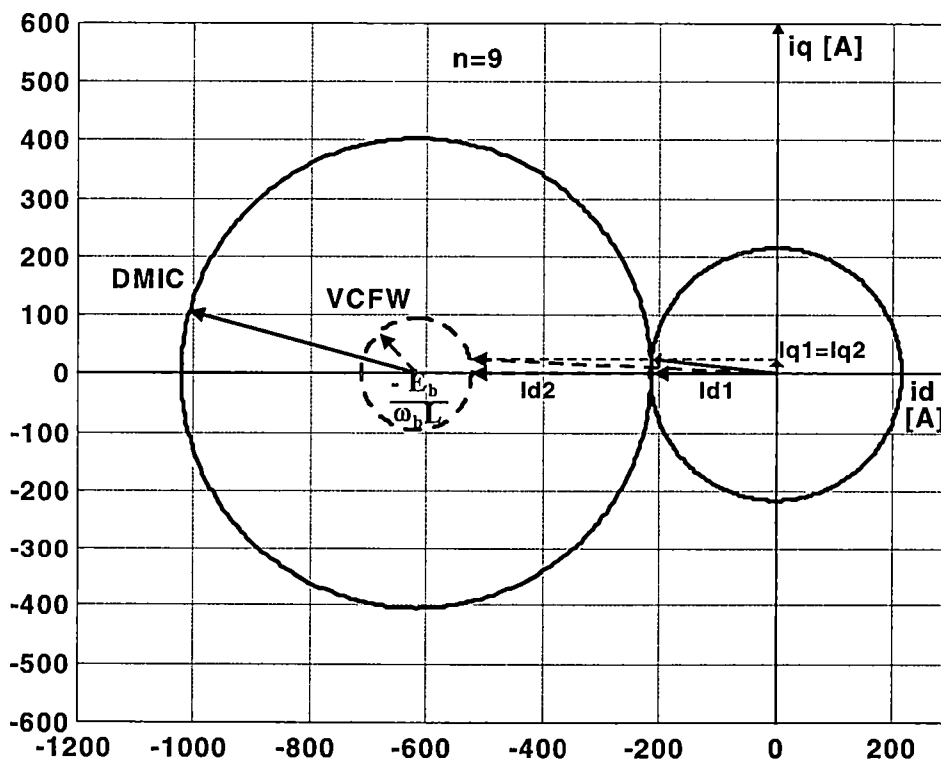


Fig. 5 11 Current and voltage limits of the PMSM using DMIC and VCFW for machine operating 9 times the base speed

However, the question about the speed limit at which the DMIC can drive PMSM developing rated power remains unanswered. This section addresses this subject to show that there is no theoretical limit of CPOR when PMSM is driven by DMIC.

As mentioned before, for the machine to develop rated torque at n times the base speed, the quadrature current at that speed I_{qn} must be controlled following Equation 5.26

$$I_{qn} = \frac{\omega_{rb} I_{max}}{\omega_r} = \frac{I_{max}}{n} \quad (5.26)$$

In order to maintain the total current equal to the current limit I_{max} , I_{dn} must be controlled following Equation 5.27

$$I_{dn} = \sqrt{I_{max}^2 - \left(\frac{I_{max}}{n}\right)^2} = \frac{I_{max}}{n} \sqrt{n^2 - 1} \quad (5.27)$$

The radius of the voltage limit circle at n times base speed is given by.

$$V_{rn} = \frac{V_{an}}{n\omega_b L} \quad (5.28)$$

where V_{an} is the amplitude of machine armature voltage at n times the base speed.

Therefore, to assure meeting both current and voltage constraints and to develop rated torque, Equation 5.29 must be satisfied

$$V_r \geq \sqrt{\left(\frac{E_b}{\omega_b L} - |I_{dn}|\right)^2 + I_{qn}^2} \tag{5.29}$$

The condition established by Equation 5.29 can be better visualized through Figure 5.12. The minimum radius of the voltage limit circle is V_r , which is the

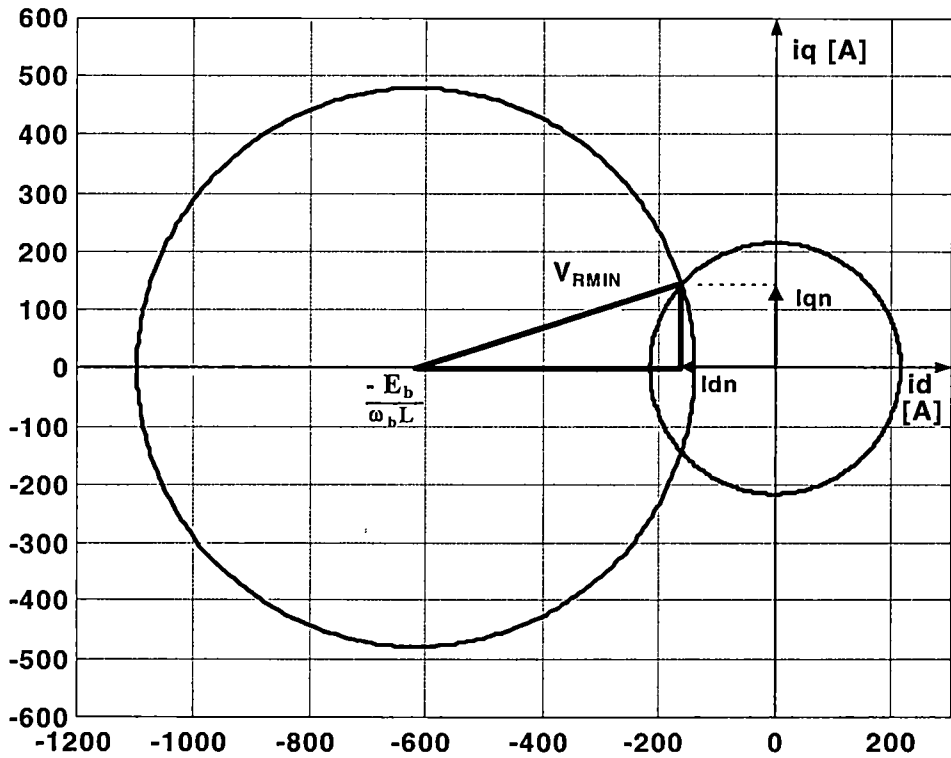


Fig 5.12 Minimum radius of the voltage limit circle for PMSM to develop rated power

hypotenuse of the Pythagorean triangle formed by I_{q_n} , $\frac{E_b}{\omega_b L} - |I_{d_n}|$, and V_r . Notice that the term $\frac{E_b}{\omega_b L}$ is the distance of the center of the voltage limit circle to the origin.

The expression of the minimum radius of the voltage limit circle is V_r as a function of the speed can be found from Equations 5.26, 5.27, and 5.28. Equation 5.30 shows this expression

$$V_r(n) = \sqrt{\left(\frac{E_b}{\omega_b L} - \frac{I_{max}}{n} \sqrt{n^2 - 1}\right)^2 + \left(\frac{I_{max}}{n}\right)^2} \quad (5.30)$$

Therefore, the minimum radius of the voltage limit circle at a certain speed can be calculated using (5.30). Figure 5.13 was plotted to compare the voltage radius provided by DMIC, VCFW, and the minimum radius given in (5.30). The radius provided by DMIC and VCFW are the columns 8 and 9 of the Table 5.1 respectively. The curve MIN represents the minimum voltage limit circle radius necessary for the machine to develop rated power. The figure shows that the DMIC provides voltage circle radius above or equal to the minimum requirement. In fact, for speeds below 5 times the base speed, the radius is bigger than the minimum required. This means that up to 5 times base speed, the machine can actually develop more power than the rated power without exceeding the current limit. On the other hand, the radius provided by VCFW is below the minimum requirement for all speeds above 2 times the base

speed This is coherent with what was stated in Chapter 4, i.e., with VCFW, the rated power can be developed only up to 1.23 times base speed. From Figure 5.13, one can also see that the minimum radius requirement and the radius provided by DMIC tend asymptotically to the 400 level as speed increases. Therefore, the radius provided by DMIC will always satisfy the condition established by (5.29). This leads to the conclusion that the theoretical limit of COPR for DMIC driving PMSM is infinity.

In order to analytically show that the limit of COPR for PMSM driven by PMSM is infinity, a function that approximates the DMIC voltage limit radius V_{R-DMIC}

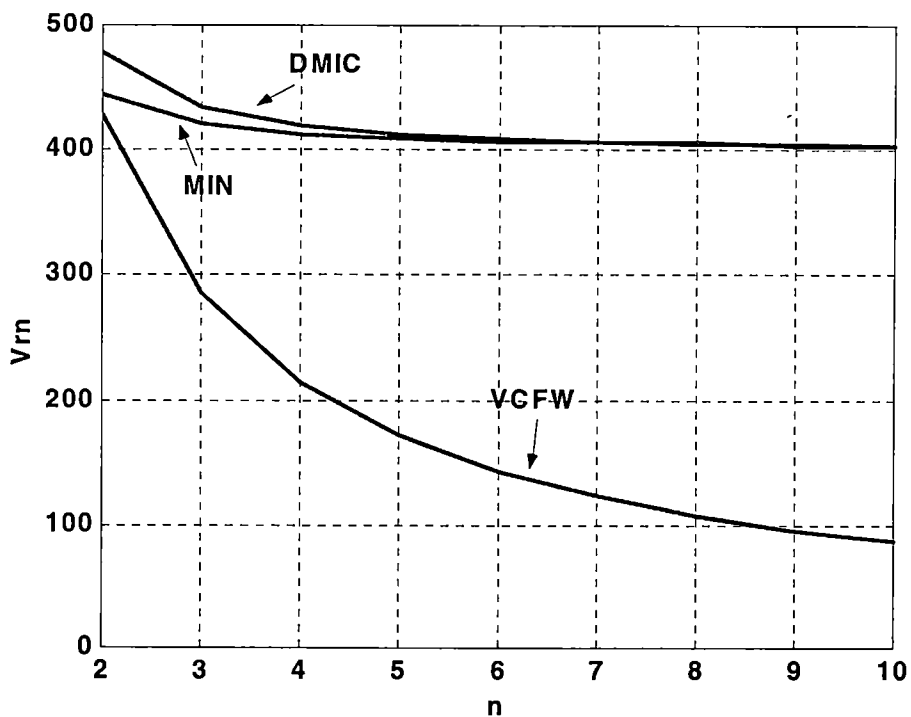


Fig 5.13 Voltage radius provided by DMIC, VCFW, and the minimum radius

as function for speed ratio n was found using the data from Table 5.1. Because the V_{R-DMIC} is similar to that of the minimum radius requirement given in Equation 5.30, the function that was found for V_{R-DMIC} was also similar, only with a different constant. The expression of V_{R-DMIC} as a function of the speed ratio is then given by

$$V_{r-DMIC_n}(n) = \sqrt{\left(\frac{E_b}{\omega_b L} - I_{max} \sqrt{\frac{n^2-1}{n^2}}\right)^2 + \left(\frac{2I_{max}}{n}\right)^2} \quad (5.31)$$

In order to compare the actual V_{R-DMIC} values with the fitting function, their values were plotted and the maximum error was calculated. Figure 5.14 shows the plot of the function versus the actual V_{R-DMIC} values. The figure shows that the function fits the points very well. The maximum error between the function and the actual points is 1.16%.

Now, in order to find a relation between the minimum voltage radius and the voltage limit radius provided by DMIC, the limits of (5.30) and (5.31) were found. Equation (5.32) gives the limit of the $V_r(n)$ as the speed goes to infinity

$$\lim_{n \rightarrow \infty} V_r(n) = \lim_{n \rightarrow \infty} \sqrt{\left(\frac{E_b}{\omega_b L} - I_{max} \sqrt{\frac{n^2-1}{n^2}}\right)^2 + \left(\frac{I_{max}}{n}\right)^2} = \frac{E_b}{\omega_b L} - I_{max} \quad (5.32)$$

The limit of $V_{r-DMIC_n}(n)$ as the speed goes to infinity is given by:

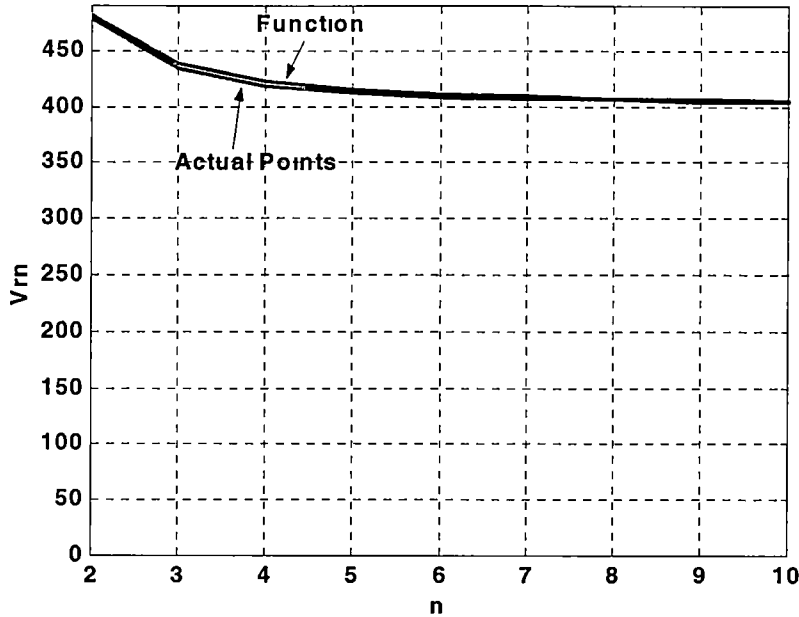


Fig 5.14 Actual and fitting function of the voltage limit radius provided by DMIC

$$\lim_{n \rightarrow \infty} V_{r-DMIC_n}(n) = \lim_{n \rightarrow \infty} \sqrt{\left(\frac{E_b}{\omega_b L} - I_{max} \sqrt{\frac{n^2 - 1}{n^2}}\right)^2 + \left(\frac{2I_{max}}{n}\right)^2} = \frac{E_b}{\omega_b L} - I_{max} \quad (5.33)$$

Equations 5.32 and 5.33 show that both $V_r(n)$ and $V_{r-DMIC_n}(n)$ go to the same value as the rotor speed goes to infinity. This value is $\frac{E_b}{\omega_b L} - I_{max}$. Therefore, this confirms what was stated previous in this section, which is that theoretically there is no limit of CPOR when PMSM is driven by DMIC. It is important to emphasize the relevance of the results given by Equations 5.32 and 5.33, i.e. theoretically a PMSM can be driven at any speed and still develop rated power. This makes possible to use

this type of machine for applications that require high-speed operation, such as electric vehicles

V.6 – Conclusions

The drive system DMIC/PMSM was analyzed in this chapter. The analysis was concerned with explanation of the drive performance above base speed from the machine perspective. Initially, the expressions of the current and voltages of the machine in the three-phase, stationary reference frame were derived. These expressions were shown to be very different from the one with the standard three-phase operation of the machine.

In order to do the analysis of the system performance, the average values of the currents and voltages were used. The average values of the i_d and i_q currents were found to be the required values for the PMSM to develop rated power. However, the armature voltage was found to be higher than that value for standard three-phase operation, and it increases as speed increases.

The plot of the current and voltage limit in the i_d - i_q plane showed that the PMSM armature voltage when DMIC is used provides a voltage limit circle that allows the machine to develop rated power at different speeds. In the same plot, it was shown that the VCFW had a much smaller voltage limit circle, and therefore rated power could not be developed. This was shown for three different speeds, two, five, and nine times the base speed.

Finally, in order to prove the limit of the CPOR when PMSM is driven by DMIC, the theoretical minimum radius of voltage limit circle required for the

machine to develop rated power was found as a function of the system parameters. A fitting function that approximates the radius of voltage limit circle provided by DMIC was found. The function was found to have the same nature of theoretical minimum radius of voltage limit circle. The limits of both functions when speed goes to infinity were found to be the same. Therefore, there is not a theoretical speed limit for DMIC/PMSM drive system. In other words, the DMIC gets rid of the voltage limit circle constraint, and the current circle is then the only constraint for high-speed operation of PMSM.

CHAPTER VI

SUMMARY

VI.1 Conclusions

In this work, Dual Mode Inverter Control driving Permanent Magnet Synchronous Machines has been proposed, simulated and analyzed. The performance of the DMIC/PMSM operating in a wide constant power range has been evaluated.

The PMSM three-phase model in stationary reference frame, as well as its two-phase dq model in synchronously rotating reference frame has been reviewed. The three-phase model is used to explain the strategy used by DMIC to drive a PMSM over the constant power range, while the dq model is used to explain how DMIC can achieve a wide constant power operation range.

The Phase Advance Angle (PHA) method driving a BDCM is described and used for comparison. The method is evaluated through simulation and its performance is found to be poor for low inductance machines. The reason of the inefficiency of PHA for low inductance machine is identified as the regeneration through the bypass diodes of the standard voltage-fed inverter.

DMIC driving a BDCM is presented, and its principle is described. In contrast, the DMIC is shown to be more effective in driving low inductance BDCM.

because of its ability to avoid the bypass diode conduction and therefore the regeneration period.

The efficacy of the DMIC driving BDCM was the motivation to propose using DMIC to drive PMSM, given the large number of similarities between BDCM and PMSM. The same principle used to drive a BDCM above the base speed is used to drive the PMSM, i.e., an ac-voltage controller interfacing the VFI and the machine to block the bypass diode conduction. The PMSM, when driven by DMIC, changes operation from purely three-phase below the base speed, to hybrid operation above the base speed. In the hybrid case, the PMSM is in three-phase operation during the commutation period and single-phase operation after the commutation period is over. The performance of DMIC/PMSM drive system is found to be excellent. Simulation results for the machine operating at five times the base speed show that the machine can develop 15% more than the rated power at this speed with the peak and rms currents exceeding just 11% and 6% the peak and rms rated values respectively.

Vector control of PMSM with field weakening (VCFW) is described and analysis of the operation limits of the system is done. This analysis considers the maximum voltage and current of the machine/inverter system. The result of this analysis shows that the constant power operation range of the PMSM when using VCFW strongly depends on the machine parameters and is narrow for low inductance machines. For the machine under study the CPOR is only 23% of the base speed. High armature current value is the cost of operating PMSM above critical base speed at rated power.

The expressions of the current and voltages of the machine in the three-phase, stationary reference frame and dq rotating reference frame have been derived for the DMIC/PMSM drive system. The average value of the voltages and currents in the dq rotating reference frame was used to model the DMIC/PMSM system from the machine point of view. The principle is found to be the same of the VCFW, where the field component of the armature current is used to weaken the air gap field. However, in VCFW the voltage limit circle is given by the maximum output voltage of the VFI and therefore shrinks fast. In the DMIC, on the other hand, the voltage limit circle is a result of the contribution of DC link voltage, the back emf, and the induced voltage provided by the derivative of the on-phase currents and it shrinks slower as speed increases compared to VCFW. Analysis of the ratio of the voltage limit circle provided by DMIC shows that this circle will always satisfy the maximum current limit condition to provide rated power above the base speed. The conclusion is that there is no inherent speed limit of CPOR when PMSM/DMIC control scheme is used because the voltage constraint is eliminated.

The drawback of the DMIC is the high pulsating torque opposing the constant torque provided by the VCFW. However, considering that the frequency of the pulsating torque is six times the fundamental frequency, the fundamental frequency is high above base speed and moreover, the inertia of the machine and load can filter out the pulsating torque. The pulsating torque should not be a problem for electric vehicle application. Therefore, DMIC is an excellent option if wide constant power operation range is required for high inertia load.

VI.2 Recommendation for future work

This work instigates questions that may be used as topics for future investigation. These questions are mainly related to the control strategy for the transition from below base speed to above base speed and converter topology.

- **Control strategy for the transition from below base speed to above base speed**

DMIC driving PMSM above base speed is addressed in this work, but operation up to base speed and slightly above base speed is not taken into consideration. Standard Vector Control with optimum torque/ampere ratio is widely accepted as the best choice for PMSM operating below base speed. If DMIC is chosen to be used above base speed, then a transition strategy must be developed. The transition has to be carefully analyzed because VC provides constant torque and DMIC provides highly pulsating torque. The two strategies that can be addressed in this topic are described below.

- In this work, the control variables used were the advance angle and the blanking angle. Therefore, a strategy for smooth transition from below base speed to above base speed using advance angle and blanking angle as control variables must be found.

- In the inner loops, VC uses i_d and i_q as the control variables, and they are controlled to be DC. A promising research subject would then be to use current control for DMIC and use the command currents to achieve smooth transition from below to above base speed. This investigation should follow the steps below.

- Generate profiles of i_d and i_q that DMIC would generate as function of speed, and use them as the current command. These profiles are given by i_d and i_q equations shown in this work
- In the transition range, make the currents smoothly changes from DC to the pulsating current required by DMIC

- **Converter topology**

The proposed converter topology works very well and is also the best topology to explain the DMIC principle. However, different topologies that may be more efficient or have lower cost can be investigated.

- **Minimum inductance**

The analysis done in this dissertation refers to a low inductance machine. However the minimum inductance required for DMIC to work was also addressed. Therefore, a complete study of the effect of the inductance in the DMIC/PMSM drive system is an important subject to be investigated.

REFERENCES

- [1] P Pillay; R Krishnan; "Modeling, Simulation, and Analysis of Permanent-Magnet Motor Drives, Part I. The Permanent-Magnet Synchronous Motor Drive", *IEEE Transactions on Industry Applications*, Vol 25, No 2, pp 265-273, March/April 1989
- [2] Thomas M. Jahns, Variable Frequency Permanent Magnet AC Machine Drives, Chapter 6 of the book "*Power Electronics and Variable Frequency Drives*", IEEE Press, New York, 1997;
- [3] J M Bailey, J S. Lawler, B Banerjee, "Five Phase Trapezoidal Back Emf PM Synchronous Machines and Drives", *Proc European Power Electron. Conference*, Florence, Italy, pp: 1-61991.
- [4] A. D P. Kinniment, A Jack, "An Integrated Circuit Controller for Brushless DC Drives", *Proc European Elec Conference (EPE)*, Florence, Vol. 4, pp 111-116, 1991.
- [5] Lee, P. W. and C Pollock, "Rotor Position Detection Techniques for Brushless PM and Reluctance Motor Drives", *IEEE-IAS Annual Meeting Rec* , pp 448-455, 1992
- [6] Wu, R , G R. Slemon, "A Permanent Magnet Motor Control Without a Shaft Sensor", *IEEE-IAS Annual Meeting Rec.*, pp 553-558, 1990.
- [7] P. Pillay; R Krishnan, "Modeling, Simulation, and Analysis of Permanent-Magnet Motor Drives, Part II: The Brushless DC Motor Drive", *IEEE Transactions on Industry Applications*, Vol 25, No 2, pp. 274-279, March/April 1989

- [8] T Sebastian, G R Slemon, "Operating Limits of Inverter-Driven Permanent Magnet Motor Drives", *IEEE Transactions on Industry Applications*, Vol. 23, No 2, pp 327-333, March/April, 1987.
- [9] J S Lawler, J M Bailey, J. W Mckeever, Extended Constant Power Speed Range of the Brushless DC Motor through Dual Mode Inverter Control, ORNL, 1999
- [10] S Morimoto, Y Takeda, T. Hirasu, "Flux-Weakening Control Method for Surface Permanent Synchronous Motors, *Proc. IPEC-Tokyo'90*, pp. 942-949, 1990
- [11] T M Jahns, "Flux-Weakening Regime Operation of an Interior Permanent-Magnet Synchronous Motor Drive", *IEEE Transactions on Industry Applications*, Vol 23, No 4, pp 681-689, July/August 1987
- [12] B Sneyers, D W Novotny, T. A. Lipo, "*Field Weakening in Buried Permanent Magnet AC Motor Drives*", *IEEE Transactions on Industry Applications*, Vol 21, No 2, pp 398-407, March/April 1985
- [13] C C Chan, J. Z. Jiang, W. Xia, K. T Chau, "Novel Wide Range Speed Control of Permanent Magnet Brushless Motor Drives", *IEEE Transactions on Power Electronics*, Vol. 10, No 5, pp 539-546, September, 1995
- [14] C S Cambier, J. F Lutz, "Brushless DC Motor Using Phase Timing Advancement", United States Patent 5677605, October 14, 1997.
- [15] P. C Krause, "*Analysis of electric machinery*", McGraw-Hill, New York, 1986

- [16] T. J. E. Miller, "*Brushless Permanent- Magnet and Reluctance Motor Drives*", Oxford University Press, New York, 1989
- [17] B. K. Bose, "A High-Performance Inverter-Fed Drive System of Interior Permanent Magnet Synchronous Machine", *IEEE Transactions on Industry Applications*, Vol 24, No 6, pp. 987-997, November/December 1988
- [18] S. Morimoto, Y. Takeda, T. Hirasaka, K. Taniguchi, "Expansion of Operating Limits for Permanent Magnet Motor by Current Vector Control Considering Inverter Capacity", *IEEE Transactions on Industry Applications*, Vol 26, No. 5, pp. 866-871, September/October 1990
- [19] M. Bodson, J. Chiasson, L. Tolbert, "A Complete Characterizations of Torque Maximization for Permanent Magnet Non-salient Synchronous Motor", IEEE American Controls Conference, June 25-27, 2001, Arlington, Virginia.
- [20] Y. Sozer, D. A. Torrey, "Adaptive Flux Weakening Control of Permanent Magnet Synchronous Motors" *IEEE-IAS Annual Meeting Rec* , pp 475-482, 1998
- [21] L. Werner, "*Control of Electrical Drives*", Springer-Verlag, Berlin, 1996
- [22] D. W. Novotny, T. A. Lipo, "*Vector Control and Dynamics of AC Drives*", Oxford University Press, New York, 1996.
- [23] A. Kumamoto, Y. Hirane, "A Flux-Weakening Method of a Buried Permanent Magnet Motor with Consideration of Parameter Detuning on System Performance",

- [24] B J Chalmers, L Musaba, D F Gosden, "Performance Characteristics of Synchronous Motor Drives with Surface Magnets and Field Weakening" *IEEE-IAS Annual Meeting Rec.*, pp 511-517, 1996
- [25] L Xu, C. Wang, "Implementation and Experimental Investigation Sensorless Control Schemes for PMSM in Super-High Variable Speed Operation", *IEEE-IAS Annual Meeting Rec.*, pp 483-489, 1998
- [26] J Kim, S. Sul, "Speed Control of Interior Permanent Magnet Synchronous Motor Drive for he Flux Weakening Operation", ", *IEEE Transactions on Industry Applications*, Vol 33, No 1, pp. 43-48, January/February 1997.
- [27] S R. Macminn, T M. Jahns, "Control Techniques for Improved High-Speed Performance of Interior PM Synchronous Motor Drives", *IEEE Transactions on Industry Applications*, Vol 27, No. 5, pp 997-1004, September/October 1991.
- [28] J A. Haylock, B. C. Mecrow, A G. Jack, D. J Atkinson, "Enhaced Current Control of PM Machine Drives Through the Use of Flux Controllers", ", *IEEE-IAS Annual Meeting Rec* , pp 467-474, 1998
- [29] Z. Q Zhu, Y. S. Chen, D. Howe, "Online Optimal Flux-Weakening Control of Permanent-Magnet Brushless AC Drives", *IEEE Transactions on Industry Applications*, Vol 36, No 6, pp 1661-1668, November/December 2000

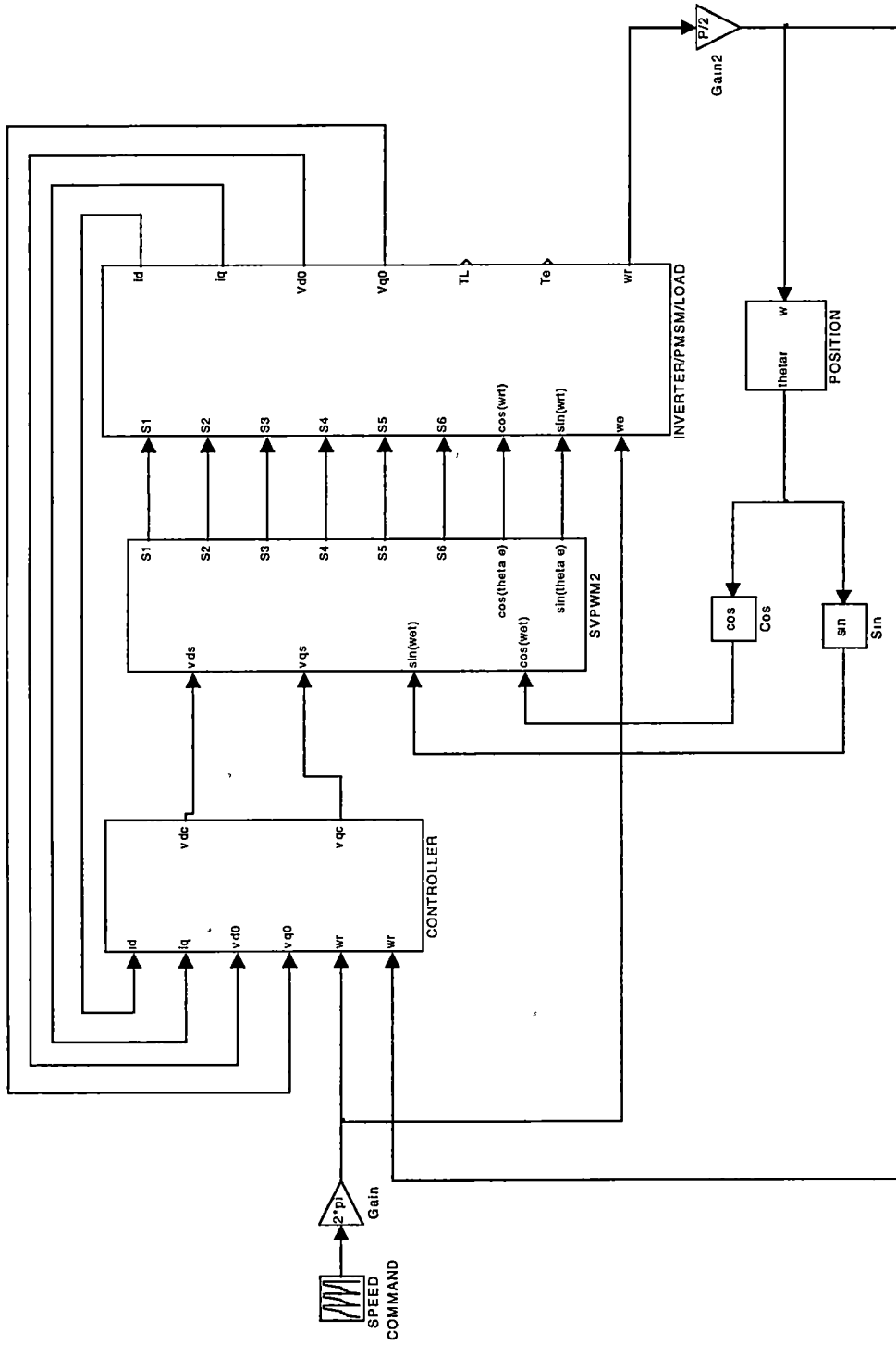
- [30] S. D. Sudhoff, K. A. Corzine, H. J. Hegner, "A Flux-Weakening Strategy for Current-Regulated Surface-Mounted Permanent-Magnet Machine Drives", *IEEE Transactions on Energy Conversion*, Vol 10, No. 3, pp 431-437, September 1995
- [31] L. Xu, L. Ye, L. Zhen, A. El-Antably, "A New Design Concept of Permanent Magnet Machine for Flux Weakening Operation", *IEEE Transactions on Industry Applications*", Vol 31, No 2, pp 373-378, March/April 1995.
- [32] P. Vas, "*Vector Control of AC Machines*" Oxford University Press, New York, 1990
- [33] C. C. Chan, W. Xin, J. Z. Jiang, K. T. Chau, M. L. Zhu, "Permanent Magnet Brushless Drives" *IEEE Industry Applications Magazine*", pp 16-22, November/December 1998.
- [34] J. O. P. Pinto, B. K. Bose, L. E. Borges and M. P. Kazmierkowski, "A neural network based space vector PWM controller for voltage-fed inverter induction motor drive", *IEEE Transactions on Industry Applications*, Vol 36, No 6, pp. 1628-1636, November/December 2000.
- [35] J. Holtz, "Pulse width modulation for electric power conversion", Proc. of the IEEE, vol 82, pp 1194-1214, August 1994.
- [36] J. O. Krah and J. Holtz, "High performance current regulation for low inductance servo motors", *IEEE-IAS Annual Meeting Rec.*, pp. 490-499, 1998.

- [37] A M Hava, R J Kerkman, and T A Lipo, "Carrier-based PWM-VSI overmodulation strategies analysis, comparison, and design", *IEEE Transactions on Power Electronics*, vol. 13, pp 674-689, July 1998
- [38] J Holtz, W Lotzkat and M. Khambadkone, "On continuous control of PWM inverters in the overmodulation range including the six-step mode", *IEEE Transactions on Power Electronics*, vol 8, pp. 546-553, October 1993
- [39] H W Van Der Broeck, H C Skudelny, G Stanke, "Analysis and realization of a pulse width modulator based on voltage space vectors", *IEEE Transactions on Industry Applications*, vol. 24, pp. 142-150, Jan /Feb. 1988
- [40] J. Kim, S. Sul, "A Novel Voltage Modulation Technique of the Space Vector PWM", *International Power Electronics Conference Rec* , Japan, April 1995
- [41] C Ong, "*Dynamic Simulation of Electric Machinery Using Matlab/Simulink*", Prentice Hall, New York, 1997.
- [41] "*MATLAB, The Language of Technical Computing- Version 5 – User's Guide*", Prentice Hall, UpperSaddle River, 1997
- [43] "*MATLAB/SIMULINK User's Guide*", The MathWorks Inc

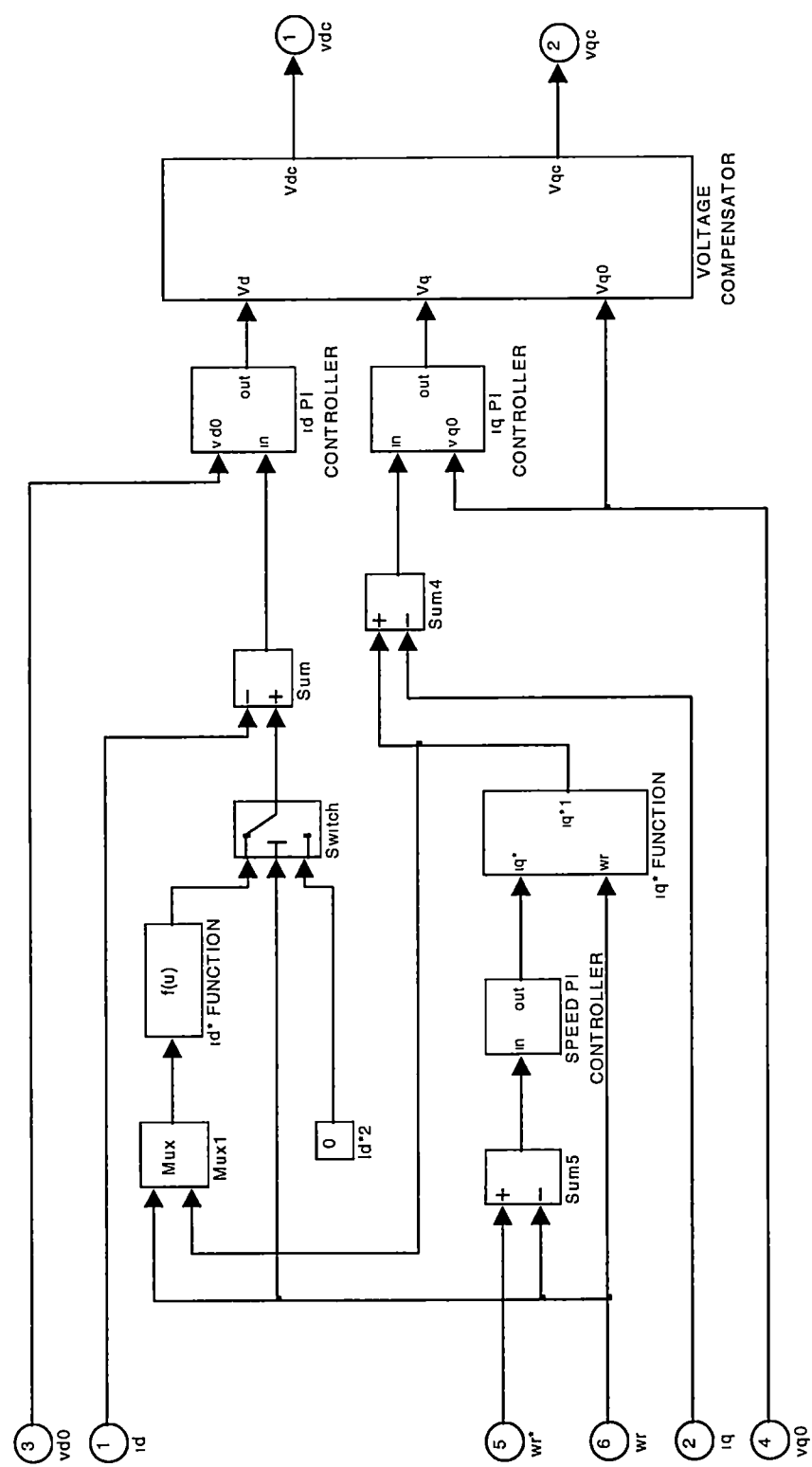
APPENDIX

SIMULATION BLOCK DIAGRAM

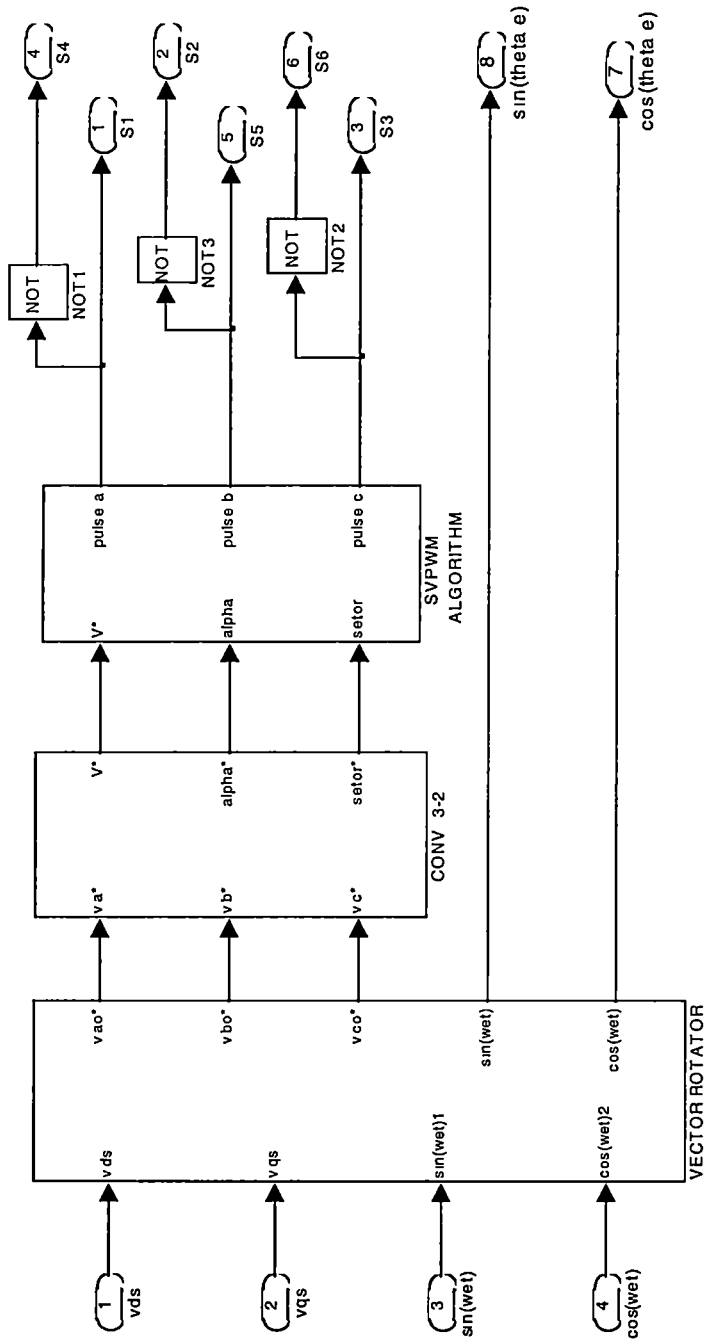
PMSMVCVFIMODEL



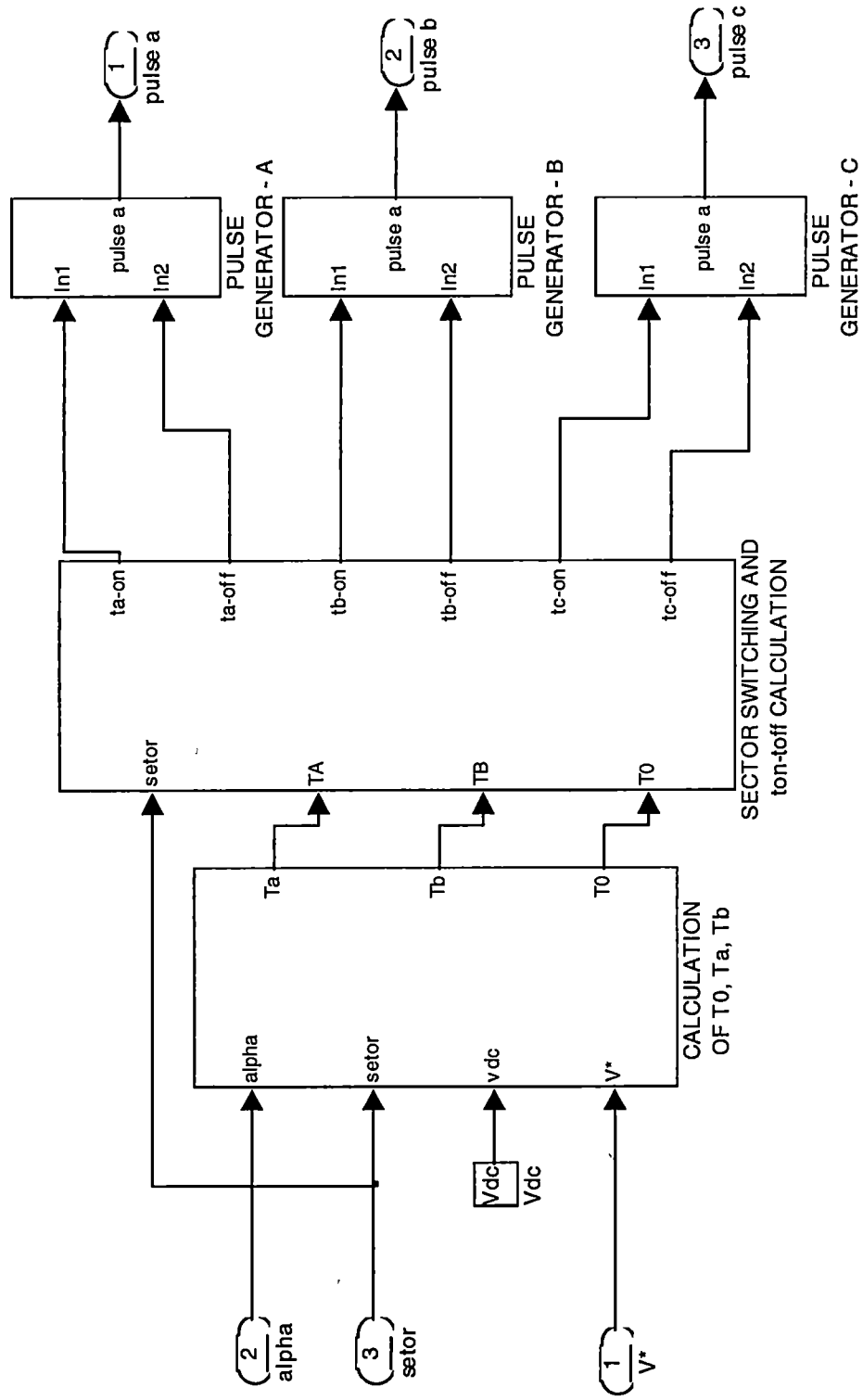
CONTROLLERS



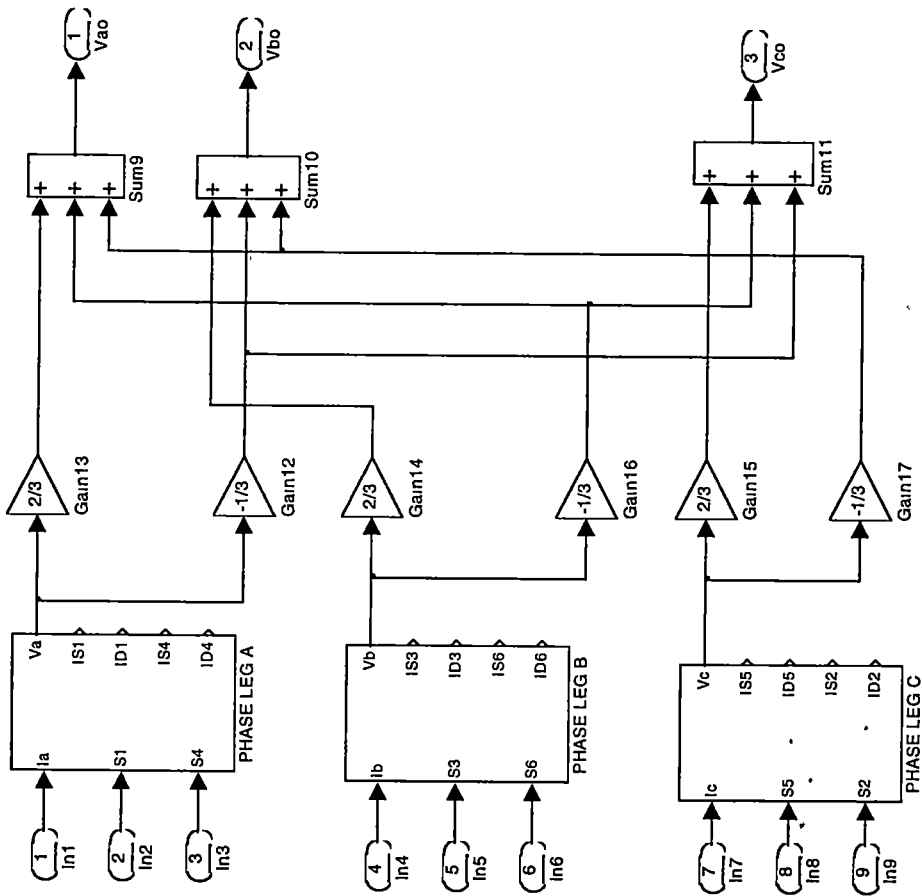
SVPWM 2



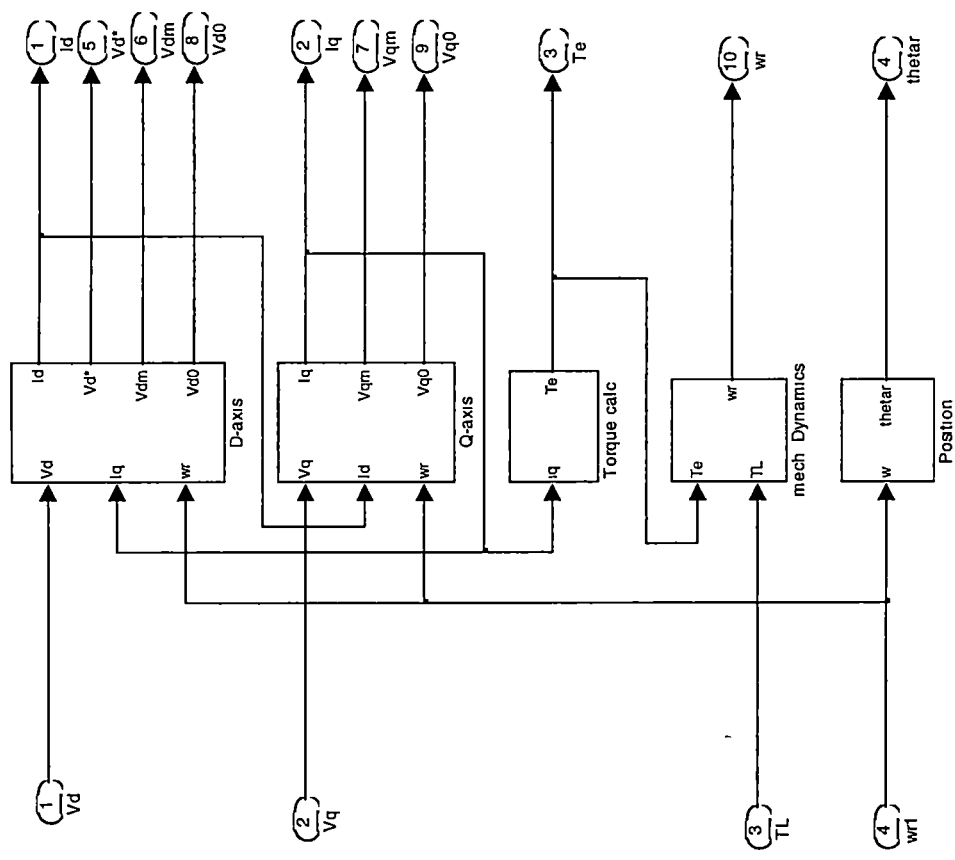
SVPWM ALGORITHM



VOLTAGE-FEED INVERTER



PMSMDQMODEL1



VITA

João Onofre Pereira Pinto was born in Valparaíso, Brazil in 1966. He attended Universidade Estadual Paulista at Ilha Solteira, SP, Brazil in 1986, where he received his Bachelor's degree in Electrical Engineering in 1990. In 1991, he attended Universidade Federal de Uberlândia, MG, Brazil where he received his Master's of Science also in Electrical Engineering in 1993.

He has been an assistant professor at Universidade Federal do Mato Grosso do Sul at Campo Grande, MS, Brazil since 1994, and is currently on leave of absence to pursue the Ph D degree in The University of Tennessee, Knoxville Department of Electrical Engineering since 1997.